Spatial and temporal variability of macrophyte growth and productivity in the Amazon floodplain.

by

Thiago Sanna Freire Silva
M.Sc., Instituto Nacional de Pesquisas Espaciais, 2004
B.Sc. (Hons.), Universidade Federal do Rio Grande do Norte, 2002

A Dissertation Submitted in Partial Fulfillment
of the Requirements for the Degree of

PhD

in the Department of Geography

Supervisory Committee

Spatial and temporal variability of macrophyte growth and productivity in the Amazon floodplain.

by

Thiago Sanna Freire Silva
M.Sc., Insituto Nacional de Pesquisas Espaciais, 2004
B.Sc. (Hons.), Universidade Federal do Rio Grande do Norte, 2002

Supervisory Committee

Dr. Maycira P. F. Costa (Department of Geography)
Supervisor

Dr. Rosaline Canessa (Department of Geography)
Departmental Member

Dr. Frederick J. Wrona (Department of Geography)
Departmental Member

Dr. Barbara Hawkins (Department of Biology)
Additional Member

Abstract

Supervisory Committee

Dr. Maycira P. F. Costa (Department of Geography)
Supervisor

Dr. Rosaline Canessa (Department of Geography)
Departmental Member

Dr. Frederick J. Wrona (Department of Geography)
Departmental Member

Dr. Barbara Hawkins (Department of Biology)
Additional Member

The main objective of the present thesis was to investigate the spatial and temporal variability of macrophyte growth and productivity in the Amazon floodplain, and the possible effects of this variability on the carbon budget of the floodplain.

In Chapter 3, two methods for estimating macrophyte biomass were compared in terms of accuracy and applicability to the Amazon floodplain conditions. Phenotypic variation was large enough to preclude indirect (phenometric) modelling of biomass, while direct sub-sampling was able to account for this variation. Sub-sampling also allowed reduction on the biomass sampling effort, presenting the best trade-off between accuracy and coverage for macrophyte biomass measurements in the Amazon floodplain.

In Chapter 4, annual net primary production (NPP) of macrophytes was estimated for a large lake on the eastern Amazon floodplain, and the uncertainty associated with these measures was assessed, offering a comparison of previous estimates of macrophyte productivity in the Amazon region. Annual net primary production was estimated at 2400 – 3500 g m^{-2} yr^{-1}, with above water production between 650 – 1100 g m^{-2} yr^{-1}, and below water production between 1700 and 2600 g m^{-2} yr^{-1}. *Echinochloa polystachya* (Poaceae) and *Paspalum fasciculatum* (Poaceae) were the most productive species, followed by *Paspalum repens* (Poaceae), *Hymenachne amplexicaulis* (Poaceae), and *Oryza perennis* (Poaceae). The four main sources of uncertainty in the estimates were macrophyte taxa, location, sampling design, and lack of measurements of dead material loss.

Chapter 5 presented a new object oriented method for combining radar and optical image time series to characterize seasonal evolution of macrophyte cover for an eastern Amazon floodplain lake. Macrophyte cover varied between 104 and 198 km^2 (10% and 20% of total floodplain area, respectively) and exhibited significant changes both seasonally and inter-annually. Two distinct growth strategies were observed: short-lived communities that thrived during low water periods and year-long communities able to survive flooding year-round. Although the majority of the macrophyte carbon fixation derived from the latter, about 17% of macrophyte NPP was attributed to the short-lived communities, which depend directly on the flood levels for a given year. The increased frequency of droughts predicted for the Amazon system could potentially result in an increase on the macrophyte-derived carbon input to the Amazon floodplain.

Table of Contents

List of Tables

List of Figures

Acknowledgments

Over the past five years, there are many people I would like to acknowledge. The list is so long I apologize beforehand if have forgotten anyone.

I am very grateful to my supervisor, Dr. Maycira Costa, and to Dr. John Melack from the University of California at Santa Barbara for giving me the chance to pursue the long sought dream of a doctorate degree in a foreign country.

I would also like to thank all my lab mates (Eddie, Nick, Jen, Terry, Keillah), all great people whom I have had great pleasure working with. I would also like to thank all faculty and staff members of the Department of Geography for taking me into their midst.

Many thanks to my colleagues at INPE (Evlyn, Eduardo, Ramon, Cláudio, Conrado, Waterloo) and at UCSB (Laura, Mary) for the very fruitful discussions and numerous contributions to my research.

Many, many thanks to Gilson Rego and all the hard working people involved on sampling kilos after kilos of macrophyte biomass at Lago Grande for a year. This thesis wouldn't exist without you.

A special thanks to all my classmates (Dave, Gerry, Raf, Megan, Ana, Kelly, Michi, Fabio, Roger, Crystal, Soo, Angela, Jaden) which have helped a "lost Brazilian" feel at home in a cold, distant land. And also another special thanks to all the "extended" geography friends (Katsy, Sharon, Brandy, Bruce, Leanne, Jordan, Shawn, Mike D., Mike C., Tomiko). You guys have been my family in Canada, and I can't thank you enough.

A big "obrigado" to all Brazilian friends I have made in Canada (Gabriel, Bruno, Chang, Joyce, Mirella, Fabiane e Rafael) for keeping a little piece of Brasil alive among us.

Special thanks to Patricia, for all the support and for trying to make me a better person during all these years.

Very, very big thanks to my family for keeping up with the distance and lack of communication, and for still spoiling me so well during my short visits.

Many thanks to my distant but still best friends (André, Fabrício, Bruno, Wagner "Baba", Melissa, Camila) for keeping the "flame" alive despite the distance, and for the kilometres of online conversations during the homesick evenings. Monstros pra sempre!

Very special thanks to Megan King for helping me manage the stress in the final days of work and for the last minute proof reading.

Funding for this research has been provided by NASA/LBA ECO, research group LC-07/LC-32, and by NSERC Discovery Grant to Dr. Maycira Costa.

Chapter 1 – Introduction

1.1 Wetland Ecosystems

Wetland ecosystems are widely renowned for their unique ecological characteristics. Many early human settlements developed along wetlands, drawing from their fertile soils (Boulé, 1994), and nowadays wetlands are recognized by their importance as agents of storage and transformation of natural elements, and as a pool of genetic diversity resulting from their combination of biotic and abiotic factors (Haslam, 2003; Mitsch and Gosselink, 2000; Keddy, 2000).

Many ecological services are provided by wetlands, such as the hydrological functions of groundwater supply recharge, flood control and reduction on shoreline erosion. Biogeochemically, they recycle many essential nutrients, and may also act as sinks for organic carbon in the form of peat. Ecologically, they usually exhibit high biodiversity and serve as breeding and habitat for many species of plants, invertebrates, fish and wildlife (Batzer and Sharitz, 2006; Mitsch and Gosselink, 2000).

Albeit very variable in terms of biotic and abiotic conditions, the presence of water is a unifying factor among all wetlands. The flooding conditions and resulting physical, chemical and biological properties are unique for wetland ecosystems. Most specialists recognize that these systems display attributes of both terrestrial and aquatic environments (plus a series of emergent properties), and for this reason tend to be overlooked by both terrestrial ecologists and limnologists or aquatic ecologists (Keddy, 2000; Mitsch and Gosselink, 2000). Being often classified as *ecotones*, transitional

systems between the terrestrial and aquatic phases, wetlands are usually considered outside the scope of terrestrial or aquatic ecology studies.

Wetlands are critical components of the global carbon cycle, being responsible for fixating, recycling and transforming large amounts of carbon (Mitsch and Gosselink, 2000). The mean net primary productivity (NPP) of world's wetlands ranges from 400 to about 2000 g C m^{-2} yr^{-1}, and is mainly a function of hydrological and geomorphologic factors. Closed, ombrotrophic (rain-fed) wetland systems tend to exhibit very low primary productivity rates because of extreme oligotrophy, while wetlands which receive nutrient enriched-water inputs from ground and surface water can figure among the most productive ecosystems in the world (Batzer and Sharitz, 2006, Mitsch and Gosselink, 2000, Schlesinger, 1997, Cao et al., 1996). Nonetheless, the total carbon pool trapped in wetland vegetation biomass is estimated to be near 7.8 Pg C, roughly 1.4% of the total global vegetation (Schlesinger, 1997). Such disparity between high productivity and low carbon storage in the vegetation implies rapid carbon turnover and/or soil accumulation rates for wetland ecosystems.

Production and emission of methane (CH_4) is another key environmental process characteristic of wetlands, and is of major interest as methane has a global warming potential approximately 20 times higher than CO_2 (Solomon et al., 2007). Estimated methane emissions from wetlands are 100 $TgCH_4$ yr^{-1}, or 72% of the total natural global emissions, representing roughly 20% of the total annual CH_4 emissions (Wuebbles and Hayhoe, 2002).

The major wetland regions of the world, as listed by Fraser and Keddy (2005), are the West Siberian Lowland in northern Russia, the Amazon River basin, the Pantanal and

the Magellanic moorland in South America, the Nile and Congo River basins and Lake Chad basin in Africa, the Prairie Potholes and Hudson Bay Lowland at the north-center of North America, the Mackenzie River basin in northwestern Canada and the Mississippi River alluvial plain in the USA. Other important wetland areas are listed by Mitsch and Gosselink (2000), such as the Orinoco River basin and the Lllanos in South America; the Rhine Delta, Mediterranean Sea deltas, Coastal Marshes of Northern Europe and various peatlands in the European continent; the Okavango Delta in Africa, the Billabongs in Oceania; and the south-eastern wetlands in Asia.

Each of these regions exhibit diverse and unique hydrological, ecological and biogeochemical characteristics, resulting in very distinct environments. Contrasting hydrology regimes, for example, can be observed between the Amazon floodplain, the ombrotrophic bogs on the Arctic tundra, and the littoral zones of the Great Lakes (Fraser and Keddy, 2005). The first is extensively flooded by overland and stream surface flows, infused with allochthonous nutrients and organic matter; ombrotrophic bogs are closed systems with slow, conservative cycles and have precipitation as their only source of exogenous material; lake littoral zones are subjected to annual variation in water stage levels, and receive significant inputs from both precipitation and surface flows.

1.2 The Amazon Floodplain

The Amazon basin houses one of the largest expanses of wetlands in the world (Fraser and Keddy, 2005). The most recent estimates from basin wide mapping using JERS-1 satellite imagery report a floodable area of about 800,000 km^2 (Melack et al., in press (a), Hess et al., 2003), and as the scale of this mapping effort does not account for

small-order streams and associated wetlands, total wetland area in the basin can exceed a million square kilometres (McClain and Elsenbeer, 2001).

The central Amazon floodplain extends over 100,000 km^2 along the river the mainstem, or 350,000 km^2 if accounting for small-order streams (Melack et al. in press (a)). Along its extent, from the eastern Andean border to the Atlantic Ocean, it exhibits a large variety of habitats and environmental conditions, reflecting the geological and hydrological conditions of its surroundings, as well as alterations due to human influence (Junk, 1997).

Differences in the estimations of the carbon budget of the entire Amazon basin have it pictured as either a sink or source of atmospheric carbon (Ometto et al., 2005; Houghton, 2003; Saleska et al., 2003), and CO_2 and CH_4 outgassing from the riverine and floodplain systems have been suggested to be one of the key missing components to accurately determine the basin C budget. Carbon dioxide evasion may account for about 500 TgC yr^{-1} (Richey et al., 2002), a value ten times higher than the floodplain's export of organic carbon to the ocean. These figures are comparable to the total emissions by deforestation in the tropical Americas (Solomon et al., 2007), and represent about 5% of the total Amazon NPP (Potter et. al. 2004) or 15% of global terrestrial tropical NPP (Grace et al., 2001). In addition, around 22 TgC yr^{-1} can be attributed to methane emissions, representing between 8 and 15% of the estimated global wetlands emissions (Solomon et al., 2007, Melack et al., 2004).

Carbon inputs into the floodplain originate from both allochthonous (ground, stream and overland flow) and autochthonous sources. While the first depend on the geology, land cover, drainage and rainfall patterns of the catchment area (McClain and

Elsenbeer, 2001), autochthonous sources are mostly regulated by the responses of floodplain vegetation to the annual and inter-annual flood dynamics, which in turn are reflected in primary production and turnover rates (Melack et al., in press (b)).

The floodplain ecology is mainly characterized by the flood pulse concept, where the annual monomodal flooding pattern controls the growth and distribution of the vegetation, the timing and availability of nutrients and the reproductive cycles of plant and animal species (Tockner et al., 2000; Junk et al. 1989). In this context, the main vegetation types (floodable forests, floodable shrubs, and herbaceous aquatic vegetation) have been associated with different successional stages in the ecosystem, each reflecting the intensity and recurrence of the flood perturbation (Piedade et al., 2001; Junk, 1997).

Primary production in the floodplain is mainly driven by flooded forest litterfall (62%) and herbaceous vegetation (macrophytes) growth (34%), with small contributions from phytoplankton and periphyton (< 3%) (Melack et al., in press (b)). This proportion, however, can vary across the floodplain depending on the extent and zonation of each vegetation type, which are in turn controlled by the flooding dynamics.

The contribution from aquatic herbaceous vegetation (macrophytes) to the carbon budget of floodplain appears to be significant, being reported as approximately 100 $TgCy^{-1}$ for the Central Amazon floodplain region (Melack et al, in press (b); Piedade et al., 1997; Piedade et al., 1991). Amazonian macrophytes have remarkably high productivity (Chapter 4; Engle et al., 2008; Costa, 2005; Hess et al., 2003; Junk and Piedade, 1993a; Piedade et al., 1991), and being the first to colonize newly exposed areas these plants can have large intra and inter-annual variations in distribution and coverage,

and are likely the most susceptible to rapid and short-lived changes in flooding patterns (Chapter 5; Junk and Piedade, 1997).

Macrophyte growth and turnover can also influence the timing of nutrient storage and release into the aquatic system (Piedade et al., 1997; Junk and Furch, 1991), and these plants are an important source of fodder for cattle, as well as a breeding habitat for fish (Camarão, 2004; Ohly and Hund, 2000; Junk, 1970) and a main food resource and determining factor for distribution and migration of the endangered Amazonian manatee (Arraut, 2008).

Despite the importance of macrophytes, previous macrophyte studies in the Amazon floodplain have been mostly restricted to small lakes (< 50 km^2) and clustered around the city of Manaus, in the central portion of the Amazon floodplain (Figure 1.1). Moreover, the uncertainties associated with these measurements have seldom been evaluated in an explicit manner. These limitations arise from the extent and inaccessibility of most areas in the floodplain, which largely constrain the ability to capture the effects of environmental variability on productivity and reduce the degree of confidence associated with extrapolations of these measurements to regional scales.

For the above reasons, further studies that describe and quantify the seasonal and inter-annual variability of macrophyte cover and productivity are needed to properly elucidate the ecological and biogeochemical role of macrophytes in the Amazon floodplain, as well as to characterize the susceptibility of these plants to climatic alterations and its possible consequences to floodplain ecological processes.

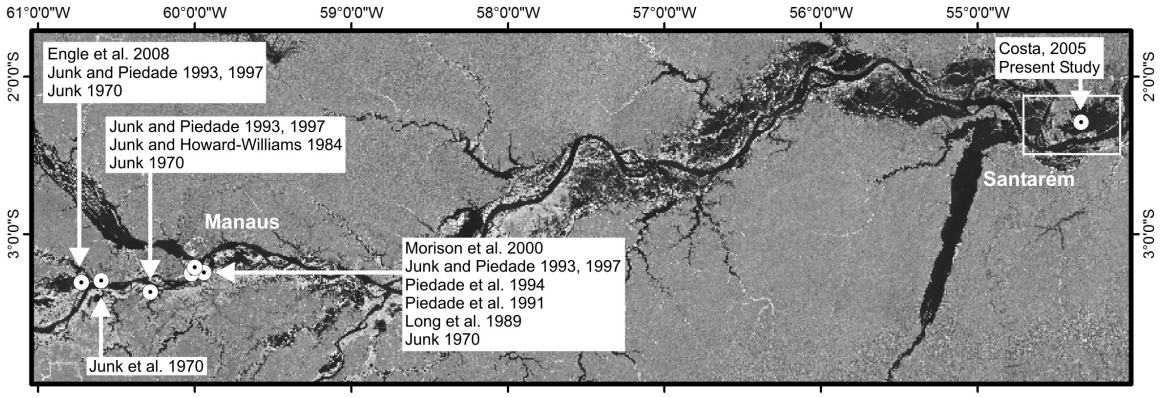

Figure 1.1 - Distribution of previous studies on macrophyte growth and productivity in the Amazon floodplain. Background image: JERS GRFM Mosaic L-HH SAR image.

1.3 Aquatic herbaceous vegetation in the Amazon floodplain

Herbaceous aquatic plants (macrophytes) are one of the major plant functional groups in the floodplain, along with flooded forest, phytoplankton and periphyton (Junk and Piedade, 1997). Amazonian macrophytes are often the first colonizers of newly exposed areas, and play a key role in the successional processes in the floodplain (Junk and Piedade, 1997; Kalliola et al., 1991).

Herbaceous plants in the Amazon floodplain are a very diverse group, with almost 400 identified species (Junk and Piedade, 1993b). Among these, grasses (Poaceae) are the most abundant, with approximately 60 species (Junk and Piedade, 1993b) followed by Cyperaceae (37), Leguminosae (30) and Compositae (30). Although most of these plants can be classified as terrestrial plants, many species have specific adaptations which allow survival during flooded periods, even if their main growth period occur during the dry phase (Junk and Piedade, 1993b).

Some grass species appear to dominate over the floodplain: *Echinochloa polystachya* (Kunth) Hitchc., *Paspalum fasciculatum* Willd. ex Flueggé, *Hymenachne*

amplexicaulis (Rudge) Nees, and *Paspalum repens* auct. non Berg, all C4 species with the exception of *H. amplexicaulis*. Floating species such as *Pistia stratiotes* L. (Araceae), *Salvinia auriculata* AUBL. (Salvinaceae) and *Eichornia* spp. (Pontederiaceae) are also ubiquitous (Junk and Piedade, 1997; Junk and Piedade, 1993b; Junk, 1970). Patches strongly dominated by *Montrichardia arborescens* SCHOTT (Araceae), a large-sized, shrub-like herb, are also characteristic of the floodplain environment.

Plant morphology is very similar among the grass species, consisting of a single, vertical stem, rooted at substrate and elongating all the way to the surface (Chapter 3; Junk 1970). Adventitious roots are common, and plant stands can occasionally detach from the substrate, forming very dense "floating islands" (Junk, 1970). These plants life cycle is mostly tied to the annual flood pulse, with the majority of growth being carried during the low, rising and high water phases, when the larger influx of nutrients occurs (Chapter 4; Junk and Piedade, 1997; Piedade et al., 1992; Junk and Piedade, 1993b; Junk 1970). Most Amazonian macrophytes can reproduce both by seed dispersal and vegetative growth, the latter being the main form of propagation (Junk and Piedade, 1997). For most grass species, new shoots start to develop from old stem nodes during the low water phase, quickly elongating as water levels start to rise (Chapters 3 and 4; Junk and Piedade, 1997, Piedade et al., 1992).

The distribution of vegetation in the Amazon floodplain is directly related to the duration and amplitude of the flood, with macrophytes colonizing areas of > 300 days of flooding, flood-tolerant shrubs colonizing areas > 230 days of flooding, and floodplain forest colonizing areas of < 230 days of flooding (Junk and Piedade, 1997). In addition, plant distribution also reflects the recurrence of flooding, with herbaceous vegetation

responding more quickly to recent flooding events, and woody vegetation being representative of decadal flooding patterns (Junk and Piedade, 1997). Macrophytes are also better adapted for colonizing areas with high sedimentation rates, and usually are responsible for stabilizing the sediments and laying the foundation for latter sucessional stages (Junk and Piedade, 1997).

1.4 Remote Sensing of Emergent Macrophytes

Remote sensing is a valuable tool for assessment of macrophyte stands and associated biophysical and ecological parameters. The use of remotely sensed images allows multitemporal studies and provides comprehensive information from surrounding areas.

The principles behind aquatic vegetation spectral characteristics are the same as behind its terrestrial counterparts. At the leaf level, presence and concentration of leaf pigments determine the response in the visible region of the spectrum, and leaf morphology and water content are the main factors acting on the infrared wavelengths. At the individual level, biophysical factors such as leaf distribution, leaf density and orientation, and overall canopy structure are important. Vertically oriented plants or reduced leaf area offer less available surface to interact with the downwelling radiation, while highly branched canopies and broadleaved plants have a more effective reflective area (Williams et al., 2003). At the community level, plant biomass and density are also important variables.

Although the spectral response of aquatic vegetation resembles that of terrestrial vegetation, the submerged or flooded conditions introduce factors that can alter its overall

spectral characteristics. The presence of water introduces variability in reflectance values due to the mixing of plant and water signals (Malthus and George, 1997), which usually results in a decrease in total reflected radiation, especially in the near to mid infrared regions where water absorption is stronger. The intensity of such effects will be determined by vegetation density and canopy structure (Jakubauskas et al., 2000), as well as by the nature of the water signal, the latter being a function of the amount and nature of suspended materials and depth of the water column, plus substratum composition for shallow depths.

Physiological status of vegetation can be another source of variation in plant spectral signatures. Best et al. (1981) demonstrated that a single species, in different phenological stages, exhibited significant variation in its reflectance. In addition, physiological stress can lead to spectral variability (Tilley et al., 2003; Peñuelas et al., 1997; Bajjouk et al., 1996; Peñuelas et al., 1993; Best et al., 1981). Stress usually implies alterations on biochemical status and morphological characteristics, which in turn determine the spectral response in the different regions of spectra.

Besides optical data, the use of Synthetic Aperture Radar (SAR) data has been long acknowledged as a valuable tool for studying wetlands. In the microwave range, differences in the signal recorded from dry and flooded vegetation allow the mapping of flooding extent (Costa 2004; Hess et al. 1995), and numerous studies have shown that SAR images can be utilized to study aquatic vegetation (Costa 2005; Kasischke et al. 2003; Moreau and Le Toan 2003; Costa et al. 2002; Novo et al. 2002; Noernberg et al. 1999; Le Toan et al. 1997; Pope et al. 1997; Kasischke and Borgeau-Chavez 1997; Hess et al. 1995).

SAR data offers information about canopy biophysical characteristics and dielectric properties (a proxy for water content), as the longer microwave wavelengths penetrate into the canopy and produce a "volumetric" signal. Radar systems operate in specific regions of the electromagnetic spectrum, and radar bands are usually coded by a single letter. The most common bands used are X (3 cm wavelength), C (5.6 cm), S (10 cm), L (23 cm) and P (75 cm). Longer wavelengths tend to have deeper canopy penetration and less sensitivity to smaller biophysical variations.

In addition to wavelength, every radar system has defined polarizations for sending and receiving the radiation pulse, either vertically (V) or horizontally (H). Same-polarization systems are usually referred as HH and VV systems, and cross-polarization systems as HV or VH. Different polarizations, as well as ratios or differences in polarizations can highlight specific characteristics for some types of targets (Lewis and Henderson, 1998).

As SAR sensors are side-looking systems, where the electromagnetic pulse hits the surface in a sub-nadir angle, most of the radiation is reflected specularly from smooth surfaces and does not return to the sensor. With increasing surface roughness and addition of volumetric components such as vegetation, the backscattered radiation increases (Lewis and Henderson, 1998). The overall radar signal from aquatic vegetation is composed primarily of the volumetric backscatter from the canopy elements, the surface backscatter from the ground/water surface, and the double-bounce interaction from radiation that is forward scattered from the surface but bounces off the canopy elements and returns to the sensor. Double bounces are caused by the interaction of the radiation with the stem/trunk, followed by a change in direction towards the surface

(water) and a strong bounce back towards the radar antenna (dihedral corner reflector behaviour), the inverse being also possible.

Overall, the total radar backscattering from wetland herbaceous plants is dependent on the interaction of the microwave energy with both the canopy and the canopy-ground. Not only plant characteristics, such as density, distribution, orientation, leaf shape, dielectric constant, height and components of the canopy, but also the sensor parameters (polarization, incidence angle and wavelength) play an important role in determining the amount of radiation backscattered toward the radar antenna. Due to this multitude of factors, visual interpretation usually requires more training and familiarity with radar imagery than optical data.

One of the main hindrances of spaceborne radar systems is that most have a single band/ polarization configuration, reducing the data available for an accurate identification of macrophyte stands (Hess et al. 2003). This limitation can be overcome with the combination of different satellite imagery (Chapter 5; Costa et al. 2002) or the use of textural and contextual measures (Simard et al., 2002, Simard et al., 2000; Noernberg et al. 1999). Also, the use of multitemporal, multi-incidence angle or multipolarization data can offer some improvement in overall discrimination (Chapter 5; Proisy et al. 2000; Hess et al. 1995).

1.5 Thesis Objective and Structure

The main objective of this thesis was to investigate the spatial and temporal variability associated with macrophyte growth and productivity in the Amazon floodplain, and the possible effects of this variability on the carbon budget of the Amazon floodplain. The document is organized into six chapters, with chapters 3 to 5 addressing

specific objectives within the main goal. Each of these three chapters corresponds to a published or submitted peer-reviewed journal article.

Chapter 2 presents an overview of the study area, details the field data collection procedures and describes remote sensing imagery acquisition and pre-processing.

Chapter 3 compares two methods for estimating macrophyte biomass from field samples, one based on phenometric measurements and other on reduced sampling (direct method) in terms of accuracy and appropriateness to the study of Amazonian macrophytes, and provides suggestions and guidelines towards the standardization of sampling methodology for Amazon aquatic herbaceous vegetation.

Chapter 4 offers an estimation of annual net primary production (NPP) of macrophytes in the study area, explicitly quantifying the sources and amount of uncertainty associated with these measurements, and offers a comprehensive comparison of the existing estimates of macrophyte NPP in the Amazon floodplain.

Chapter 5 presents a new hierarchical, object oriented method for combining multisource and multidate optical and SAR remote sensing data to map seasonal changes in macrophyte cover in the Amazon floodplain, and offers for the first time a consistent characterization of the seasonal evolution of macrophyte cover along a yearly flooding cycle for an eastern Amazon floodplain lake, alongside some considerations on the possible effects of this variability on the ecological and biogeochemical processes of the Amazon floodplain.

Chapter 6 presents general conclusions and future recommendations regarding the outcomes of the present study.

Chapter 2 – Study Area and Data Collection

2.1 Study Area

The study area (Figure 2.1) consists of two locations within the limits of 54º00'W to 54º45'W and 02º00'S to 02º30'S in the state of Pará, Brazil. Both sites are situated at about 900 km from the Amazon River's mouth, near its confluence with the Tapajós River, and can be regarded as representative of the environmental conditions found in the eastern portion of the Amazon floodplain.

Open water surface in Monte Alegre Lake varies seasonally between 1000 – 1200 km^2. Annual water level variation is about 3 – 6 m, rising from December to May, reaching a peak in June and July, and receding to a minimum in November. Although most of the lake water is derived from sediment-rich Amazon River water (traditionally known as "white" water), smaller rivers and creeks can contribute with waters rich in particulate and dissolved organic substances ("black" water) or with low contents of organic and inorganic matter ("clear" water), creating a variety of conditions. A similar pattern has been described for the nearby Curuai Lake (Bonnet et al., 2008).

Hymenachne amplexicaulis (Rudge) Nees (Poales : Poaceae) and *Paspalum fasciculatum* Willd. ex Flueggé (Poales : Poaceae) were the dominant species in the region, usually forming dense and extensive stands (> 100 m2). Other species, such as *Oryza perennis* Moench (Poales : Poaceae), *Paspalum repens* auct. non Berg. (Poales : Poaceae), and *Echinochloa polystachya* (Kunth) Hitchc. (Poales : Poaceae) occurred in specific regions within the study area, forming distinct community clusters. Genera such as *Eichornia*, *Pistia*, *Salvinia*, *Ceratophyllum*, *Ludwigia*, *Urena*, *Scoparia*, *Nymphaea*,

Nymphoides, and *Victoria* were also observed, mostly interspersed with the dominant vegetation or, in rarer occasions, forming monospecific stands (e.g., *Eichornia*). Due to the high turbidity and limited light penetration, submerged species (e.g., *Utricularia* spp.) were less common, but found occasionally in places where low currents or clear water input resulted in increased sedimentation and less turbid conditions.

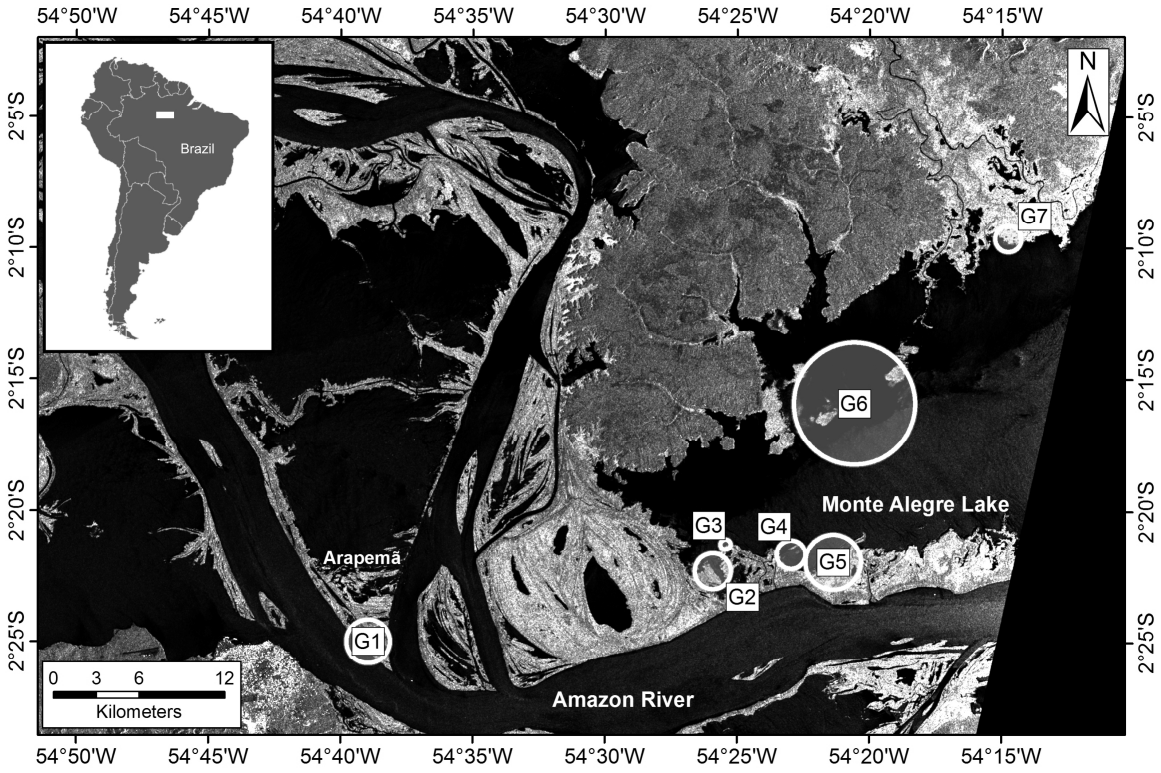

Figure 2.1: Monte Alegre Lake and the seven main sampling sites chosen for our study. Shaded circles represent the maximum radius covered by sampling points at each location. Background Image: Radarsat 1 C-HH seasonal backscatter average.

2.2 Field Sampling

Ten field campaigns were undertaken during the period of December 2003 to November 2004, with the best possible regularity within existing logistical constraints (Figure 2.2). The data collection design was established to accommodate both field measurements of macrophyte biomass and ground truthing of satellite imagery analysis. The full dataset comprised a total of 357 sampling points, with a minimum of 16 and a maximum of 40 points sampled per campaign (Table 2.1).

The sampling design was stratified into seven main sampling sites based on known macrophyte occurrence. Six sites were established at Monte Alegre Lake (sites G2 to G7), and a single site was selected at a location near a small community known locally as Arapemã (site G1) (Figure 2.1). This region was included because it is representative of an *Echinochloa polystachya* dominated community, commonly found at other locations on the floodplain, and which have been the focus of the majority of previous studies carried in the Amazon.

Within each site, one or more sampling transects were determined based on the extent and shape of the stands, reaching up to 100 m into the stand. Five to ten sampling points were visually distributed along the transect(s), and triplicate measurements were done at each point by randomly placing a 0.25 m^2 aluminum quadrat in the immediate vicinity of the point.

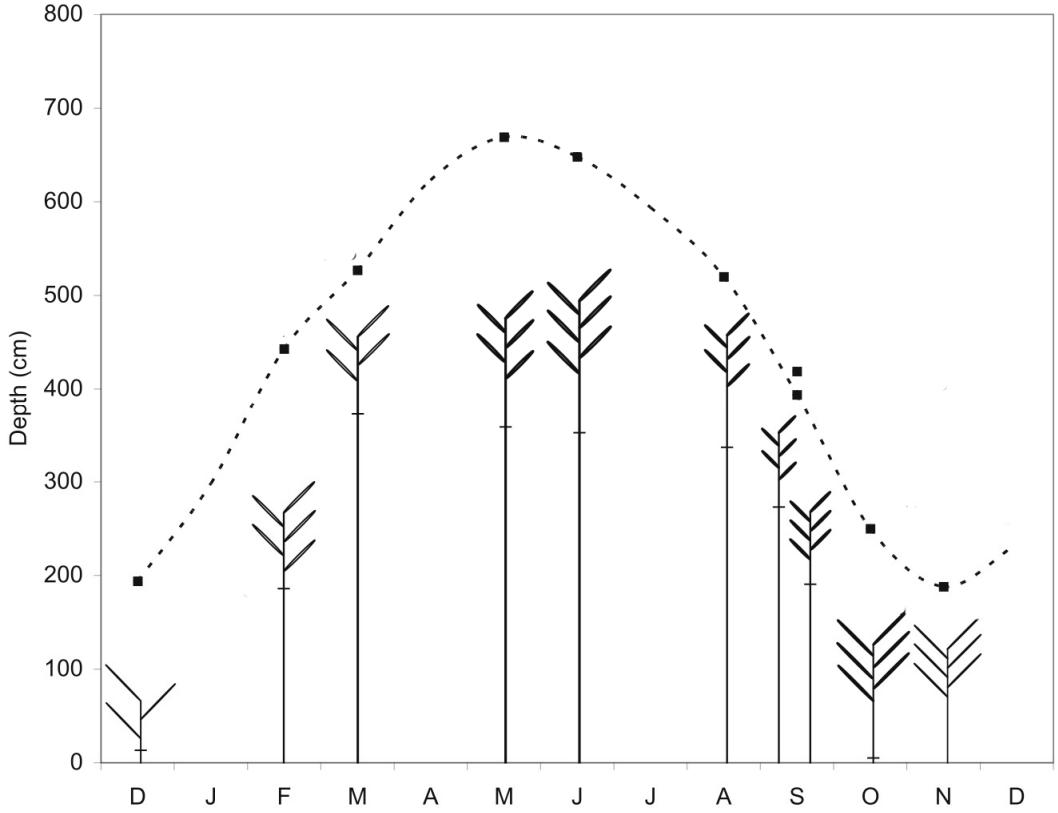

Figure 2.2: Distribution of field campaigns along the annual flood cycle (black squares). Plant schematics are drawn in proportion to average Stem Length, Stem Diameter, Leaf Length, Leaf Width and Number of Leaves for all samples. The horizontal notch indicates the division between Emergent and Submerged Stem Length. Amazon River stage data for the studied period (2003 - 2004) was obtained from the Óbidos gauging station (ANA, 2006). Please note that stage values refer to river depths, and do not reflect actual depths at Monte Alegre lake.

Three types of samples were established for data collection:

Partial Samples (PS): Ten percent (10%) of the total number of individual plants in the quadrat were clipped, with a minimum of 9. Plants were first clipped at the water surface, and then submerged parts were sampled by pulling the stems from the soft substratum. Samples included all aboveground plant parts (leaves, stems and adventitious roots) (n = 217).

Complete Samples (CS): Similar to the partial samples, but with further sampling of all remaining individuals in the quadrat after the initial collection of the ten percent sample, weighed separately (n = 64).

Observation Samples (OS): Only the presence of macrophytes and the dominant species occurring at the location (estimated visually) were recorded, along with photographs and geographical location. These samples were intended to aid in remote sensing imagery interpretation and validation (n = 96).

After sampling, roots and any detached litter material were removed and plants were placed inside fine mesh bags and hand washed to remove mud and fine debris. Emergent and submerged biomasses were weighed separately. Dry biomass was determined by oven-drying (80ºC) to constant weight, to the nearest 0.1 g (Downing and Anderson, 1985).

Water depth and phenometric plant variables were recorded for each quadrat, for both CS and PS samples. For the phenometric data, at least three random individuals were measured inside each quadrat, and the average was recorded. The obtained data were aggregated by averaging the values of the triplicate quadrat samples at each point, yielding a single average value per geographical location. The phenometric variables selected to be used in the following study are presented in Table 2.2, and an explanatory diagram of the phenometric measurements is shown on Figure 2.3.

Table 2.1: Sample sizes and species distribution at sampling sites in Monte Alegre Lake (Amazon, Brazil). The values represent the number of samples collected for each combination of dominant species (columns) and sampling site (G1–G7, rows) during December 2003 to November 2004. "Others" include *Scoparia* (Scrophulariaceae), *Urena* (Malvaceae), and *Eichornia* (Pontederiaceae). Table does not include observation points (n = 96).

Group	*H. amplexicaulis*	*P. fasciculatum*	*O. perennis*	*P. repens*	*E. polystachya*	Others	**Total**
G1	7	6	0	9	13	0	**35**
G2	45	0	4	2	0	1	**52**
G3	0	24	0	0	0	0	**24**
G4	9	23	0	1	0	2	**35**
G5	21	38	7	5	0	0	**71**
G6	12	0	10	0	0	0	**22**
G7	21	0	1	0	0	0	**22**
Total	**115**	**91**	**22**	**17**	**13**	**3**	**261**

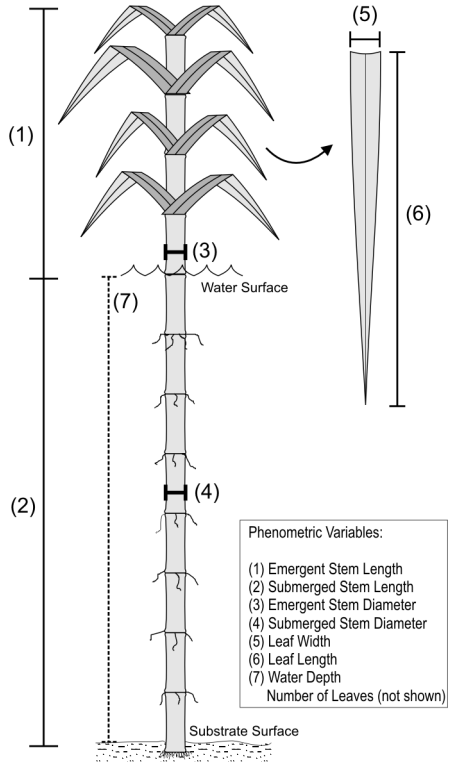

Figure 2.3 - Explanatory diagram of phenometric measurements.

2.3 Remote Sensing Data

Table 2.3 lists characteristics and availability of the image data used for the present study. Radarsat-1 images were acquired as Level 1 SGF (path) images, processed by the Alaska Satellite Facility. Level 1 images include basic georeferencing using the satellite orbit and attitude data, and radiometric calibration of the radar signal to Radar Cross Section (RCS) values in 16-bit digital numbers. Conversion to sigma-naught ((σ^0) backscattering values in dB was obtained by application of a reverse scaling function (Shepherd, 2000):

$$\sigma_j^0 = 10\log_{10}[(DN_j^2 + A3)/A2_j] + 10\log_{10}(\sin I_j) \qquad \text{(Eq. 2.1)}$$

where DN is the digital number, $A3$ is the fixed offset value, $A2_j$ is the calibration gain applied to every pixel j, and I_j is the incidence angle of the radar beam at pixel j. $A2_j$ values are included in the original SGF files and interpolated for each pixel j based on a Look-Up Table (LUT) generated using absolute and relative calibration parameters for the Radarsat sensor. These parameters are maintained by regular calibration operations that re-assess system error and noise. Because of very low variation in elevation observed for the study area, incidence angles (I_j) for the present study were derived simply by using the WGS84 earth ellipsoid (Freeman, 1992). Stability of the radiometric calibration of the radar scenes was assessed by taking homogenous samples ($n > 100$ pixels) of dense upland forest along the radar range. Variations along range were < 2dB, indicating that calibration was stable (Srivastava et al., 1999). Images were processed using the MapReady (former ASF Convert) software, provided by the Alaska Satellite Facility (http://www.asf.alaska.edu/sardatacenter/softwaretools).

As the system georeferencing error was considered too high for the present application (< 750m, Radarsat International, 2002), further geo-referencing was carried for all images through selection of ground control points, using as reference an Ortho-Rectified Landsat ETM+ scene provided by the Global Land Cover Facility (GLCF) (http://glcf.umiacs.umd.edu/index.shtml). Overall accuracy was of $0 < RMSE < 2$ pixels for all scenes.

MODIS 09 daily surface reflectance products where acquired as MOD09 GQ (Terra) and MYD09GQ (Aqua) products, which are processed to Level 2G. MOD-09 images were processed by the Modis Reprojection Tool (https://lpdaac.usgs.gov/lpdaac/tools/modis_reprojection_tool), for conversion to the same UTM-WGS84 coordinate system as the radar imagery. The MOD-09 product offers pre-calibrated estimates of Surface Reflectance (Justice et al., 2002) in 16-bit signed integer digital number values.

The atmospheric calibration algorithm for MODIS land products corrects the effect of gaseous and aerosol scattering and absorption. Gaseous absorption is estimated based on a combination of ancillary atmospheric composition data and elevation, and aerosol optical thickness is derived by MODIS bands located at specific aerosol absorption intervals, as well as AVHRR and SeaWiFS data or modelled according to the 6S algorithm (Vermote and Vermeulen, 1999, Vermote et al., 1997). Corrections are also performed for non-lambertianieity through the use of Bidirectional Reflectance Distribution Functions (BRDFs), and contamination by thin cirrus clouds is corrected using a cloud-detection algorithm (Vermote and Vermeulen, 1999).

Digital numbers can be converted to reflectance values by application of a simple scale factor (Vermote and Kotchenova, 2008):

$$\rho = DN \times 0.0001 \qquad \text{(Eq. 2.2)}$$

To improve the spatial resolution of MODIS, images were submitted to an image restoration procedure, which attempts to recover a portion of the signal degraded by the optical image acquisition (Silva et al., 2007). This degradation can be approximated by a Gaussian blur model (Fonseca e Mascarenhas, 1987), similar to

Table 2.2: Macrophyte phenometric data collected at Monte Alegre Lake (Amazon, Brazil), from December, 2003 to November, 2004.

Variable Name	Description
Dry Biomass	Dry biomass per individual plant.
Dominant Species	The dominant species based on visual assessment.
Depth	Water depth at the sample location.
Density	Total number of individuals (stems) per square meter.
Emergent Stem Length	Stem height as measured from the water surface (emergent length).
Emergent Stem Diameter	Diameter of the emergent portion of the stem, measured at half-length.
Number of Leaves	Number of leaves present.
Leaf Length	Length from petiole/sheath insertion to the tip.
Leaf Width	Width at maximum leaf width.
Submerged Stem Length	Length of the submerged part of the stem.
Submerged Stem Diameter	Diameter of the submerged part of the stem at half-length.
Total Stem Length	Sum of emergent and submerged stem lengths.
Total Stem Diameter	Average of emergent and submerged stem diameters.

a low-pass filter, and a restoration (high-pass) filter can be applied to the image to reduce the blurring effect. The image restoration procedure resulted in MODIS images with 125m nominal spatial resolution, as opposed to the 250m spatial resolution of the original files.

The RESTAU restoration algorithm used in the present work was based on a Modified Inverse Filter (MIF) technique (Fonseca et al., 1993; Boggione, 2003). The MIF was designed based on the EIFOV (Effective Instantaneous Field of View) sensor parameter, which is a function of the frequency in which the MTF (Modulation Transfer Function) is equal to 50% of its maximum value. For MODIS images, the MTF values indicated by Barnes et al. (1998) have been used to calculate the EIFOV values for each band. Previous studies have shown that an increase in the accuracy of areal and (to a lesser degree) shape determinations from MODIS can be achieved by the application of the RESTAU algorithm, without significant alterations in the radiometric properties of the images (Silva et al., 2007b).

Three image sources were used as aids for visual interpretation of Radarsat-1 and MODIS data. Cloud-free Landsat TM 5 images were acquired for all the possible dates during the study period, as well as four cloud free scenes from the CBERS-2 High Resolution Camera (HRC) sensor. Both image sets were georeferenced to the aforementioned ortho-rectified Landsat ETM+ reference image. Geocoded digital videography mosaics from the 1999 VOAM survey (Hess et al., 2002) were obtained from the National Institute for Space Research (INPE) in Brazil. An existing archive of about 250 overlapping true-color analog aerial photographs at approximately 1:15000

resolution obtained during 1996 for the studies by Costa (2005, 2004) was also employed.

Table 2.3: Availability and characteristics of satellite imagery used in the present study.

Sensor	Characteristics	Available Dates	
Radarsat 1	Synthetic Aperture Radar C band (5.6cm), HH polarization Incidence Angle = 24.2º-31.2º (ST2 mode) Pixel Size = 12.5m	2003-12-20 2004-01-13 2004-02-06 2004-03-01 2004-03-25 2004-04-18 2004-06-05	2004-06-29 2004-07-23 2004-08-16 2004-09-09 2004-10-27 2004-11-20 2004-12-14
MODIS	MOD-09 Daily Surface Reflectance Product Band 1: 620-670 nm Band 2: 841-876 nm Pixel Size = 250m	2003-12-16 2003-01-03 2003-02-27 2004-03-30 2004-04-10 2004-05-01 2004-06-27	2004-07-29 2004-08-19 2004-09-13 2004-10-22 2004-11-09 2004-12-11
Landsat TM 5	Surface Reflectance Band 1: 450 – 520 nm Band 2: 520 – 600 nm Band 3: 630 – 690 nm Band 4: 760 – 900 nm Band 5: 1550 – 1750 nm Band 7: 2080 – 2350 nm Pixel Size = 30m	2004-05-27 2004-06-12 2004-07-14	2004-08-31 2004-11-03 2004-12-21
CBERS HRC	Panchromatic Band (500 – 800 nm) Pixel Size = 2.7m	2008-11-04 (2 scenes) 2008-11-30 (2 scenes)	
SRTM	DEM	2000-02	
Aerial Videography	True Color RGB Image Pixel Sixe ~1m	1996-06	
Aerial Photography	Analog True Color 1:15000	1997-03	

Chapter 3 – Assessment of two biomass estimation methods for aquatic vegetation growing on the Amazon Floodplain[1].

3.1 Abstract

Aquatic macrophytes are an important component of carbon dynamics on the Amazon floodplain. These plants have short life cycles that respond to variations in the flooding conditions, and often have high net primary productivity. Studies of macrophyte productivity in the Amazon region are limited by accessibility and costs; hence, they may suffer from reduced sample size and representativity. The present study compares a phenometric (indirect) method and a sub-sampling (direct) method in terms of accuracy and applicability to estimation of aquatic macrophyte biomass in the Amazon. The results show that phenometric models were not as effective as selective sub-sampling for the estimation of macrophyte biomass under the studied conditions. Phenometric models performed more acceptably for predicting emergent biomass, and less for submerged and total biomass. Species-specific phenometric models were able to slightly improve accuracy, but phenotypic variation across the studied region was large enough to preclude the generalization of phenometric relationships into accurate numeric models, while the direct sub-sampling method was able to account for this variation. Sub-sampling also allowed a significant reduction on the physical effort of biomass sampling, which directly translated into wider and more complete sampling. We suggest that direct sub-sampling presents the best trade-off between accuracy and coverage for macrophyte biomass measurement in the Amazon floodplain.

3.2 Introduction

Studies of macrophyte productivity in the Amazon floodplain are often limited by travel time, difficult accessibility and high costs due to the long distances and

[1] Submitted to *Aquatic Botany*

waterlogged nature of the floodplain environment. The consequence is reduced sample effort and/or incomplete data sets, limiting both the quantity and quality of the obtained data, notably the spatial and temporal representativity of the samples (Vis et al., 2003).

In addition, the significant volume of living plant mass (up to 40 kg m^{-2} of fresh biomass) makes manual harvesting of Amazonian macrophytes an energy- and time-consuming activity, making it especially difficult to obtain the necessary amount of material to accurately estimate plant biomass and productivity.

Techniques for determining the net primary productivity (NPP) of aquatic plants include direct biomass sampling (Costa, 2005; Junk and Piedade, 1993a; Downing and Anderson, 1985), indirect phenometric estimation (also known as morphometric or allometric) (Daoust and Childers, 1998; Leeuw et al., 1996; Hopkinson et al., 1980), measurements of plant gas exchange (Piedade et al., 1994; Fisher and Carpenter, 1976,) and measurement of carbon uptake through eddy covariance systems (Morison et al., 2000, Oechel et al., 2000).

Direct measurements of biomass are usually employed because of the easier computation method and lesser degree of error introduction. However, these methods prevent continuous monitoring of the same plant stands, and might introduce greater spatial variability from the necessity of sampling different plots each time (Dai and Wiegert, 1996). Indirect methods, in contrast, offer the ability to continuously monitor growth and phenology on the same individuals and can reduce the effort involved in biomass harvesting, but depend on the existence of strong relationships between the predictor variables and plant biomass (Daoust and Childers, 1998). Also, many authors emphasize that different methods of measuring and calculating NPP from biomass

measurements can lead to varying results (Sala et al., 1988; Linthurst and Reimold, 1978).

In attempting to deal with the sampling limitations imposed by the environment, biomass and productivity studies in the Amazon have employed different sampling and measurement methods (Engle et al., 2007; Costa, 2004; Morison et al., 2000; Piedade et al., 1994; Piedade et al.,1991). These variations can limit the comparability of results between different studies, and an effort towards standardization of the sampling techniques is desirable in order to assure consistency.

The present paper addresses the issues of biomass sampling and estimation in the Amazon floodplain conditions by: (1) comparing two biomass estimation techniques, one based on phenometric measurements (indirect method) and other on selective sub-sampling (direct method), in terms of accuracy and appropriateness of each method to the study of Amazonian macrophytes; and (2) providing suggestions and guidelines towards the standardization of sampling methodology for Amazon aquatic herbaceous vegetation.

3.3 Methods

3.3.1 Biomass Estimation Methods

Biomass per square meter ($\hat{B}$) was estimated by multiplying the average biomass per stem ($\overline{B}_i$) in quadrat q by the number of stems per square meter in quadrat q ($D_{(q)}$), similar to the method used by Piedade et al. (1991):

$$\hat{B} = \frac{1}{q}\sum_{q=1}^{3}(\overline{B}_{i(q)} \times D_{(q)}) \qquad \text{(Eq. 3.1)}$$

Separate values were calculated for emergent ($\hat{B}_e$) and submerged ($\hat{B}_s$) biomass, and total biomass was calculated as $\hat{B}_t = \hat{B}_e + \hat{B}_s$.

Average biomass per individual **(** $\overline{B}_i$**)** was obtained by using two different methods, which are the main focus of the present paper. The first method, hereby called the *sub-sampling* method, consisted of directly determining $\overline{B}_i$ from the partial samples:

$$\overline{B}_{i(q)} = (B_{p(q)})/(I_{(q)}) \qquad \text{(Eq. 3.2)}$$

where $I_{(q)}$ is the number of stems harvested for biomass in the 10% sample in quadrat *q*, and $B_{p(q)}$ is the biomass of the 10% sample in quadrat *q*.

The second method, called the *phenometric* method, consisted of establishing multiple regression models to predict individual biomass ($\hat{B}_i$) from the morphological measurements, and then indirectly calculating $\hat{B}$ as stated in equation Eq. 3.1, using $\hat{B}_i$ instead of $\overline{B}_i$.

The morphological variables evaluated for phenometric modeling were Stem Length, Stem Diameter, Number of Leaves, Leaf Length, and Leaf Width. Depth was also included as an additional potential explanatory variable for biomass. Besides these, two additional combined variables were computed to provide simplified models and minimize colinearity between predictors:

1. *Stem Volume* - computed as a cylindrical volume ($V_{stem} = L_{stem} \times 0.25 \times \pi \times D_{stem}^2$, where L_{stem} is the length of the stem, and D_{stem} is the average Stem Diameter). Emergent, Submerged and Total Values were calculated separately.

2. *Total Leaf Area* - computed as the sum of the areas of a triangle ($A_{leaf} = \sum_{i=0}^{n_{leaf}} (0.5 \times L_{leaf} \times W_{leaf})$, where L_{leaf} is the average Leaf Length, W_{leaf} is the average Leaf Width and n_{leaf} is the total number of leaves). The triangle was considered as the shape that better approximated the leaf shape of the studied species.

The Pearson's Correlation Coefficient (*r*) for all pairs of selected variables was used in a first step to quantify the expected degree of association between morphological traits and biomass and to highlight possible colinearity between predictors. The correlation analysis was performed for all available data pooled together, as well as individually for each of the five main species occurring at the study site.

Phenometric models were fitted by multiple linear regression, with three models adjusted separately for emergent, submerged and total biomass. In addition, two sets of variables were used to fit each model; the first including the original variables considered relevant to the prediction of biomass in each compartment (*extended* model), and the second including only the respective combined variables (*combined* model). The final number of models equalled 2 sets (extended and combined) × 3 biomass compartments (emergent, submerged, total) (Table 3.1). After the initial adjustment, models were simplified when necessary by re-adjustment after the removal of non-significant predictors ($p > 0.05$).

To evaluate the influence of interspecific variability in biomass predictions, the same two sets of models were also fitted exclusively to the data observed for

Hymenachne amplexicaulis and *Paspalum fasciculatum*, the only two species for which sample sizes were deemed sufficient to satisfactorily model the relationship between the predictors and plant biomass. Analyses of the species-specific models were identical to the ones performed for the pooled data model.

Table 3.1: Original and simplified multiple regression models for macrophyte biomass estimation in Monte Alegre Lake (Amazon, Brazil). (*E, S, T*) = Emergent, Submerged, Total; (*SL*, *SD*, *SV*) = Stem Length, Stem Diameter, Stem Volume; (*LL*, *LW*, *NL*, *TLA*) = Leaf Length, Leaf Width, Number of Leaves, Total Leaf Area; *Dp* = Depth.

Emergent Biomass		Initial Model	Adjusted Model
All Spp.	Extended	$\hat{B}_i = \mathrm{f}(ESL, ESD, LL, LW, NL)$	$\hat{B}_i = \mathrm{f}(ESL, ESD, LL, NL)$
	Combined	$\hat{B}_i = \mathrm{f}(ESV, TLA)$	$\hat{B}_i = \mathrm{f}(ESV, TLA)$ a
H. amplexicaulis	Extended	$\hat{B}_i = \mathrm{f}(ESL, ESD, LL, LW, NL)$	$\hat{B}_i = \mathrm{f}(ESL, ESD, LL, LW, NL)$ [a]
	Combined	$\hat{B}_i = \mathrm{f}(ESV, TLA)$	$\hat{B}_i = \mathrm{f}(ESV)$
P. fasciculatum	Extended	$\hat{B}_i = \mathrm{f}(ESL, ESD, LL, LW, NL)$	$\hat{B}_i = \mathrm{f}(ESL, LL, LW, NL)$
	Combined	$\hat{B}_i = \mathrm{f}(ESV, TLA)$	$\hat{B}_i = \mathrm{f}(ESV)$
Submerged Biomass			
All Spp.	Extended	$\hat{B}_i = \mathrm{f}(SSL, SSD, Dp)$	$\hat{B}_i = \mathrm{f}(SSL, SSD, Dp)$ [a]
	Combined	$\hat{B}_i = \mathrm{f}(SSV, Dp)$	$\hat{B}_i = \mathrm{f}(SSV)$
H. amplexicaulis	Extended	$\hat{B}_i = \mathrm{f}(SSL, SSD, Dp)$	$\hat{B}_i = \mathrm{f}(SSD, Dp)$
	Combined	$\hat{B}_i = \mathrm{f}(SSV, Dp)$	$\hat{B}_i = \mathrm{f}(SSV)$
P. fasciculatum	Extended	$\hat{B}_i = \mathrm{f}(SSL, SSD, Dp)$	$\hat{B}_i = \mathrm{f}(SSL, Dp)$
	Combined	$\hat{B}_i = \mathrm{f}(SSV, Dp)$	$\hat{B}_i = \mathrm{f}(SSV)$
Total Biomass			
All Spp.	Extended	$\hat{B}_i = \mathrm{f}(TSL, TSD, LL, LW, NL, Dp)$	$\hat{B}_i = \mathrm{f}(TSL, TSD, LW, NL, Dp)$
	Combined	$\hat{B}_i = \mathrm{f}(TSV, TLA, Dp)$	$\hat{B}_i = \mathrm{f}(TSV, TLA)$
H. amplexicaulis	Extended	$\hat{B}_i = \mathrm{f}(TSL, TSD, LL, LW, NL, Dp)$	$\hat{B}_i = \mathrm{f}(TSD, LL, LW, NL)$
	Combined	$\hat{B}_i = \mathrm{f}(TSV, TLA, Dp)$	$\hat{B}_i = \mathrm{f}(TSV, TLA)$
P. fasciculatum	Extended	$\hat{B}_i = \mathrm{f}(TSL, TSD, LL, LW, NL, Dp)$	$\hat{B}_i = \mathrm{f}(TSL, LL, LW, Dp)$
	Combined	$\hat{B}_i = \mathrm{f}(TSV, TLA, Dp)$	$\hat{B}_i = \mathrm{f}(TSV, TLA, Dp)$ [a]

[a] No variables excluded from the original model.

Model fit was assessed by the Coefficient of Determination (R^2) and by the Root Mean Square Error (RMSE), which indicates the average deviation between observed and predicted values:

$$RMSE = \sqrt{\frac{1}{N}\sum_{n=1}^{N}(\hat{B}_{pred} - B_{obs})^2} \qquad \text{(Eq. 3.3)}$$

Model robustness was assessed by the calculation of confidence intervals for R^2, RMSE and model coefficients through bootstrap sampling. This method is based on the generation of multiple bootstrap samples, obtained by resampling the original data set with replacement, and using this new sample to re-compute the statistics of interest. The process is repeated many times, and thus a probability distribution of the statistics of interest can be obtained, from where confidence intervals can be drawn (Efron and Tibshirani, 1986). A total of ten thousand bootstrap samples were used to generate the model parameter distributions, and the confidence intervals were calculated by simply taking the ($\alpha = 0.025$, $1 - \alpha$) percentiles of each generated distribution. All analyses were performed with R statistical software, version 2.7.0 (www.r-project.org).

3.3.2 Validation

Both methods were validated by using a simple linear regression of predicted versus observed biomass values, the latter obtained from the CS samples. Agreement was evaluated in terms of R^2 and RMSE values, as well as by the closeness of the regression coefficients to an ideal 1:1 relationship. The same bootstrap technique was used to produce confidence intervals for the validation models.

3.4 Results

3.4.1 Descriptive Analysis

The main species found at the study site were *Hymenachne amplexicaulis* (Rudge) Nees (Poales:Poaceae) (*n* = 112) and *Paspalum fasciculatum* Willd. ex Flueggé (Poales:Poaceae) (*n* = 88), which dominated over about two thirds of the data set (Figure 3.1). These species usually formed dense and extensive stands, covering hundreds of square meters. Other species, such as *Oryza perennis* Moench (Poales:Poaceae) (*n* = 19), *Paspalum repens* auct. non Berg. (Poales:Poaceae) (*n* = 13) and *Echinochloa polystachya* (Kunth) Hitchc. (Poales:Poaceae) (*n* = 13) were mostly restricted to areas with specific environmental conditions, (*e.g.,* strong currents and steeper banks for *E. polystachya* and high influx of river water for *P. fasciculatum*).

The average phenometric characteristics of each of the main species are presented in Table 3.2. Stem density was usually high in all cases, ranging from about 80 stems m^{-2} to more than 400 stems m^{-2} during initial establishment phases of *O. perennis*. Larger densities were consistently attained by species with smaller stem diameter.

Plant length and diameter was similar for most species, in the vicinity of 2.0 - 2.5 m total length (about 0.6 m emergent), and a diameter of 0.5 cm. *E. polystachya* represented an exception due to its larger size, averaging a total length of more than 3 meters with 1 meter or more being emergent, and a diameter of about 1 cm. The number of leaves for all species ranged mostly between 4 and 8, and leaf length and width were

about 20 – 30 cm and 1 – 2 cm respectively, with *E. polystachya* exhibiting considerably longer leaves (70 cm).

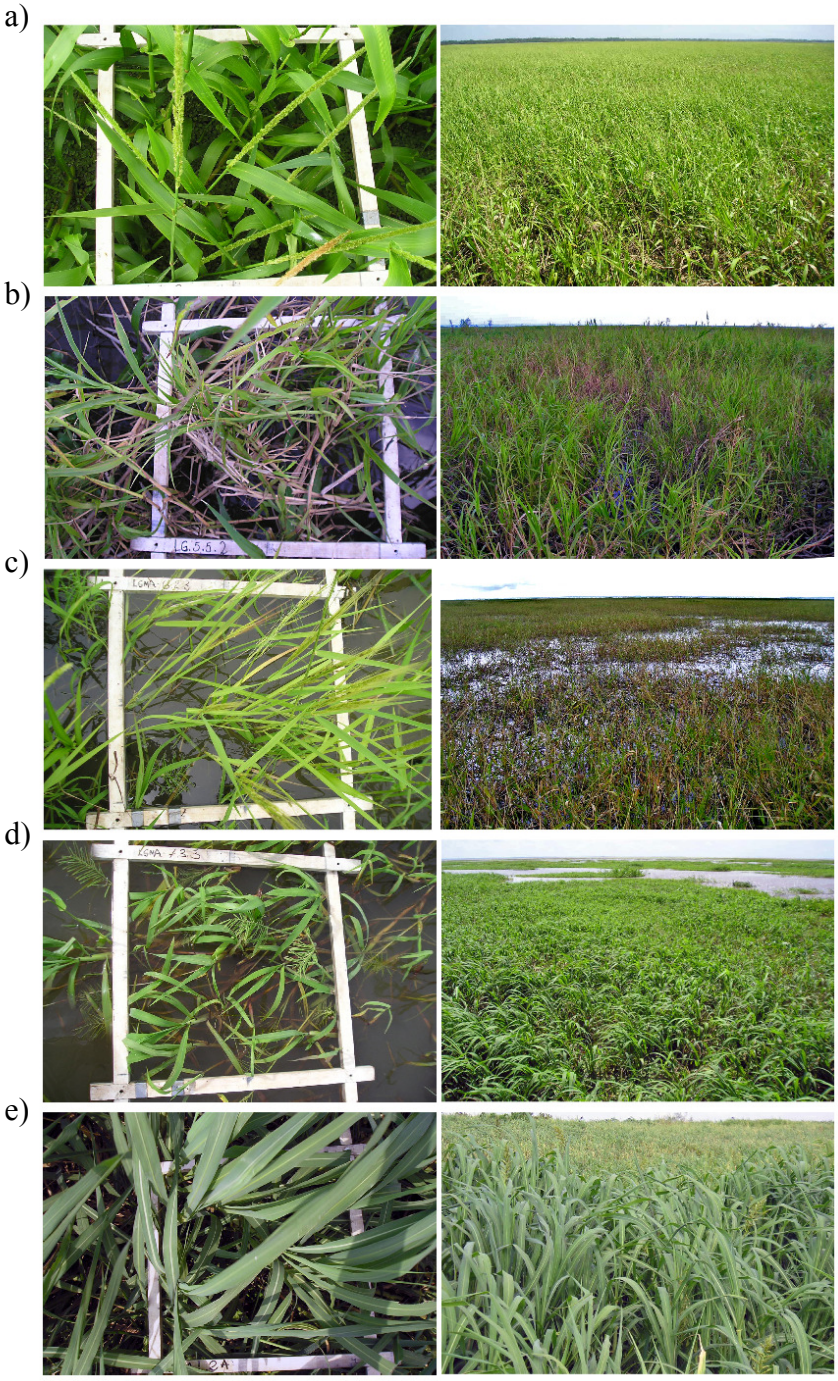

Figure 3.1- Main species found at the study site. From top to bottom, close-up and stand pictures of: a) *Hymenachne amplexicaulis*, b) *Paspalum fasciculatum*, c) *Oryza perennis*, d) *Paspalum repens* and e) *Echinochloa polystachya*.

3.4.2 Correlation Analysis

For the pooled data (*i.e.,* all species together), correlation analysis revealed that stem and leaf variables were both highly correlated with emergent biomass measurements (Table 3.3). Emergent Stem Length showed the highest correlation coefficient ($r = 0.82$, $p < 0.05$), followed by Leaf Length ($r = 0.76$, $p < 0.05$) and Emergent Stem Diameter ($r = 0.69$, $p < 0.05$). The use of combined variables (Emergent Stem Volume and Total Leaf Area) was able to improve these coefficients, both achieving the highest observed values ($r = 0.87$ and $r = 0.85$ respectively, $p < 0.05$).

For submerged biomass, Submerged Stem Length and Diameter showed the highest correlation values, with $r = 0.61$ and $r = 0.67$ respectively ($p < 0.05$). The use of Submerged Stem Volume improved the correlation to $r = 0.75$ ($p < 0.05$). Depth did not exhibit a high correlation with submerged biomass ($r = 0.38$, $p < 0.05$). Total Stem Diameter and Total Stem Length also had the highest correlations with total biomass measurements, at $r = 0.67$ ($p < 0.05$) and $r = 0.59$ ($p < 0.05$) respectively. For the combined variables, correlation coefficients were $r = 0.76$ ($p < 0.05$) for Total Stem Volume, and $r = 0.50$ ($p < 0.05$) for Total Leaf Area.

Table 3.2: Mean and Standard Deviation values for the phenometric variables collected at Monte Alegre Lake (Amazon, Brazil).

Variable	All sp.	*H. amplexicaulis*	*P. fasciculatum*	*O. perennis*	*P. repens*	*E. polystachya*
Density (ind./m^2)	202.24 ± 216.46	238.21 ± 212.91	112.84 ± 62.07	403.32 ± 395.04	190.46 ± 134.01	78.46 ± 25.76
Depth (cm)	104.97 ± 91.44	145.25 ± 91.76	52.57 ± 58.2	141.89 ± 72.42	146.31 ± 92.21	105.31 ± 100.69
Em. Stem Length (cm)	69.37 ± 39.83	68.28 ± 27.58	69.47 ± 44.08	60.96 ± 11.01	67.3 ± 23.74	150.18 ± 45.08
Sub. Stem Length (cm)	144.21 ± 107.47	191.15 ± 77.91	92.07 ± 94.51	184.59 ± 80.86	167.85 ± 91.96	207.95 ± 194.88
Tot. Stem Length (cm)	221.36 ± 115.86	262.73 ± 91.7	164.22 ± 85.53	273.21 ± 41.34	232.92 ± 91.92	358.13 ± 196
Em. Stem Diameter (cm)	0.55 ± 0.26	0.54 ± 0.21	0.54 ± 0.16	0.36 ± 0.17	0.77 ± 0.26	1.12 ± 0.27
Sub. Stem Diameter (cm)	0.54 ± 0.36	0.62 ± 0.3	0.46 ± 0.36	0.46 ± 0.25	0.64 ± 0.31	0.75 ± 0.63
Tot. Stem Diameter (cm)	0.55 ± 0.27	0.59 ± 0.24	0.5 ± 0.19	0.42 ± 0.21	0.67 ± 0.23	0.93 ± 0.43
Number of Leaves	5.39 ± 2.6	4.08 ± 0.94	7.28 ± 2.89	3.86 ± 1.38	5.56 ± 2.08	7.08 ± 1.82
Leaf Length (cm)	26.6 ± 17.2	20.08 ± 8.24	29.6 ± 16.12	21.67 ± 9.69	38.26 ± 13.42	70.31 ± 16.01
Leaf Width (cm)	1.37 ± 0.71	1.66 ± 0.82	1.13 ± 0.34	0.81 ± 0.19	1.37 ± 0.38	1.99 ± 0.42
Em. Stem Volume (cm^3)	27.13 ± 44.39	20.96 ± 24.92	20.69 ± 21.9	7.68 ± 6.05	38.63 ± 27.85	163.32 ± 102.99
Sub. Stem Volume (cm^3)	68.02 ± 97.75	79.1 ± 68.47	42.3 ± 51.13	48.76 ± 81.76	68.84 ± 49.46	263.25 ± 280.96
Tot. Stem Volume (cm^3)	84.4 ± 128.95	90.79 ± 78.47	45.41 ± 49.19	51 ± 58.82	98.66 ± 66.89	392.54 ± 382.83
Tot. Leaf Area (cm^3)	127.65 ± 172.77	78.03 ± 72.12	150.16 ± 158.2	30.23 ± 11.9	158.9 ± 92.77	544.16 ± 305.68
N (emergent)	265	113	88	19	18	13
N (submerged)	273	114	91	22	13	13
N (total)	258	112	88	19	13	13

Table 3.3: Correlation coefficients for macrophyte dry biomass (g/ind.) and phenometric variables measured at Monte Alegre Lake (Amazon, Brazil). Em. = Emergent, Sub. = Submerged, *H. amplex.* = *Hymenachne amplexicaulis*, *P. fascic.* = *Paspalum fasciculatum*, *O. peren.* = *Oryza perennis*, *P. Rep.* = *Paspalum repens* and *E. poly.* = *Echinochloa polystachya*. Values in bold correspond to $p < 0.05$.

Variables	All Spp.	*H. amplex.*	*P. fascic.*	*O. peren.*	*P. rep.*	*E .poly.*
Emergent Biomass						
Em. Stem Length (cm)	**0.82**	**0.82**	**0.81**	**0.72**	**0.83**	**0.79**
Em. Stem Diameter (cm)	**0.69**	**0.73**	**0.66**	**0.49**	**0.62**	**0.74**
N. of Leaves	**0.58**	**0.46**	**0.78**	0.19	**0.50**	**0.88**
Leaf Width (cm)	**0.42**	**0.73**	**0.50**	0.32	**0.53**	**0.83**
Leaf Length (cm)	**0.76**	**0.47**	**0.68**	0.12	**0.61**	**0.87**
Em. Stem Volume (cm^3)	**0.87**	**0.91**	**0.86**	**0.61**	**0.79**	**0.88**
Total Leaf Area (cm^2)	**0.85**	**0.80**	**0.82**	**0.58**	**0.81**	**0.94**
Submerged Biomass						
Depth (cm)	**0.38**	**0.27**	**0.79**	**0.68**	**0.64**	0.81
Sub. Stem Length (cm)	**0.61**	**0.43**	**0.90**	**0.80**	0.60	**0.93**
Sub. Stem Diameter (cm)	**0.67**	**0.76**	**0.71**	**0.68**	0.20	0.83
Sub. Stem Volume (cm^3)	**0.75**	**0.82**	**0.84**	**0.72**	0.27	**0.93**
Total Biomass						
Depth (cm)	**0.24**	**0.12**	**0.68**	**0.47**	**0.62**	**0.73**
Total Stem Length (cm)	**0.59**	**0.43**	**0.87**	**0.79**	**0.66**	**0.95**
Total Stem Diameter (cm)	**0.67**	**0.74**	**0.66**	**0.74**	0.27	**0.84**
N. of Leaves	**0.35**	**0.36**	0.19	0.22	0.06	0.41
Leaf Width (cm)	**0.37**	**0.65**	0.15	0.30	0.48	**0.58**
Leaf Length (cm)	**0.41**	**0.39**	-0.13	-0.01	-0.00	**0.73**
Total Stem Volume (cm^3)	**0.76**	**0.79**	**0.78**	**0.81**	0.38	**0.93**
Total Leaf Area (cm^2)	**0.50**	**0.65**	0.08	**0.50**	0.22	**0.61**

For the species-specific relationships, emergent biomass was best correlated with Emergent Stem Length, ranging from $r = 0.72$ to $r = 0.83$ ($p < 0.05$), the only exception being *E. polystachya* with its highest correlation against Number of Leaves ($r = 0.88$, $p < 0.05$). Emergent Stem Diameter was seldom included among the variables with highest coefficients. Submerged Stem Length had the highest correlation to submerged biomass of *P. fasciculatum* ($r = 0.90$, $p < 0.05$), *E. polystachya* ($r = 0.93$, $p < 0.05$), and *O. perennis* ($r = 0.80$, $p < 0.05$), while Submerged Stem Diameter had the highest correlation for *H. amplexicaulis* ($r = 0.76$, $p < 0.05$). Depth was well correlated to the submerged biomass of all species ($r > 0.6$) except *H. amplexicaulis* ($r = 0.27$, $p < 0.05$) . As this species represents about 42 percent of the entire data set, it explains the lower correlation also observed for the pooled data.

Total Stem Length had the best correlation with total biomass for *E. polystachya* ($r = 0.95$, $p < 0.05$), *P. repens* ($r = 0.66$, $p < 0.05$), *P. fasciculatum* ($r = 0.87$, $p < 0.05$), and *O. perennis* ($r = 0.79$, $p < 0.05$), while Total Stem Diameter had the highest correlation to *H. amplexicaulis* total biomass ($r = 0.74$, $p < 0.05$). Depth was fairly well correlated with total biomass for most species except *O. perennis* ($r = 0.47$, $p < 0.05$) and *H. amplexicaulis* ($r = 0.12$, $p < 0.05$). The use of combined variables improved the correlation coefficients in many cases (Table 3.3).

Due to the small sample sizes available for *O. perennis*, *P. repens* and *E. polystachya*, correlation results for these species should be interpreted only as general indicators of possible relations. Further sampling would be required to properly quantify these relationships, and for this reason these species were not subjected to any further modeling analysis.

3.4.3 Phenometric Model Building and Adjustment

Most of the multivariate regression models fitted initially produced non-significant coefficients ($p > 0.05$) for variables that exhibited lower correlation coefficients or redundancy (colinearity). Thus, the extended and combined models were simplified into the models described in Table 3.1. The removal of non-significant variables had no noticeable impact on regression parameters, and simplification led to univariate regression models for the emergent and submerged species-specific combined models.

The results of model fitting after simplification are summarized in Table 3.4. The fit from extended and combined models were generally similar. Confidence intervals for R^2 and *RMSE* between extended and combined models did not reveal significant differences in any cases (*i.e.*, the intervals had a large overlap).

3.4.4 Validation

The validation results are presented in Table 3.5. Validation was performed for the direct calculations from the sub-sampling method and for the values predicted by the phenometric models. Only the species-specific models for emergent biomass of *H. amplexicaulis* and *P. fasciculatum* were validated, as limited sample sizes prevented proper validation of the remaining species-specific cases.

Table 3.4: Statistics and coefficients for phenometric models of macrophyte biomass from Monte Alegre Lake (Amazon, Brazil). *(E, S, T)* = Emergent, Submerged, Total; (*SL, SD, SV*) = Stem Length, Stem Diameter, Stem Volume; (*LL, LW, NL, TLA*) = Leaf Length, Leaf Width, Number of Leaves, Total Leaf Area; *Dp* = Depth. P0.025 and P0.975 = 95% confidence interval limits for model parameters. CV = coefficient of variation for model parameters. % Sig = percentage of bootstrap samples resulting in significant parameters.

	Extended Model						Combined Model				
	P0.025	**Median**	P0.975	CV	% Sig.		P0.025	**Median**	P0.975	CV	% Sig.
Emergent – All species											
R^2	0.72	**0.77**	0.82	0.14	-	R^2	0.73	**0.83**	0.89	0.19	-
RMSE	1.63	**1.95**	2.22	0.30	-	RMSE	1.34	**1.70**	2.07	0.43	-
Intercept	-6.23	**-5.24**	-4.15	-0.40	100.00	Intercept	-0.13	**0.19**	0.47	3.16	31.65
ESL	0.03	**0.05**	0.06	0.49	100.00	*ESV*	0.02	**0.05**	0.07	1.10	99.26
ESD	2.12	**3.68**	5.37	0.88	99.85	*TLA*	0.01	**0.01**	0.02	1.50	100.00
LL	0.00	**0.04**	0.06	1.47	74.15						
NL	0.21	**0.36**	0.47	0.73	99.67						
Emergent – H. amplexicaulis											
R^2	0.78	**0.84**	0.89	0.14	-	R^2	0.71	**0.83**	0.90	0.23	-
RMSE	0.56	**0.69**	0.81	0.36	-	RMSE	0.61	**0.71**	0.82	0.29	-
Intercept	-2.87	**-2.18**	-1.56	-0.60	100.00	Intercept	0.38	**0.54**	0.70	0.58	100.00
ESL	0.03	**0.04**	0.05	0.47	100.00	*ESV*	0.06	**0.07**	0.07	0.23	100.00
ESD	2.23	**4.20**	5.86	0.87	99.86						
LL	0.06	**0.53**	1.07	1.92	75.40						
NL	-0.11	**-0.08**	-0.05	-0.89	99.94						
Emergent – P. fasciculatum											
R^2	0.77	**0.84**	0.91	0.16	-	R^2	0.61	**0.75**	0.85	0.31	-
RMSE	1.08	**1.58**	2.08	0.63	-	RMSE	1.54	**1.99**	2.44	0.45	-
Intercept	-10.09	**-5.51**	-4.61	-0.99	100.00	Intercept	-0.53	**-0.10**	0.31	-8.12	2.12
ESL	0.03	**0.07**	0.09	0.92	99.06	*ESV*	0.13	**0.16**	0.19	0.35	100.00
LL	1.66	**3.86**	6.67	1.30	99.55						
LW	0.39	**0.60**	0.91	0.87	99.69						
NL	-0.16	**-0.10**	-0.01	-1.57	77.93						
Submerged – All Species											
R^2	0.47	**0.54**	0.61	0.27	-	R^2	0.43	**0.56**	0.70	0.48	-
RMSE	6.92	**8.34**	9.74	0.34	-	RMSE	6.72	**8.04**	9.29	0.32	-
Intercept	-4.20	**-2.77**	-1.72	-0.89	99.71	Intercept	1.34	**2.34**	3.27	0.83	99.45
SSL	0.04	**0.07**	0.10	0.81	100.00	*SSV*	0.08	**0.10**	0.12	0.39	100.00
SSD	11.51	**15.31**	19.42	0.52	100.00						
Dp	-0.08	**-0.06**	-0.04	-0.82	99.95						
Submerged – H. amplexicaulis											
R^2	0.52	**0.62**	0.73	0.33	-	R^2	0.59	**0.69**	0.80	0.30	-
RMSE	2.98	**4.75**	6.55	0.75	-	RMSE	2.81	**4.20**	5.64	0.67	-
Intercept	-3.62	**-1.84**	-0.70	-1.59	68.49	Intercept	-1.40	**0.42**	1.85	7.80	28.61
SSD	14.64	**19.04**	24.17	0.50	100.00	*SSV*	0.07	**0.09**	0.13	0.66	100.00
Dp	-0.02	**-0.01**	-0.01	-1.21	82.96						

Table 3.4 (continued). Statistics and coefficients for the phenometric models of macrophyte biomass at Monte Alegre Lake, Amazon, Brazil, 2004. (*E, S, T*) = Emergent, Submerged, Total; (*SL, SD, SV*) = Stem Length, Stem Diameter, Stem Volume; (*LL, LW, NL, TLA*) = Leaf Length, Width, Number of Leaves, Total Leaf Area; *Dp* = Depth. P0.025 and P0.975 = 95% confidence interval limits for model parameters. CV = coefficient of variation for model parameters. % Sig = percentage of bootstrap samples resulting in significant parameters.

	Extended Model						Combined Model				
	P0.025	**Median**	P0.975	CV	% Sig.		P0.025	**Median**	P0.975	CV	% Sig.
Submerged – P. fasciculatum											
R^2	0.75	**0.84**	0.91	0.19	-	R^2	0.52	**0.72**	0.93	0.56	-
RMSE	3.97	**5.58**	7.19	0.58	-	RMSE	3.88	**7.29**	9.69	0.80	-
Intercept	-1.63	**-0.80**	-0.10	-1.91	2.85	Intercept	-0.02	**1.61**	3.38	2.11	28.79
SSL	0.07	**0.19**	0.25	0.97	99.79	*SSV*	0.17	**0.24**	0.31	0.58	100.00
Dp	-0.19	**-0.09**	0.12	-3.43	68.64						
Total - All Species											
R^2	0.52	**0.62**	0.70	0.30	-	R^2	0.41	**0.59**	0.73	0.53	-
RMSE	7.70	**9.16**	10.54	0.31	-	RMSE	7.99	**9.51**	10.98	0.31	-
Intercept	-21.38	**-16.25**	-12.02	-0.58	100.00	Intercept	2.78	**4.49**	6.09	0.74	100.00
TSL	0.04	**0.06**	0.09	0.71	100.00	*TSV*	0.07	**0.08**	0.10	0.40	100.00
TSD	22.03	**29.02**	37.52	0.53	100.00	*TLA*	0.00	**0.01**	0.02	2.00	57.47
LW	0.81	**1.31**	1.93	0.86	99.86						
NL	-5.89	**-3.10**	-0.50	-1.74	75.12						
Dp	-0.06	**-0.04**	-0.02	-1.16	92.34						
Total – H. amplexicaulis											
R^2	0.56	**0.69**	0.83	0.39	-	R^2	0.55	**0.66**	0.78	0.35	-
RMSE	2.97	**5.02**	7.21	0.84	-	RMSE	3.41	**5.23**	6.98	0.68	-
Intercept	-19.09	**-13.60**	-8.67	-0.77	100.00	Intercept	-0.53	**1.61**	3.06	2.23	52.32
TSD	17.99	**25.04**	31.86	0.55	100.00	*TSV*	0.08	**0.12**	0.15	0.62	100.00
LL	1.13	**3.58**	6.76	1.57	76.75	*TLA*	-0.05	**-0.03**	0.00	-2.04	44.10
LW	1.33	**2.34**	3.29	0.84	97.95						
NL	-0.56	**-0.33**	-0.15	-1.23	86.54						
Total – P. fasciculatum											
R^2	0.73	**0.83**	0.90	0.21	-	R^2	0.41	**0.69**	0.91	0.73	-
RMSE	4.36	**6.07**	7.82	0.57	-	RMSE	4.32	**8.11**	11.16	0.84	-
Intercept	-20.02	**-10.81**	0.99	-1.94	77.24	Intercept	-3.43	**0.88**	5.54	10.21	19.17
TSL	0.10	**0.19**	0.25	0.82	100.00	*TSV*	0.06	**0.15**	0.24	1.23	95.79
LL	-0.50	**-0.25**	0.01	-2.02	73.89	*TLA*	0.00	**0.02**	0.03	1.50	58.43
LW	-8.24	**6.75**	18.31	3.93	55.06	*Dp*	0.01	**0.11**	0.20	1.72	81.95
Dp	-0.20	**-0.08**	0.09	-3.74	61.12						

The results indicate a high degree of agreement between estimated and observed data for emergent biomass estimated through the sub-sampling method, with R^2 and *RMSE* values of 0.86 (0.82, 0.88) and 136.7 g/m^2 (123.1, 150.9) respectively (values in parentheses represent the ($\alpha = 0.025$, 1- α) confidence interval limits obtained from the

bootstrap method) (Figure 3.2). Good agreement was also observed for total biomass (R^2 = 0.90 (0.87, 0.93), albeit with a larger variance margin (*RMSE* = 286.9 g/m^2 (242.8, 329.6)), while estimation of submerged biomass had a lower agreement (R^2 = 0.71 (0.61, 0.80) , *RMSE* = 355.1 g/m^2 (295.6, 408.47), Figure 3.3).

For the phenometric method, lesser agreement was observed for all cases. R^2 values ranged from a minimum of 0.15 (0.04, 0.32) to a maximum of 0.79 (0.75, 0.83), and RMSE for estimated emergent biomass ranged from 117.5 g/m^2 (110.5, 124.7) to 571.8 g/m^2 (438.9, 681.8) (Figure 3.2). Submerged biomass RMSE varied between 730.4 g/m^2 (667.1, 786.3) and 884.5 g/m^2 (631.3, 1076.3) for the extended and combined models respectively, and RMSE for total biomass ranged from 1388.8 g/m^2 (1135.3, 1622.1) to 2512.8 g/m^2 (1067.8, 3341.5) for the combined and extended model respectively (Figure 3.3).

Intercept coefficients for the validation models (β_0) were significantly different from zero ($\alpha = 0.05$) on less than 15% of the bootstrap samples for the sub-sampling method. Slope (β_1) parameters were significant in more than 90 percent of the cases, approaching the unity value at 0.94 - 1.15 for emergent, 0.62 - 1.81 for submerged and 0.91 - 1.35 for total biomass. Values and distribution of model coefficients were similar for *Hymenachne amplexicaulis* and *Paspalum fasciculatum* (Table 3.5).

The validation regression coefficients for the phenometric method validation indicated a poorer fit between predicted and observed biomass values than observed for the sub-sampling method (Table 3.5). Intercepts were significantly different from zero on 27 to 97 percent of the bootstrap samples, with the exception of some models for

emergent biomass (< 19% were significant). Slope coefficients were significant in more than 90 percent of the cases, with values ranging between -0.85 and 5.43.

Table 3.5: Regression coefficients and significance for validation of phenometric and direct estimations of macrophyte biomass at Monte Alegre Lake (Amazon, Brazil). *H. amp.* = *Hymenachne amplexicaulis*, *P. fas.* = *Paspalum fasciculatum*.

Validation Model	Intercept	% Sig.	Slope	% Sig.	*N*
Phenometric					
Emergent Extended - All	-90.83 (-501.02, 183.68)	18.9	1.26 (0.76, 2.11)	100	58
Emergent Combined - All	98.74 (34.68, 160.26)	70.7	0.81 (0.68, 0.99)	100	58
Submerged Extended - All	592.73 (83.40, 1299.72)	51.8	1.06 (0.42, 1.84)	90.6	8
Submerged Combined - All	741.41 (-59.17, 1228.79)	33.9	0.94 (0.36, 2.43)	56.8	8
Total Extended - All	-1780.14 (-4587.62, 324.07)	53	2.71 (1.14, 5.44)	99.9	19
Total Combined - All	1495.91 (577.12, 2511.28)	96.8	0.43 (-0.86, 1.32)	36.8	19
Emergent Extended - *H. amp.*	-168.76 (-328.96, -37.57)	66.7	1.62 (1.26, 2.01)	100	27
Emergent Combined - *H. amp.*	75.24 (-46.15, 157.45)	26.9	0.80 (0.55, 1.07)	100	27
Emergent Extended - *P. fas.*	22.15 (-103.88, 193.31)	0.9	1.06 (0.44, 1.31)	95.4	17
Emergent Combined - *P. fas.*	93.13 (-63.40, 298.76)	1.5	1.04 (0.56, 1.46)	95.2	17
Sub-sampling					
Emergent - All	-11.35 (-51.87, 26.49)	0.8	1.02 (0.94, 1.15)	100	58
Submerged - All	43.87 (-323.71, 514.85)	8.5	1.09 (0.62, 1.81)	89.9	8
Total - All	-67.03 (-220.51, 99.09	6.9	1.18 (0.90, 1.38)	100	20
Emergent - *H. amp.*	-108.92 (-276.17, -29.39)	14.4	1.37 (1.04, 1.74)	100	27
Emergent - P. *fas.*	- 34.01 (-109.52, 32.01)	1.71	1.03 (0.75, 1.17)	99.9	17

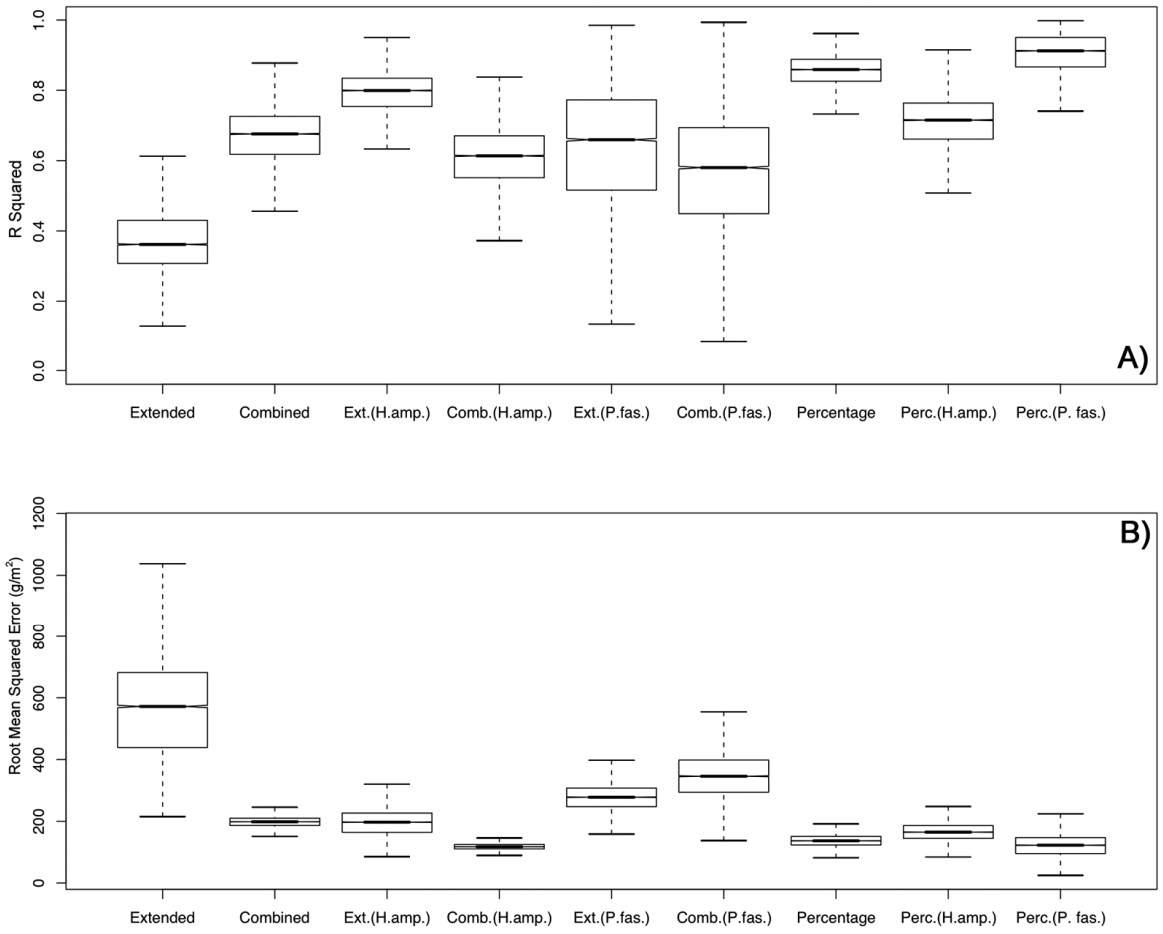

Figure 3.2: Bootstrap distributions of A) R^2 and B) *RMSE* for the phenometric and sub-sampling methods, for estimation of emergent macrophyte biomass at Monte Alegre Lake (Amazon, Brazil).

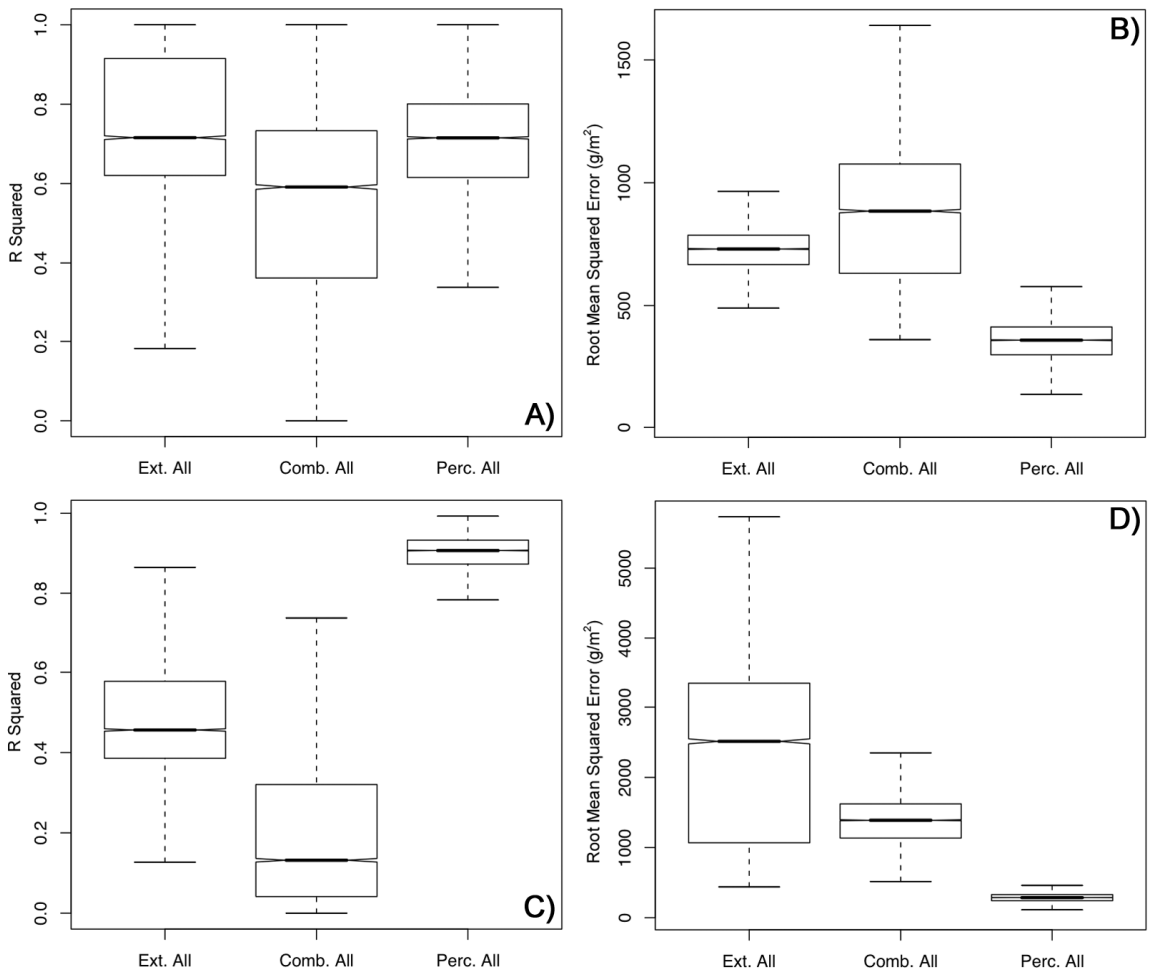

Figure 3.3: Bootstrap distributions of R^2 and *RMSE* for the phenometric and sub-sampling methods, for estimation of (A and B) submerged and (C and D) total macrophyte biomass at Monte Alegre Lake (Amazon, Brazil).

3.5 Discussion

3.5.1 Phenometric Analysis and Modeling

The prevalence of *H. amplexicaulis* and *P. fasciculatum* seems to be a natural characteristic of Monte Alegre Lake, which differs from the *Echinochloa polystachya* dominated macrophyte stands observed on studies carried on the middle Amazon region

(Engle et al., 2008; Junk and Piedade, 1993a; Piedade et al., 1991). Limnological conditions in Monte Alegre and other lower Amazon lakes differ from those observed in the upstream, region, with the former exhibiting significantly larger lakes. Also, differences in physical attributes such as littoral exposure, currents and general circulation, as well as substrate erosion and sedimentation are likely to result in alternative species distributions (Junk, 1997).

Most phenometric variables had strong correlation with plant biomass. Stem variables (Length, Diameter, Volume) had the strongest relationships as the stem constitutes about 70 to 80 percent of plant living mass in Amazonian macrophytes (Piedade et al., 1991). The combination of related variables into single predictors also seemed to better capture the relationship between morphology and biomass, resulting in increased correlation coefficients in many cases. Morphological variability among species was evidenced by the correlation coefficients obtained for species-specific analysis, which were overall higher than for the pooled analysis. In addition, diverging variables reached the highest correlations for each individual species, such as Stem Length for *P. fasciculatum* versus Stem Diameter for *H. amplexicaulis* (submerged biomass, Table 3.3). As much as the grass-like vegetation of the Amazon floodplain tends to a similar morphology, differences in habitats and life history of each species are likely to modulate the phenometric relationships. *Paspalum repens*, for example, detaches itself from the substratum and forms floating mats, exhibiting a significant amount of lateral modular growth, while *H. amplexicaulis*, *P. fasciculatum* or *E. polystachya* remain mostly rooted to the substratum and show individual vertical growth (Junk ,1997; Junk and Piedade, 1993b; Piedade et al., 1991).

The weak correlation between depth and stem length observed for *H. amplexicaulis* can be explained by the differences between plant growth and water level change: during rising water, wetland plants invest heavily in stem elongation to prevent submersion, while later in the season investment can be shifted towards stem thickening and growth of adventitious roots (Vartapetian and Jackson, 1997); during falling water, biomass loss happens at a slower rate than the decrease in river stage. Also, the fact that *H. amplexicaulis* is widely distributed across the lake would imply in populations subjected to variable flooding and general environmental conditions (controlled by local hydrography, pedology and geomorphology), affecting in turn the growth patterns of each population.

The process of model simplification reinforced the fact that the biomass of different species can be better explained by different morphological factors, as the final choice of variables changed when considering each species individually. Variable elimination also highlighted the main morphological factors determining biomass in general, with some parameters being included ubiquitously in almost all models (Stem Length, Stem Volume, Depth).

3.5.2 Comparison of Methods

The sub-sampling method produced equal or better estimations than the phenometric method in all evaluated cases (Table 3.5). In general, predictions were more accurate for emergent biomass, less so for total biomass and the least accurate for submerged biomass values in both cases. Such differences, however, can to some extent be attributed to the differences in sample sizes among biomass components.

In the sub-sampling method, non-significant intercept coefficients and unitary slope coefficients for the validation models indicated a close approach to a 1:1 relationship, showing that this method closely predicted real biomass values (Figure 3.4). The agreement was inferior for the submerged component, with a tendency to overestimate large values. For the phenometric models, regression lines exhibited a much more pronounced deviation from the 1:1 relationship, often resulting in overestimation of high values and underestimation of small values (Figure 3.4).

The comparison between the combined and extended phenometric models revealed that combined models produced lower or similar errors in most cases, despite R^2 values being higher for the extended models (Figures 3.2 and 3.3). As R^2 always increases with the addition of variables while not necessarily implying better performance, the combination of variables into compound values improved the results of phenometric biomass estimation (Figure 3.4c).

The better performance of the sub-sampling method can be attributed to its lesser susceptibility to inter and intraspecific variation, as each calculation considers only the individuals living close together in the sampled quadrat. The phenometric method, on the other hand, depends on a generalization of the phenometric relationships across various species and populations subjected to diverging biotic and abiotic conditions, which will tend to exhibit phenotypical variability. The detrimental effect of variability in the phenometric approach is demonstrated by the slight increase in explanatory power for species-specific versus pooled data models.

This same variability in phenometric relationships has been demonstrated for phenometric modeling of different species: Gouraud et al. (2008) required specific

models for different populations of *Schoenoplectus maritimus* (L.) Lye in different years, related to variations in water level and topography across an area of about 50 km^2. The same was observed by Morris and Haskin (1990) for *Spartina alterniflora* Loisel. and by Daoust and Childers (1998) for various species, in areas smaller than 25 km^2, and Miao et al. (2008) observed phenometric changes in leaves of *Cladium jamaicense* Crantz. and *Typha domingensis* Pers. along an 8 km P enrichment gradient. Given the very large extent of the sampled area in the present study (over 1600 km^2), it is likely that environmental conditions such as depth, substrate quality, nutrient availability, littoral exposure and other factors vary to a great extent, thus reducing the explanatory power of phenometric models.

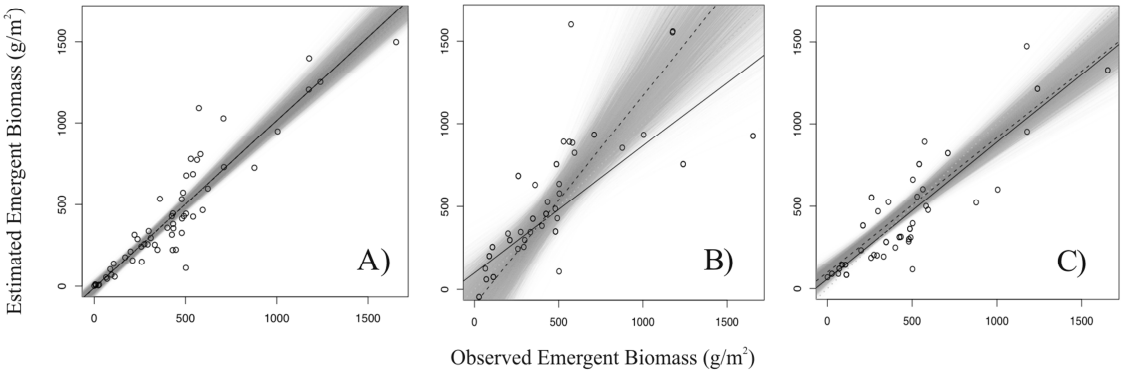

Figure 3.4: Scatter plots of observed versus estimated emergent pooled dry macrophyte biomass at Monte Alegre Lake (Amazon, Brazil). A) Sub-sampling Method, B) Phenometric Extended Model, C) Phenometric Combined Model. Solid black lines represent the regression line obtained from a single regression using all data pairs, dashed lines represent the median slope and intercept obtained from the bootstrap distributions of regression parameters. Shaded areas indicate the distribution of regression lines obtained from each bootstrap sample, *i.e.* the degree of certainty about the true regression line.

Chapter 4 – Annual net primary production of macrophytes in the eastern Amazon floodplain[2]

4.1 Abstract

Aquatic herbaceous macrophytes contribute significantly to the carbon input in the Amazon floodplain. These plants have large seasonal variations in areal coverage and high productivity. The present study estimates annual net primary production (NPP) of aquatic herbaceous macrophytes in a large lake on the eastern Amazon floodplain, assesses the sources and amount of uncertainty associated with these measures, and offers a comparison among the estimates of herbaceous macrophyte productivity in the Amazon region. Plant biomass accumulated during the rising water stage of the annual flood cycle, peaking at 2300 – 6100 g m^{-2} and decreasing later in the year. Annual net primary production was estimated to range from 2400 – 3500 g m^{-2} yr^{-1}, with above water production between 650 – 1100 g m^{-2} yr^{-1}, and below water production between 1700 – 2600 g m^{-2} yr^{-1}. *Echinochloa polystachya* and *Paspalum fasciculatum* were the most productive species, followed by *Paspalum repens*, *Hymenachne amplexicaulis,* and *Oryza perennis*. The four main sources of uncertainty in the estimates were macrophyte taxa, location, sampling design, and lack of measurements of dead material loss.

4.2 Introduction

Net primary productivity (NPP) is one of the basic parameters that characterize an ecosystem, as it defines the maximum amount of resource available for all the consumer organisms (Etherington, 1983). In terms of total dry weight, wetland NPP variation is

[2] Published in *Wetlands* 29(2): 747–758, 2009.

within the range of 600 to 2000 g m^{-2} yr^{-1} (Mitsch and Gosselink, 2000). Modeled values of carbon fixation for wetlands range from 45 to 820 g C m^{-2} yr^{-1}, with lower values associated with arctic bogs, and the highest with tropical swamps (Cao et al., 1996). The mean NPP for world's wetlands is around 1300 g C m^{-2} yr^{-1} (Schlesinger, 1997), placing wetland environments among the most productive ecosystems in the world (Keddy, 2000; Schlesinger, 1997). The total carbon pool trapped in wetland vegetation biomass is estimated to be near 7.8 PgC, roughly 1.4% of the total global vegetation (Schlesinger, 1997).

The amount of photosynthetic fixation in wetlands is a function of the energy input (light and temperature), but above all of the nutrient limitation exhibited by these ecosystems. In some wetlands, the influxes of water bring a continuous amount of nutrients to the system, and the relaxation of limiting pressures allow high rates of biomass production (Costa, 2005; Keddy, 2000; Junk and Piedade, 1997). On the other hand, ecosystems such as northern wetlands tend to have very low productivity, being subjected to low temperatures and light availability, short growth season and poor nutrient recycling (Wrona et al., 2005; Schlesinger, 1997; Gorham 1991).

Previous studies of macrophyte net primary productivity in the Amazon floodplain have revealed very high productivity rates, emphasizing the importance of macrophyte contributions to the total input of carbon in the floodplain system. Most of these studies, however, have been restricted to small lakes (< 50 km^2) and clustered around the city of Manaus, in the central portion of the Amazon floodplain. Moreover, the uncertainties associated with these measurements have seldom been evaluated in an explicit manner.

Given that the total extent of the Amazon floodplain bordering is about 900,000 km^2 in area and has considerable intra- and interannual variations in flood extent, as well a high degree of spatial ecological heterogeneity (Hess et al., 2003; Rosenqvist et al., 2002; Sippel et al., 1998), such limitations largely restrain the ability to capture the effects of environmental variability on productivity, and reduce the degree of confidence associated with current extrapolations of these measurements to regional scales.

Our study addresses the aforementioned shortcomings by 1) measuring annual net primary production (NPP) of aquatic herbaceous macrophytes in a large floodplain lake system (> 1000 km^2) representative of the eastern Amazon floodplain, 2) explicitly quantifying for the first time the uncertainty associated with these measures, and 3) offering a comprehensive comparison among the existing estimates of macrophyte NPP in the Amazon floodplain.

4.3 Methods

4.3.1 Net Primary Production Determination

Annual net primary production was estimated by the method of Milner and Hughes (1968), calculated as the sum of increments in average monthly biomass ($\Delta\overline{B}_i = \overline{B}_t - \overline{B}_{t-1}$) from one sampling time to the next, measured through the whole growing season (Equation 4.1). Biomass values were calculated according to the sub-sampling method (See Section 3.3).

$$NPP = \sum_{i=1}^{i} (\Delta\overline{B}_i) \quad \text{for all} \quad \Delta\overline{B}_i > 0 . \qquad \text{(Eq. 4.1)}$$

Total net primary production was calculated by determining the emergent and submerged NPP estimates separately and then summing the values at the end of the calculations ($NPP_{(t)} = NPP_{(e)} + NPP_{(s)}$). As our study did not include measurements of dead biomass loss, this element was not directly incorporated into NPP calculations. Instead, production values were adjusted *a posteriori* based on contributions of dead biomass loss previously reported in the literature (Table 4.3). All productivity values reported were rounded to the nearest multiple of 10.

The uncertainty of the NPP estimates was assessed using randomized bootstrap resampling. The method is based on the generation of multiple bootstrap samples, resampling the original data set with replacement, and using each new sample to re-compute the estimator of interest (i.e., NPP). By repeating this process many times, an approximate distribution of the estimator can be obtained (Efron and Tibshirani, 1986). For the present study, 10,000 bootstrap samples were used, and a bootstrapped NPP estimation was calculated by taking the mean value of the generated NPP distribution. In addition, confidence intervals were calculated by taking the 2.5 and 97.5% percentiles of the generated distribution (Manly, 2001; Efron and Tibshirani ,1986). The relationships between macrophyte growth and water depth were assessed through Pearson's correlation coefficients. All calculations and statistical analysis were performed with R statistical software, version 2.7.0 (http://www.r-project.org/).

The influence of macrophyte taxa and growth location as sources of uncertainty on NPP estimates was evaluated by separately computing production and confidence intervals from subsets of the original data. For individual species, NPP values were calculated using only samples where each of the five main occurring species was

dominant. To assess spatial variation, NPP was determined separately for samples belonging to each of the main sampling sites (G1–G7) (Figure 2.1). Furthermore, to reduce the effect of species variation among sites, the same calculations were performed on subsets restricted by both site and dominant species. Only locations where sample size and temporal coverage were deemed representative were analyzed, and thus not all possible combinations of species vs. site could be assessed. Bootstrapped NPP calculations for taxa and site-specific NPP were performed in the same manner as for the entire data set.

4.4 Results

4.4.1 Growth and Biomass

Macrophytes rapidly increased stem length during the initial flooding phase, with the plants usually achieving most of their maximum emergent length within the first three months, and further additions to plant growth being observed mostly in submerged parts (Figures 4.1 and 4.2). For most species, total elongation rates followed the rate of depth increase during the beginning of the flooding season, and then progressively slowed until reaching a stable peak of 300 cm between March and July, coinciding with high water levels.

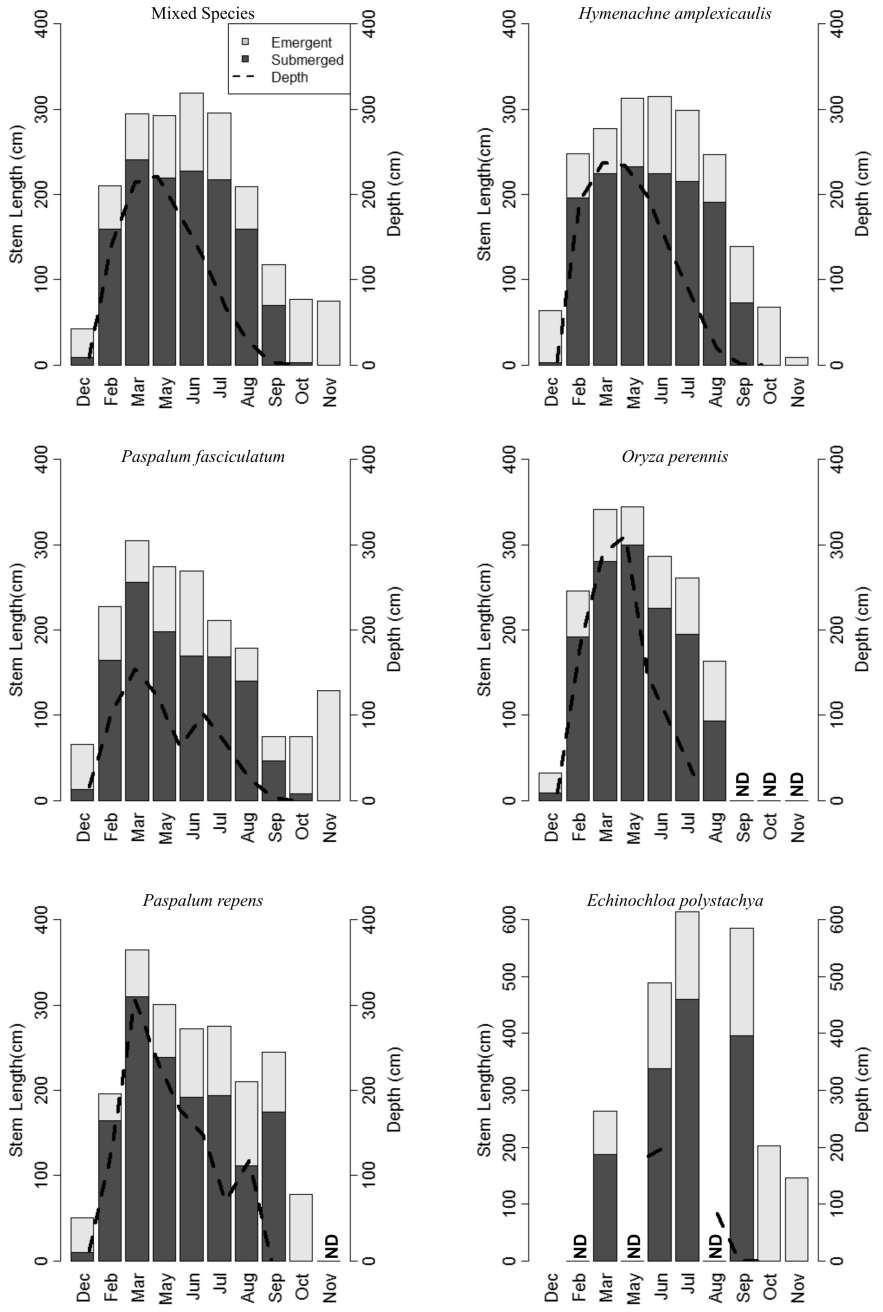

Figure 4.1: Depth and emergent and submerged stem length of pooled and individual dominant macrophyte species at Monte Alegre Lake (Amazon, Brazil). Depth curves for each graph are derived from the subsets of depth samples associated with each species. Note the different scale used for *E. polystachya*. ND = no data.

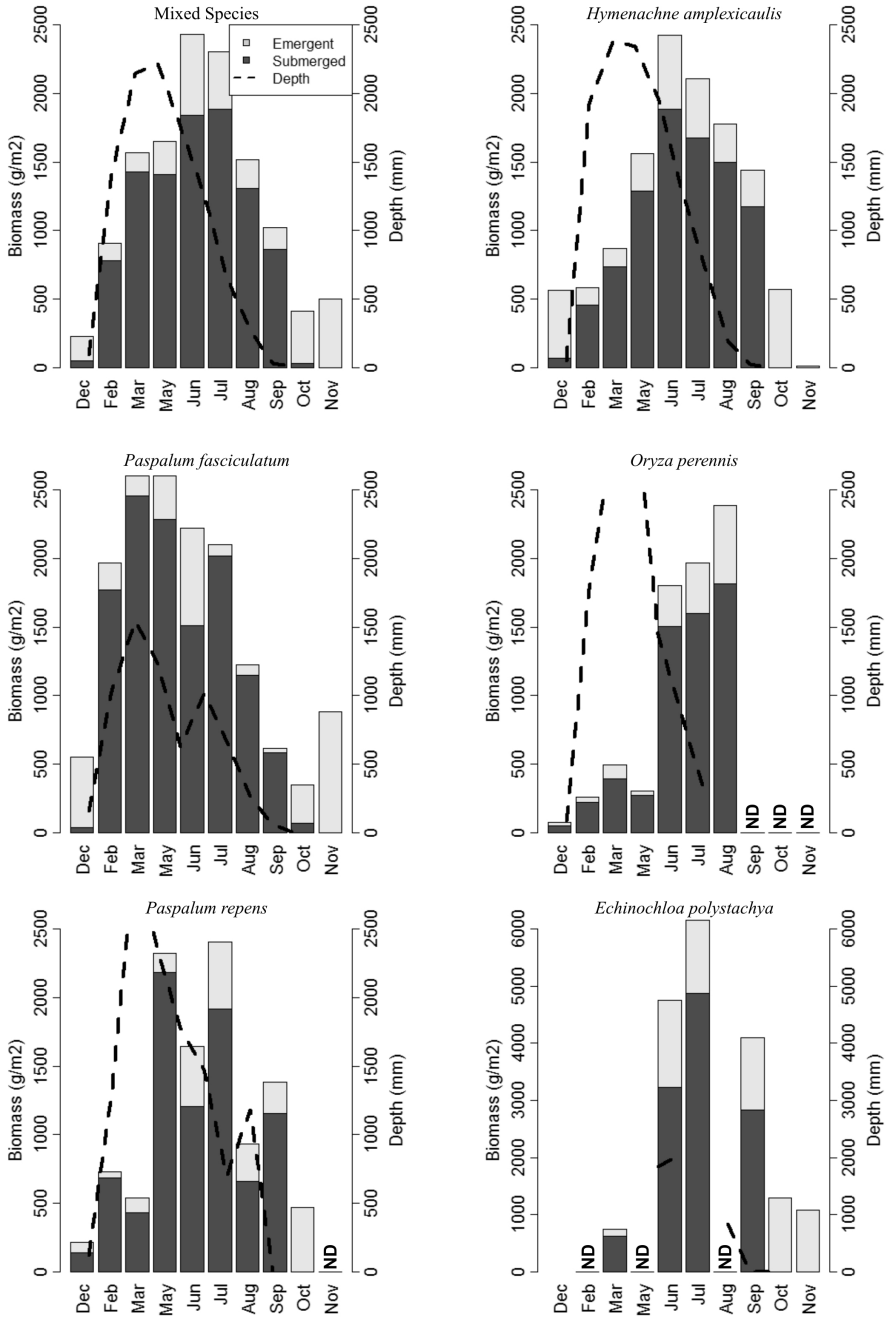

Figure 4.2: Depth and emergent and submerged biomass of pooled and dominant macrophyte species in Monte Alegre Lake (Amazon, Brazil). Depth curves for each graph are derived from the subsets of depth samples associated with each species. Note the different scale used for *E. polystachya.* ND = no data.

Submerged stem length was strongly correlated to depth, ranging between r = 0.90 and r = 0.97 ($p < 0.05$) for all species except *E. polystachya*, which had r = 0.78 ($p < 0.05$). No significant correlation was observed between stem length and depth for the emergent component of any species. However, total stem length (submerged + emergent) was still correlated with depth for all species, ranging between r = 0.65 to 0.92 ($p < 0.05$).

Paspalum fasciculatum and *P. repens* had the earliest peak growth (March), while *E. polystachya* continued to grow until late in the season, reaching a maximum length of about 600 cm during early August (Figure 4.1). The lowest lengths were registered around November and December, when most of the substratum became exposed. The number of stem nodes followed a similar trend for all species, rising from about 5 to 10 nodes during low water to 20 to 30 nodes during high water.

Average stem diameter ranged between 0.22 and 0.74 cm and reached a maximum value early in the season (~1 cm for *E. polystachya* and ~0.6 cm for the remaining species). *Echinochloa polystachya* had the largest leaves, over 80 cm in length and 2.5 cm in width, as well as the highest average number of leaves (7). *Paspalum fasciculatum* had a maximum number of 20 leaves in June. For other species, leaf length was about 20 to 40 cm, and the number of leaves increased steadily with flooding, reaching an average maximum of 4 to 7 leaves during peak flooding. Most species had densities ranging from 50 to 200 individual stems per square meter, but maximum density reached values up to 500 to 600 stems m^{-2} (*O. perennis*, *P. repens*). A maximum of 1933 seedlings was observed in a newly developing patch of *H. amplexicaulis* in November 2004.

Biomass accrual rate initially followed the rise in water level, but kept increasing even after maximum flooding was reached, peaking around June for *E. polystachya*, *P. repens*, and *H. amplexicaulis*, and later for *O. perennis* and *P. fasciculatum* (Figure 4.2). Biomass values were similar for most species, with the exception of *E. polystachya*, which accumulated about twice the biomass of the other species. However, the correspondence between plant biomass and flood cycle, especially for the submerged component, was not in synchrony.

For the pooled species, Pearson's r correlation coefficients achieved maximum values when comparing submerged or total biomass with water depth from the preceding month ($r = 0.91$ and $r = 0.93$, respectively, $p < 0.05$). For *H. amplexicaulis* alone, the best correlation was achieved between submerged or total biomass and depth from two months earlier ($r = 0.89$ and $r = 0.92$, respectively, $p < 0.05$), while for *P. fasciculatum* the best correlation was found between submerged or total biomass and depth from the same month ($r = 0.97$ and $r = 0.91$, respectively, $p < 0.05$). For all tested species, no significant correlation was found between emergent biomass and depth regardless of time lag. Testing of correlation for *O. perennis*, *P. repens*, and *E. polystachya* was precluded by the incomplete time series available for these species.

4.4.2 Net Primary Production

Net primary production estimates of 2600 g m^{-2} yr^{-1} in dry mass were partitioned in approximately 30% (800 g m^{-2} yr^{-1}) as above water biomass, and the remaining two thirds (1800 g m^{-2} yr^{-1}) allocated to submerged plant material. The bootstrapped estimation of NPP resulted in slightly larger figures, totalling 2900 g m^{-2} yr^{-1} divided

between 900 g m^{-2} yr^{-1} emergent and 2000 g m^{-2} yr^{-1} submerged. Since the bootstrap method provides more robust estimates of NPP, only bootstrapped values are reported in the remainder of the text (simple field derived NPP calculations are provided in Table 4.1). In addition, as production is sometimes estimated as being equivalent to peak biomass (standing crop) (Linthurst and Reimold, 1978), peak seasonal values (highest average monthly biomass) are also reported, and the maximum biomass values observed in a single sample are included to demonstrate the maximum attainable biomass for each species.

4.4.3 Sources of NPP Uncertainty

Net primary production varied among species by a factor of 2.2. The highest annual values were observed for *E. polystachya* and *P. fasciculatum*, with a total NPP of 5300 g m^{-2} yr^{-1} (1500 g m^{-2} yr^{-1} emergent and 3800 g m^{-2} yr^{-1} submerged) and 4500 g m^{-2} yr^{-1} (1500 g m^{-2} yr^{-1} emergent and 3000 g m^{-2} yr^{-1} submerged), respectively. *Paspalum repens* was the third most productive species, with 3600 g m^{-2} yr^{-1} (600 g m^{-2} yr^{-1} emergent and 2300 g m^{-2} yr^{-1} submerged), and the remaining species (*H. amplexicaulis*, *O. perennis*) had productivity values, in the range of 2000 to 2500 g m^{-2} yr^{-1} (Table 4.1). Emergent NPP ranged from 17% (*P. repens*) to 33% (*P. fasciculatum*) of total production.

Net primary production among the seven main sites had a large range of variation. The highest NPP values were attained from samples collected at the G1 site, with 1700 g m^{-2} yr^{-1} emergent NPP, 3500 g m^{-2} yr^{-1} submerged NPP, and 5200 g m^{-2} yr^{-1} total biomass.

Table 4.1: Net primary production (g m^{-2} y^{-1}) of macrophyte species at Monte Alegre Lake (Amazon, Brazil). Maximum biomass was for a single plot, Peak biomass was a monthly average, NPP was calculated after Milner and Hughes (1968), and the Bootstrapped NPP was the average NPP value generated using 10000 bootstrap samples of the original data (C.I. = Confidence interval).

	Maximum Biomass	Peak Biomass	NPP	**Bootstrapped NPP**	Lower C.I.	Upper C.I.
All Species Pooled						
Emergent	1852	590	816	**869**	649	1096
Submerged	5009	1884	1822	**2017**	1695	2575
Total	6501	2430	2639	**2886**	2471	3487
Hymenachne amplexicaulis						
Emergent	1287	569	720	**753**	349	1358
Submerged	3706	1884	1814	**1820**	1309	2235
Total	4195	2427	2533	**2573**	1881	3363
Paspalum fasciculatum						
Emergent	1539	881	810	**1480**	1091	1805
Submerged	4830	2455	2923	**3049**	1409	4116
Total	5002	2601	3733	**4529**	2901	5632
Oryza perennis						
Emergent	573	573	417	**507**	311	632
Submerged	2560	1816	340	**1864**	1394	2415
Total	2986	2389	757	**2371**	1857	2946
Paspalum repens						
Emergent	728	492	443	**618**	347	929
Submerged	3555	2187	2635	**2996**	1369	5116
Total	3730	2409	3079	**3614**	1910	5789
Echinochloa polystachya						
Emergent	1852	1530	1443	**1549**	42	2242
Submerged	5009	4873	4250	**3777**	843	4596
Total	6501	6152	5694	**5326**	2218	6575

The lowest NPP values occurred in samples collected at the G7 site, with 200 g m^{-2} yr^{-1} emergent, 600 g m^{-2} yr^{-1} submerged, and 800 g m^{-2} yr^{-1} total NPP. The other sites had values ranging from 1000 to 1500 g m^{-2} yr^{-1} for emergent, 2500 to 4500 g m^{-2} yr^{-1} for submerged, and 3200 to 5700 g m^{-2} yr^{-1} for total NPP.

For the calculations of NPP constrained by site and species, emergent NPP of *H. amplexicaulis* ranged from 300 g m^{-2} yr^{-1} at G7 (n = 21) to 700 g m^{-2} yr^{-1} at G5 (n = 21), submerged NPP ranged between 600 g m^{-2} yr^{-1}at G1 (n= 7) and 2700 g m^{-2} yr^{-1} at G2 (n = 45), and total NPP ranged between 900 g m^{-2} yr^{-1} at G7 (n = 21) and 3400 g m^{-2} yr^{-1} at G2 (n = 45). For *P. fasciculatum*, emergent NPP ranged from 800 g m^{-2} yr^{-1} at G1 (n = 6) to 1500 g m^{-2} yr^{-1} at G3 (n = 24), submerged NPP ranged between 0 g m^{-2} yr^{-1}at G1 (n = 7) and 3500 g m^{-2} yr^{-1} at G3 (n = 45), and total NPP ranged between 800 g m^{-2} yr^{-1}at G1 (n = 7) and 5000 g m^{-2} yr^{-1} at G3 (n = 24). Small sample size influenced the zero value for *P. fasciculatum* because it increased the probability of bootstrap samples yielding zero net production.

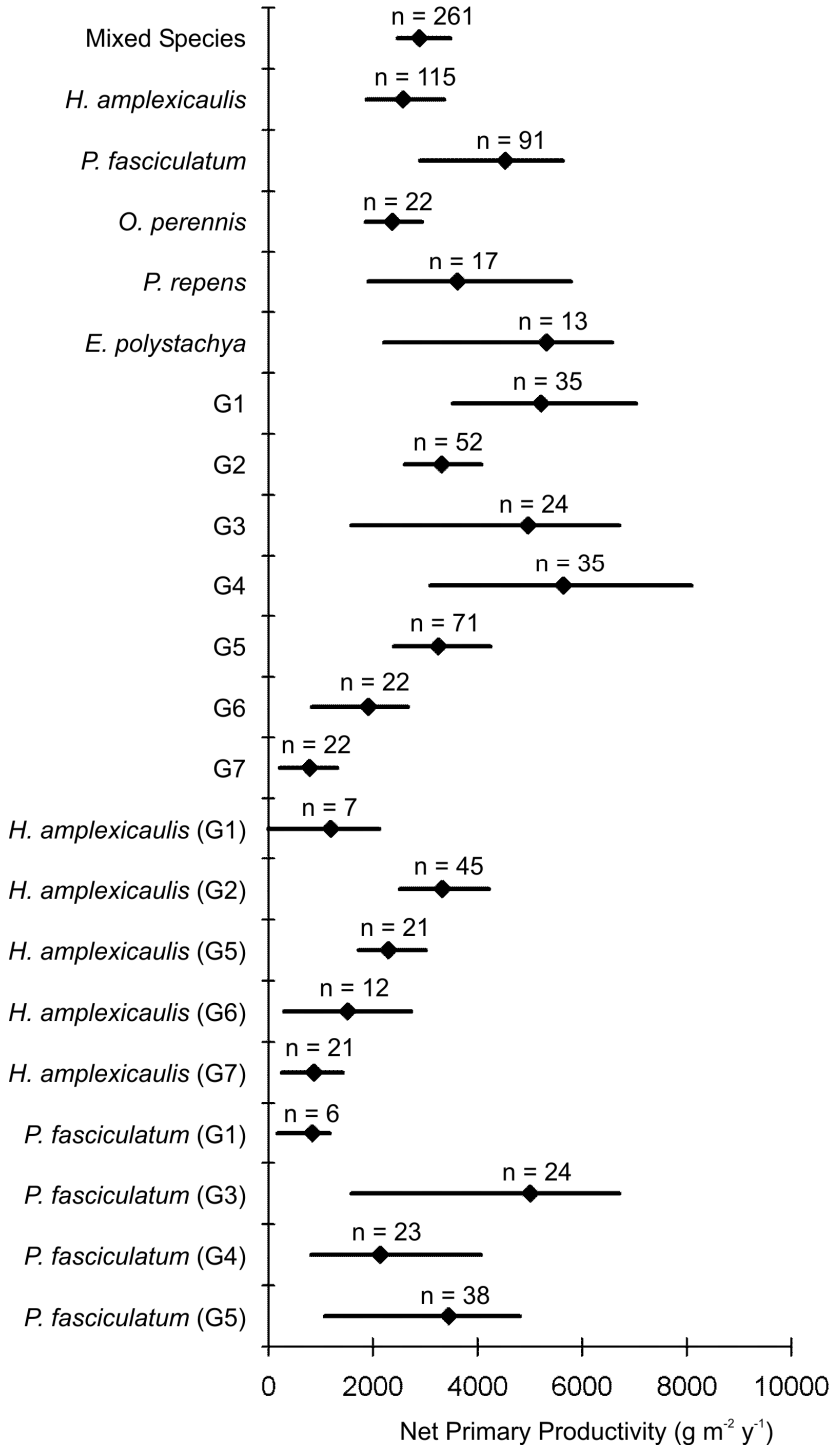

Figure 4.3: Graphical representation of average macrophyte NPP values and bootstrap confidence intervals calculated for pooled species, individual species, different sampling sites (G1–G7) and for the two main species (*Hymenachne amplexicaulis* and *Paspalum fasciculatum)* at each individual sampling site in Monte Alegre Lake (Amazon, Brazil).

4.5 Discussion

The differences in the timing of peak growth among different species suggest a temporal partition of resources among the species as also observed by Engle et al. (2008). Junk and Piedade (1993) note that such temporal partitioning of resources often implies higher overall primary production in the ecosystem, as different species can reach peak biomass values at unique times over the yearly cycle. The increase in number of stem nodes suggests that growth occurs mainly through the addition of new nodes, and less by internodal elongation (Piedade et al., 1991).

Overall NPP estimates for mixed species were within the range of values reported in other studies (Table 4.2). A difference was observed however from the estimates by Costa (2005) in the same study area. This difference might be explained by the combined effect of the smaller sample size utilized in the latter study (98 samples distributed among 5 collection dates), and by differences in duration and timing of the sampling in each of the studies (Table 4.2).

Net primary production variation among species reached up to 33% (coefficient of variation) in our study. *Echinochloa polystachya* and *Paspalum fasciculatum* attained the highest NPP values (4500–5500 g m^{-2} yr^{-1}), while *Hymenachne amplexicaulis* and *Oryza perennis* were slightly less productive (2000–3000 g m^{-2} yr^{-1}), with *Paspalum repens* in between (3500 g m^{-2} yr^{-1}). In addition, variations could be observed for all species when comparing our results to estimates obtained from studies at varying conditions and locations (Table 4.2).

Table 4.2: Comparison between Monte Alegre Lake (Amazon, Brazil) and published values of net primary production for Amazonian macrophytes at other locations (see Figure 1.1). Values in parenthesis represent 95% confidence intervals.

Source	Species	NPP (g m^{-2} yr^{-1})	Months Sampled (Period)
Present study	Mixed Population	2886 (2471–3487)	10 (Dec.–Nov.)
Junk and Piedade (1993)[a]	Mixed population 1*	1600 (1450–1750)	10 (Sep.–July)
Junk and Piedade (1993)[a]	Mixed population 2**	3000	10 (Sep.–July)
Marlier (1965)[b,c]	Mixed population***	5000	N. A.
Present Study	*Hymenachne amplexicaulis*	2573 (1881–3363)	10 (Dec.–Nov.)
Costa (2005)[a]	(field) *Hymenachne amplexicaulis*	3490	5 (Extrapolated
Costa (2005)[a]	(satellite) *Hymenachne amplexicaulis*	4553	linearly to 12)
Junk and Piedade (1997)[d]	*Hymenachne amplexicaulis*	2270 (2262–2278)	1 (April)
Present study	*Paspalum fasciculatum*	4529 (2901–5632)	10 (Dec.–Nov.)
Junk and Piedade (1993)[a]	*Paspalum fasciculatum*	7000	230 days
Junk and Howard-Williams (1984)[a,e]	*Paspalum fasciculatum*	3900	18 (Sep.–Feb.)
Present Study	*Oryza perennis*	2371 (1857–2946)	10 (Dec.–Nov.)
Engle et al. (2008)[a,d]	*Oryza perennis* (40% loss)	2660	12 (Across
Engle et al. (2008)[d]	*Oryza perennis*	1900 (1116–2684)	3 years)
Junk and Piedade (1993)[a]	*Oryza perennis*	2300–2700	5 (Nov.–Mar.)

Table 4.2 (Continued): Comparison between Monte Alegre Lake (Amazon, Brazil) and published values of net primary production for Amazonian macrophytes at other locations (see Figure 1.1). Values in parenthesis represent 95% confidence intervals.

Source	Species	NPP (g m^{-2} yr^{-1})	Months Sampled (Period)
Present Study	*Paspalum repens*	3614 (1910–5789)	10 (Dec.–Nov.)
Engle et al. (2008)[a,d]	*Paspalum repens* (40% loss)	5600	12 (Across
Engle et al. (2008)[d]	*Paspalum repens*	4000 (2628–5372)	3 years)
Junk and Piedade (1993)[a]	*Paspalum repens*	2500–3300	6 (Dec.–May/ Jan.–Jun.)
Junk (1970)[b]	*Paspalum repens*	600–800	N.A.
Present Study	*Echinochloa polystachya*	5326 (2218–6575)	10 (Dec.–Nov.)
Engle et al. (2008)[a,d]	*Echinochloa polystachya* (40% loss)	10220	12 (Across
Engle et al. (2008)[d]	*Echinochloa polystachya*	7300 (5982–8672)	3 years)
Morison et al. (2000)[f]	*Echinochloa polystachya*	8540	2 (High/Low Water)
Piedade et al. (1994)[g]	*Echinochloa polystachya*	8930	18 (July.–Dec.)
Piedade et al. (1991)	*Echinochloa polystachya*	9930 (8617–11243)	18 (July.–Dec.)
Long et al. (1989)[a,e]	*Echinochloa polystachya*	9925	
Long et al. (1989)[a]	*Echinochloa polystachya*	9425	12 (Sep.–Oct.)
Long et al. (1989)[e]	*Echinochloa polystachya*	8680	
Long et al. (1989)[h]	*Echinochloa polystachya*	6300	

[a] Method includes loss of dead biomass.

[b] No details about estimation method available.

[c] Value as reported in Junk (1970).

[d] Standing crop (peak biomass) only.

[e] Method includes root (belowground) biomass.

[f] Calculated by gas exchange/eddy covariance measurements.

[g] Calculated by leaf CO_2 exchange measurements.

[h] Method does not account for roots or loss of dead biomass.

[*] *O. perennis* and *P. repens* plus various Cyperaceae.

[**] *H. amplexicaulis* and *Aeschynomene sensitiva* plus various Gramineae and Cyperaceae.

[***] Undisclosed species, *Paspalum fasciculatum* dominated.

While the NPP of most individual species was within the ranges currently reported in the literature, peak biomass and net primary production of *E. polystachya* were lower than observed for previous studies (Table 4.2). Flood amplitude is much

larger at central portions of the Amazon floodplain, where the previous studies on *E. polystachya* have been carried, and thus likely explains the larger biomass observer for the species at this site.

Stem length and biomass appeared to be connected to flood dynamics, as most other abiotic factors remained fairly constant throughout the year due to the equatorial location (Irion et al., 1997). Photosynthetically available radiation (PAR) values can fluctuate seasonally due to cloud cover and aerosol concentrations, and greening has been observed for upland forested regions during dry seasons (Huete et al., 2006). Nevertheless, the range of annual PAR levels (1000 and 1500 µmols m^{-2} s^{-1}) approaches light saturation levels of macrophytes (Junk and Piedade, 1997; Piedade et al., 1994), and photosynthetic rates of Amazonian macrophytes have been shown to be limited by leaf carbon concentrations due to changes in stomatal conductance, with photosynthesis achieving near-optimal rates during the high water season (Piedade et al., 1994). Since seasonal variations of precipitation and evapotranspiration are both translated into flood dynamics and water levels (see summary in Irion et al., 1997) and an influx of nutrient-rich water is observed during the rising water phase (Forsberg et al., 1988), it is reasonable to assume that flooding is the main abiotic factor controlling the distribution, growth, and productivity of Amazonian macrophytes.

Table 4.3: Macrophyte NPP values (g dry mass m^{-2} y^{-1}) for Monte Alegre Lake (Amazon, Brazil), with a range of biomass loss rates published for Amazonian macrophytes

Species	Present estimate	+10% loss[a]	+25% loss[a]	+40% loss[b]	+ 40% loss[b] + 5% root biomass[c].
Mixed population	2886	3175	3608	4040	4242
Hymenachne amplexicaulis	2573	2831	3216	3602	3783
Paspalum fasciculatum	4529	4982	5661	6340	6657
Oryza perennis	2371	2608	2964	3319	3484
Paspalum repens	3614	3976	4518	5060	5313
Echinochloa polystachya	5326	5859	6658	7457	7830

[a]As estimated by Junk and Piedade (1993) and Piedade et al. (1991) by quantifying the amount of dead material present in biomass samples.

[b]As estimated by Engle et al. (2008) by the difference between measured and expected monthly biomass (calculated from measured daily growth rates).

[c]As reported by Junk and Piedade (1997).

Spatial variation in NPP was higher than 50% (coefficient of variation) for macrophyte communities at different sites, reaching a maximum of 62% for *P. fasciculatum* communities (Figure 4.3). These results suggest that local biotic and abiotic conditions result in significant differences in growth and biomass accumulation for macrophytes, even within different populations of the same species. Factors such as sediment quality and topography, water chemistry, turbulence, nutrient input, and intra and interspecific competition have all been demonstrated to influence plant establishment and growth (Junk and Piedade, 1997; Junk, 1970). In addition, anthropogenic pressure, mostly in the form of cattle grazing, can influence final productivity of macrophytes (Camarão et al., 2004; Ohly and Hund, 2000).

An observation of the spatial distribution of sampled sites at the landscape scale suggests some possible causes for environmental variation. Sites G6 and G7, which had the lowest NPP values, are located further from the Amazon river main stem, and thus likely to receive smaller nutrient inputs. In addition, site G1 is very close to the mouth of a few black-water creeks, and could suffer from dilution effects. Black-water rivers are notably absent of macrophyte growth, since the low nutrient concentrations and low pH strongly inhibit the growth of Amazonian macrophytes (Junk and Piedade, 1997; Junk and Piedade, 1993b).

Exposure and water velocity could also explain the reduction in NPP observed for sites G3 – G6, as can be readily observed by the eastward increasing return in the radar image caused by wind fetch and water roughness (Figure 2.1). Furthermore, interspecific competition could explain the low productivity observed for both *H. amplexicaulis* and *P. fasciculatum* at the G1 site, where *E. polystachya* populations are dominant and likely better adapted to the local environmental conditions. Further studies associating plant growth and distribution with variations in biotic and abiotic conditions are necessary to further elucidate their effect on macrophyte biomass and productivity.

Our results also demonstrate how sampling and choice of computation method can influence the degree of uncertainty and reliability of estimates. The bootstrap estimation method has shown that a fair degree of uncertainty and potential underestimation are associated with simple point estimations of NPP (Milner and Hughes, 1968). The bootstrapped NPP estimate resulted in a value at least 9% larger than the simple point estimate, and confidence interval limits estimated for total net primary

production in our study imply values 15% smaller or 23% higher than the estimated average.

The impact of uncertainty is evident when extrapolating the present values to the central Amazon floodplain. Assuming a macrophyte cover of 26,000 km^2 (Hess et al., 2003) and a carbon content of 50% (Melack and Forsberg, 2001), the NPP value of 2300 g m^{-2} y^{-1} implies on an annual macrophyte production of 29 TgC yr^{-1}. The use of the bootstrapped distribution of the NPP estimate increases this value to about 37 (95% confidence interval limits: 32–45) TgC yr^{-1}, and by further considering the previously reported 10%, 25%, and 45% biomass loss rates (Table 4.3), we could obtain 41 (35–50), 45 (39–54), and 54 (47–66) TgC yr^{-1}, respectively. Incorporating a 20% mapping error to the areal estimate (reasonable for large scale mapping) increases the uncertainty range to a final estimate of 54 (32–79) TgC yr^{-1}. This estimate brackets the macrophyte contribution to the central floodplain carbon budget suggested by Richey et al. (2002). Engle et al. (2008) report a much higher value of ~100 TgC yr^{-1} for macrophyte NPP in the same area, but their calculations integrated flooded woodland and mixed classes (from Hess et al. 2003), with flooded macrophytes, into a single flooded herbaceous class. Using this assumption, our estimate would be increased to 106 (63–155) TgC yr^{-1}.

Given a total outgassing estimate of 216 TgC yr^{-1} for the central Amazon floodplain (Richey et al., 2002), our estimates show that macrophytes could be responsible for fixing more than half of the total carbon lost to the atmosphere, as also suggested by Engle et al. (2008). Quay et al. (1992) calculated a 40% macrophyte contribution to the respired carbon in the Amazon floodplain based on the C4-originated fraction of the $^{13}\delta$C signature in the river mainstem. If C3 (e.g., *H. amplexicaulis)*

dominance observed at our study sites is the norm for eastern floodplain lakes, then an even higher percentage of macrophyte-originated carbon emissions could be expected for the Amazon region.

Seasonal partitioning of macrophyte phytomass accumulation and loss during the flooding season is likely to create a pulse of available nutrients and organic material (Piedade et al., 1997), which in turn could strongly affect ecological processes of the floodplain. Moreira-Turcq et al. (2003) report much larger seasonal changes in transport of total organic carbon (TOC) for white water rivers (main macrophyte habitats) than for black and clear water rivers, and a gain of 4 TgC yr^{-1} in the TOC exported through the Amazon mainstem originating from white water lakes in the floodplain.

Uncertainty associated with our estimates indicates the need for an integrative method to assess plant productivity on floodplains. Satellite and aerial imagery provide spatially continuous information to permit integration of spatial variability in biomass and mitigating problems of inadequate spatial coverage (Silva et al., 2008). Remotely sensed data are commonly used to estimate upland vegetation NPP (Houghton, 2003; Field et al., 1995), and can be used to estimate area and productivity of macrophytes on the Amazon floodplain (Silva et al., 2007a; Costa, 2005; Hess et al., 2003). Satellite-based techniques, however, do not address the second main source of uncertainty in estimates, inadequate measurements of dead material loss; few measurements of loss are available for Amazonian macrophytes. The development of a methodology for deriving macrophyte biomass from satellite data, associated with field sampling that includes measurements of dead biomass loss and is stratified to capture the main macrophyte

habitats and communities throughout the floodplain, would present the best approach to effectively reduce the uncertainty of scaling up macrophyte NPP to the whole floodplain.

Chapter 5 – Spatio-temporal variability of macrophyte cover and productivity in the Eastern Amazon floodplain: a remote sensing approach[3]

5.1 Abstract

The Amazon floodplain plays an important role in the Amazon system carbon budget. Floodplain ecology, biogeochemistry and vegetation zonation are mainly determined by the annual flooding cycle (flood pulse concept), and macrophytes (herbaceous aquatic vegetation) are the most susceptible to changes in flooding patterns. Quantification of macrophyte contribution to the floodplain carbon balance is hindered by intra and inter-annual variability of plant cover. The present study offers a new hierarchical, object oriented method for combining radar and optical image time series to characterize the evolution of seasonal macrophyte cover along a yearly flood cycle, for an eastern Amazon floodplain lake. Macrophyte cover varied between 104 – 198 km^2 for the mapped area, and exhibited significant changes both seasonally and inter-annually. Two distinct growth strategies have been observed: short-lived communities that thrive during low water periods, and year-long plant communities that are able to survive flooding. Although the majority of the macrophyte carbon fixation is derived from the latter, about 9% of macrophyte NPP can be attributed to the short-lived communities, which depend directly on the observed low water levels for a given year. The increased frequency of droughts predicted for the Amazon system can thus result in an increase in the macrophyte-derived carbon input in the Amazon floodplain system.

[3] Submitted to *Remote Sensing of Environment*

5.2 Introduction

Macrophytes production is one of the major sources of carbon input in the Amazon floodplain (Melack et al., in press (b)). These plants cover about 12% - 15% of the mainstem Amazon floodplain (Melack et al, in press (a)), but can dominate primary productivity in many areas due to their high productivity (Chapter 4; Engle et al., 2009; Costa, 2005; Piedade et al., 1991; Quay et al., 1992).

One important aspect unique to macrophytes is the remarkable spatial and temporal variability exhibited by plant stands across the floodplain environment. Because of their fast growth rates and rapid life cycles, macrophytes can quickly occupy newly exposed areas of substrate (Piedade et al., 1991). This variability in turn, can greatly affect the contribution of the plants to the ecological and biogeochemical processes in the Amazon floodplain.

Hess et al. (2003) used JERS-1 L band (HH) SAR imagery to produce floodplain cover maps at for the lowest and highest flooding conditions of the entire Amazon floodplain, showing a significant difference in the cover and distribution of macrophytes between seasons. Melack et al. (in press (a)) further analysed these results by dividing the main floodplain into five geomorphic sub-units, which revealed a progressive increase in the extent of macrophyte cover from the easternmost unit (110 km^2) towards the confluence of the Amazon and Tapajós river (4910 km^2), the farthest reach of the Amazon free from tidal influence.

At a finer scale, Costa (2004) used a combination of Radarsat-1 C-band (HH) and JERS-1 L-band (HH) to produce macrophyte cover maps of a lake system in the eastern floodplain region over five different stages along the flooding cycle, and Silva et al. (2007a) have shown that MODIS imagery offered an acceptable trade-off between spatial and temporal resolution for mapping macrophyte cover in the floodplain. Both studies have reinforced the aspect of macrophyte cover variability along the seasonal cycle, and its connection to water level variation and flooding conditions.

The usefulness of multitemporal image series to map and characterize time series has been long acknowledged in the field of agricultural remote sensing (Quegan et al., 2000; Le Toan et al., 1997; Nemani and Running, 1997), and has been successfully applied to the study of wetland environments (Townsend et al., 2001; Kasischke and Borgeau-Chavez, 1997). Temporal changes in soil moisture, plant phenology or flooding often result in more pronounced differences in radiometric responses than physico-chemical and structural differences between cover types in a single moment in time. Martinez and LeToan (2007) explored the possibility of characterizing land cover types based on seasonal changes in the Amazon floodplain.

Combination of multiple remote sensing sources can also improve land cover discrimination, as radiometric properties of land targets can be very distinct among the different regions of the electromagnetic spectrum. Graciani and Novo (2003) investigated the potential for combining optical and radar imagery to map macrophyte cover.

However, none of the previous remote sensing or field studies in the Amazon floodplain have succeeded in providing a complete spatial and temporal characterization of the seasonal variation in macrophyte cover for the floodplain, necessary to properly

quantify the amount and timing of carbon uptake and release in the floodplain. Such understanding of short and long term variability is a key component for proper determination of the participation of macrophytes into the floodplain carbon cycle, as well, as the possible effects of climate variability and habitat alteration on the ecological role of macrophytes.

Thus, the present study offers 1) a new hierarchical, object oriented method for combining multisource and multidate optical and SAR data to map seasonal changes in macrophyte cover in the Amazon floodplain, 2) a consistent characterization of the seasonal evolution of macrophyte cover along a yearly flooding cycle for an eastern Amazon floodplain lake, and 3) some considerations on the possible effects of macrophyte Spatio-temporal dynamics on the ecological and biogeochemical processes of the Amazon floodplain.

5.3 Methods

5.3.1 Classification Method

The proposed classification method is grounded by the flood pulse concept (Junk, 1989), taking as its basic premise that the seasonal variation of flooding is the main determinant of land cover type and dynamics in the Amazon floodplain. Using this defining trait, a hierarchical classification scheme is proposed where cover classes are first characterized in the temporal domain, and then this information is used *a posteriori* to constrain single date image classification (Figures 5.1 and 5.2). The present scheme also acknowledges the nature of the information contained in the radar imagery and

attempts to be consistent with previous remote sensing studies in the floodplain (Silva et al., 2007a; Martinez and Le Toan, 2007; Costa, 2005; Hess et al, 2003).

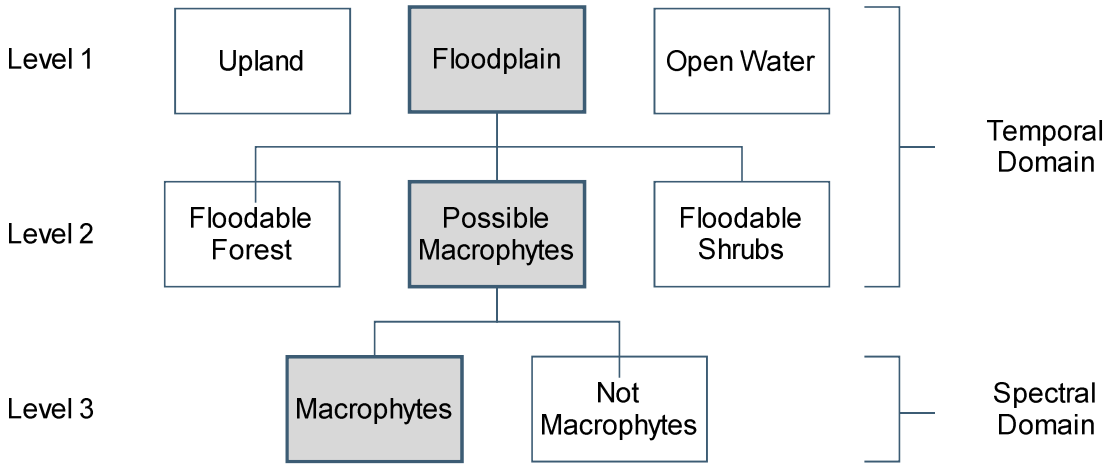

Figure 5.1: Classification Levels used defined for the present classification method. Highlighted boxes indicate the classes of interest for the present study.

The first hierarchical classification level (Level 1) represents the most readily observable partitioning of land cover from the temporal point of view, and includes three classes: Upland (non-floodable areas), Floodplain and Open Water (permanent). The second classification level partitions the Floodplain area into three possible cover types: Floodable Forest, Floodable Shrubs and Possible Macrophytes. This level is based on the assumption that forest and shrub cover are spatially constant during the studied period and only have two transient states (flooded / non-flooded), while exposed soil, macrophyte and open water areas can be thought of as alternate states that can be observed at the same spatial location throughout the flooding season (Junk and Piedade, 1997).

The third classification level (Level 3) partitions the Possible Macrophytes class into actual macrophyte cover and other cover types at each isolated date, in order to generate a time series of macrophyte cover evolution throughout the season. This level assumes that only the three aforementioned cover types (actual macrophytes, bare soil, and open water) are observable within the Possible Macrophytes class.

The method was implemented using Definiens Developer 7.0 (www.definiens.com), using an object-oriented classification framework. Image objects consist of homogenous groups of pixels (objects), generated by an image segmentation algorithm which iteratively partitions the image space based on radiometric and spatial properties of adjacent pixels (Definiens Imaging, 2007). Object-oriented analysis is particularly desirable for radar classification, since the underlying radiometric signature of each target must be estimated by averaging backscatter across a group of pixels, due to radar speckle (Laur et al., 1994). Also, the use of objects as basic analysis units allows for the incorporation of multiple object properties (features) into the classification process, such as average radiometric response, standard deviation of radiometric response, object size and shape, and relationships between multiple objects, instead of relying on a single piece of information (pixel value).

The first step in the analysis consisted of signature extraction and radiometric characterization of each thematic class in the Radarsat-1, MODIS and SRTM imagery. Training areas were selected based on visual interpretation of the image dataset by an analyst familiar with the location and aided by the existence of previous field data collected in the region (Chapter 2). The minimum size *n* in pixels established for each training area was of 100 pixels, based on the calculations specified by Laur et al. (1994)

for correct estimation of multi-look radar backscattering intensity (σ^0) with an error boundary of ± 1 dB at the 95% confidence level.

After signature extraction, image objects were generated for the temporal domain by segmenting a set of two images: a derived image of average radar backscatter for the whole Radarsat-1 ST2 time series, and a single image corresponding to the lowest flood level in the time series. While the first was able to characterize most of the distinct temporal classes and greatly reduce the effect of radar speckle on object identification, the latter was necessary to ensure proper segmentation of areas only exposed during the lowest flooding stage, and thus suppressed in the average image.

Once image objects were generated, image classification was performed hierarchically to achieve each classification level. Level 1 classification was carried for the entire scene, while Level 2 classes were derived only for objects belonging to the "Floodplain" class at Level 1. Both levels were generated based on the temporal information, thus yielding a single classification result for the whole time series.

Level 3 classes were then identified for each single date image, restricted to the areas identified as "Possible Macrophytes" at Level 2. A new segmentation was applied prior to classification to account for changes in actual cover among dates, and MODIS images were introduced at this level in order to achieve the best separation between exposed soil and newly vegetated areas.

The same classification algorithm was used for each level, consisting of a two-step procedure. In the first step, image objects were classified using user-defined simple rules (thresholds), specified based on visual analysis of the radiometric intervals observed during signature analysis, representing areas of little or no overlap among class signatures

(*e.g.* all objects with average seasonal radar backscatter > -5.3 dB belonging to the "Floodplain" class, all objects with average SRTM height larger than 18m belonging to the "Upland" class). At the second step, a supervised nearest neighbour (N-N) algorithm was used to classify the remaining unclassified objects.

A total of 32 object features were used as inputs for the N-N classification, including average seasonal backscatter, average backscatter at each date (14 images), standard deviation of backscatter at each date (14 images), average SRTM height and three user-defined features:

$$\text{High/Low Image Ratio} = \sum(h_1 + h_2) / \sum(l_1 + l_2) \qquad \text{(Eq. 5.1)}$$

$$\text{Normalized Seasonal Difference} = \frac{\sum(h_1 + h_2) - \sum(l_1 + l_2)}{\sum(h_1 + h_2) + \sum(l_1 + l_2)} \qquad \text{(Eq. 5.2)}$$

$$\text{Cumulative Difference} = \sqrt{\sum_{t=1}^{14}(i_{t+1} - i_t)^2 + (i_1 - i_{14})^2} \qquad \text{(Eq. 5.3)}$$

, where h_1 and h_2 are the images associated with the two highest water level dates, l_1 and l_2 are the images associated with two lowest water levels, and i_t refers to each single image at date t. The last term of Eq. 5.3 was included to account for the differences between low water stages one seasonal cycle apart. For each classification level, an optimized subset of this original set was generated by taking the combination of features that produced the largest average minimum distance between class samples. Distances were normalized by the square root of the number of features included in each combination, to prevent distance inflation from increasing numbers of features (Definiens Imaging, 2008). The whole classification process is summarized on Figure 5.2.

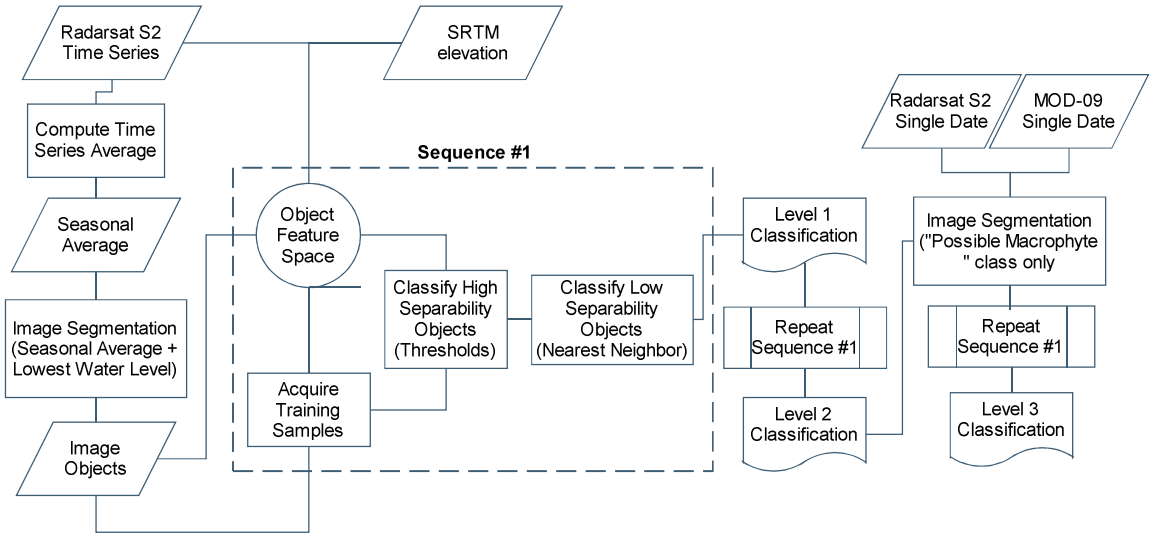

Figure 5.2: Overview of the proposed classification method. Chart flows from left to right, and top to bottom.

5.3.2 Accuracy assessment

For levels 1 and 2, a validation set was generated by randomly distributing 350 points across the study area (16 to 134 points per class), which were then manually classified through visual interpretation of high resolution CBERS-2 HRC images, digital videography data and analog aerial color photography.

This set of points was used to produce error matrices for the classifications, and for calculation of the following accuracy measurements (Congalton, 1991):

Percent accuracy: percentage of the validation points corresponding to correctly classified areas for the whole image;

Omission errors: also known as Producer's accuracy or exclusion errors, represents the ratio of correctly classified pixels (diagonal values) to the total number of reference pixels in each class (column totals), expressed as percentages;

Commission errors: also known as User's accuracy or inclusion errors, corresponds to the ratio of correctly classified pixels (diagonal values) to the total number of classified pixels in each class (row totals), expressed as percentages;

K-hat statistic: also know as *kappa* (κ) or KIA (kappa index of agreement), is a multivariate statistical index that measures the amount of agreement between reference and classification data in relation to the amount of agreement expected for any two classifications due to chance alone (omission and commission errors). It is calculated as:

$$\hat{K} = \frac{N\sum_{i=1}^{k} x_{ii} - \sum_{i=1}^{k}(x_{i+} \times x_{+i})}{N^2 - \sum_{i=1}^{k}(x_{i+} \times x_{+i})} \qquad \text{(Eq. 5.4)}$$

, where k is the number of rows/columns (land cover classes), x_{ii} is the number of observations in row i and column i, x_{i+} and x_{+i} are the marginal totals for row i and column i respectively, and N is the total number of observations.

For the level 3 classification, accuracy was determined both by comparison with the 350 point validation set and by comparison with a set of field observations of macrophyte occurrence collected at the field during the studied period (Chapter 2). At this level, only the correct differentiation between macrophyte and non-macrophyte cover was assessed.

5.3.3 Net primary production simulation

The effect of seasonal cover change on annual net primary production in the studied area was assessed by simulation, combining field total biomass values (Chapter 3) and the present individual maps. The best possible pairing between field and image dates was used, for a total of 11 dates, and the biomass values from December 2003 were associated to both December 2003 and December 2004 images.

Net primary production was simulated by first randomly assigning one biomass observation to each pixel classified as macrophyte in each field-image pair, and then taking the per-pixel sum of positive increments in biomass throughout the observed period (Section 4.3):

$$NPP = \sum_{i=1}^{i} (\Delta \overline{B}_i) \quad \text{for all} \quad \Delta \overline{B}_i > 0 \qquad \text{(Eq. 5.5)}$$

A total of 100 realizations of the above simulation were performed in order to estimate the mean and standard deviation of NPP values across the studied area.

Simple extrapolations of annual production were also calculated for the remaining primary producers, as a simple multiplication of cover area by the NPP values reported in Melack et al. (in press (b)). In accordance with the aforementioned study, flooded forest and flooded shrubs were assumed to have the same associated NPP values.

5.4 Results

5.4.1 Signature Analysis

The analysis of the Radarsat 1 radiometric signatures for the different cover types revealed a fair amount of overlap even at the most basic classification level, at any given single date (Figure 5.3). In general, floodplain cover types had the highest backscattering values and largest amount of variability (-18 dB to 1 dB), while upland cover types occupied the middle range of backscattering values (-16 dB to -4 dB) and open water areas exhibited the lowest backscattering response (-25 dB up to -5 dB) (Figure 5.3). A distinct bi-modal pattern could be observed for open water areas. Still water areas had a very low radiometric response, while the presence of waves at the main lake surface resulted in significantly higher radar return, overlapping the radiometric intervals observed for the remaining classes. This effect was more predominant closer to the near range, where the combination of water wave angle and radar incidence angle more often resulted in specular reflection back at the sensor, saturating the radiometric response. Towards the far ranges, only progressively steeper (rougher) water waves caused saturation.

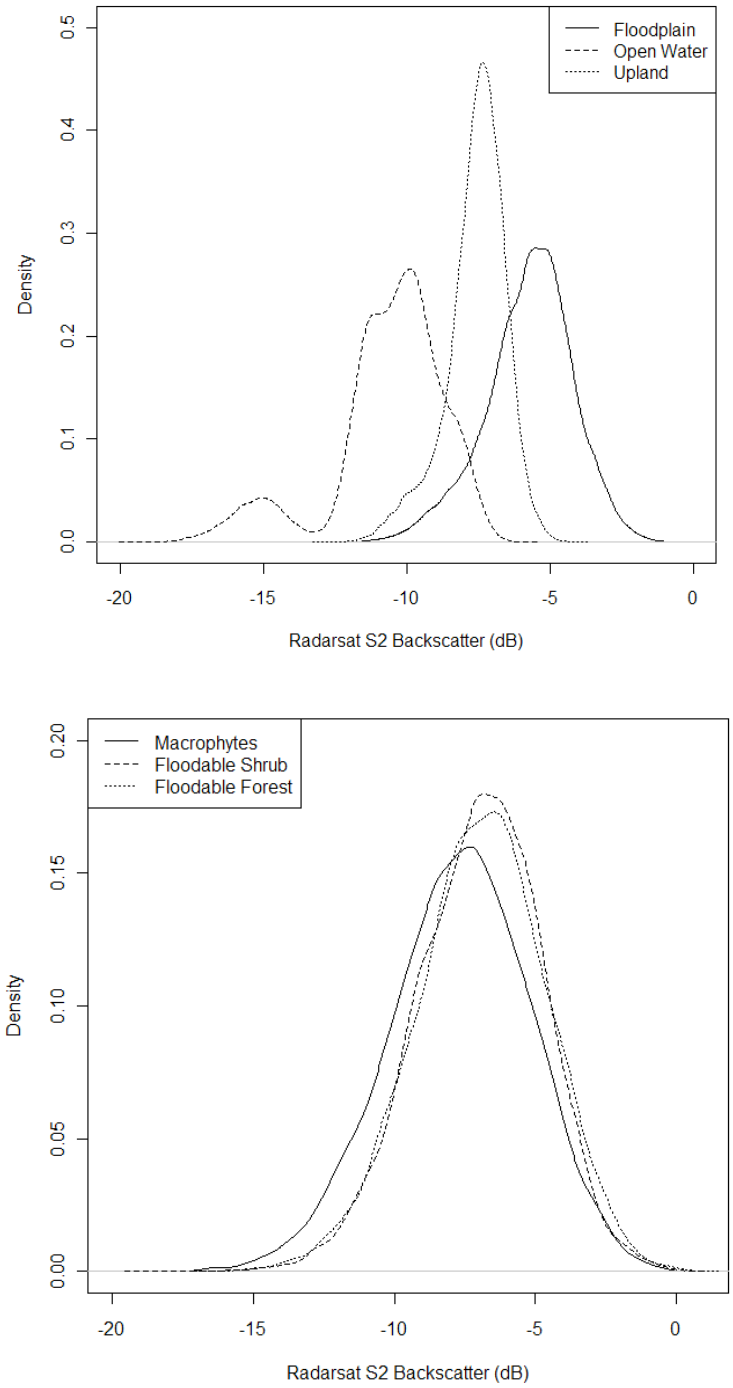

Figure 5.3: Kernel density plots of average annual backscatter for Level 1 (above) and Level 2 (below) classes at Monte Alegre lake (Amazon, Brazil).

The analysis of the radiometric information in the temporal domain indicated a noticeable seasonal variation for floodplain cover types, in synchrony with the annual flood pulse, while upland and open water classes remained relatively stable throughout the season (Figures 5.4 to 5.6). Some discriminating features could be observed for the floodable vegetation classes based on the temporal features: floodable shrubs had noticeably higher backscattering during the peak flood season (-3 to -4 dB range), while macrophytes had a noticeable drop from around -6 dB during high water to under -10dB at the end of the growing season, as well as the highest amplitude in temporal variability of backscattering (Figure 5.6). In all cases, however, the existence of considerable overlap between spectral ranges at each date suggested potential confusion among floodable vegetation classes during classification. MODIS reflectance data revealed good separation between exposed soil and macrophyte vegetation, especially in the near infrared (band 2) range (Figure 5.7).

5.4.2 Classification Accuracy

The error matrices for Level 1 and Level 2 classifications are presented in Tables 5.1 to 5.3. Level 1 accuracy was very high, with about 95% agreement and a k-hat index of 0.92. Classification errors were equally distributed among classes and between producer's (omission) and user's (commission) error types.

For Level 2 classification results, the percentage of agreement was 84%, with a k-hat index of 0.78. The highest accuracy was observed for the Possible Macrophyte class, followed by Flooded Forest and Flooded Shrubs (Table 5.2).

Table 5.1: Error matrix for Level 1 classification of land cover in Monte Alegre lake (Amazon, Brazil). Ov. = Overall Accuracy.

	Reference Data				
	Upland	Floodplain	Open Water	**Row Total**	*Omission*
Upland	63	3	0	**66**	*5%*
Floodplain	4	142	7	**153**	*5%*
Open water	0	4	127	**131**	*3%*
Column Total	**67**	**149**	**134**	**350**	
Commission	*6%*	*5%*	*5%*	*Ov. = 94.9%*	*K-hat =0.92*

Table 5.2: Error matrix for Level 2 classification of land cover in Monte Alegre lake (Amazon, Brazil). F. = Flooded, Ov. = Overall Accuracy.

	Reference Data						
	Upland	F.Forest	F. Shrubs	Macroph.	Open Water	**Row Total**	*Omission*
Upland	63	2	0	1	0	**66**	*5%*
Flooded Forest	3	24	8	17	1	**53**	*55%*
Flooded Shrubs	0	4	6	2	0	**12**	*50%*
Macrophytes	1	6	2	73	6	**88**	*17%*
Open Water	0	0	0	4	127	**131**	*3%*
Column Total	**67**	**36**	**16**	**97**	**134**	**350**	
Commission	*6%*	*33%*	*63%*	*25%*	*5%*	*Ov. = 83.7%*	*K-hat = 0.78*

Table 5.3 - Error Matrix for Level 3 Classification of macrophyte cover in Monte Alegre lake (Amazon, Brazil) for the low water (Nov 2004 – above) and high water (June 2004 – below) stages of the Amazon River. Ov. = Overall Accuracy.

	Reference Data – Nov 2004 (Low Water)			
	Macrophyte	Not Macrophyte	**Row Total**	*Omission*
Macrophyte	25	11	**36**	*31%*
Not Macrophyte	12	22	**34**	*35%*
Column Total	**37**	**33**	**70**	
Commission	*32%*	*33%*	*Ov. = 67.1%*	*K-hat = 0.34*
	Reference Data – June 2004 (High Water)			
	Macrophyte	Not Macrophyte	**Row Total**	*Omission*
Macrophyte	39	4	**43**	*9%*
Not Macrophyte	1	33	**34**	*3%*
Column Total	**40**	**37**	**77**	
Commission	*2%*	*11%*	*Ov. = 93.5*	*K-hat = 0.87*

Validation of the single date Level 3 classifications indicated an increase in accuracy for the months of high water stage (Table 5.3). For June 2004, agreement was 93% between classification results and visually interpreted reference points, and 65% against the field collected samples. For November 2004, accuracy values were 67% and 56%, respectively.

5.4.3 Classification Results

The results of the Level 1 and Level 2 multitemporal classifications are shown in Figure 5.8. Level 3 classification results for low and high water levels are presented in Figure 5.9 and Appendix A. Visual inspection of the mapped distribution of cover types indicated agreement with observations from field and high resolution imagery, especially concerning the interspersed patches of floodable forest, floodable shrub and possible macrophytes on the south-eastern part of the lake.

The classification results show the predominance of floodable vegetation along the areas receiving water influx from the Amazon River on the western and southern portions of the lake, and from the Curuá River in the northeast. At Level 1, floodable areas comprised 984 km^2 (38% of the classified area), while upland areas and permanently open water represented 588 km^2 (22)% and 1041 km^2 (40%) respectively. At Level 2, the floodplain area was further partitioned into 341 km^2 of Floodable Forest (35%), 80 km^2 of Floodable Shrubs (8%) and 563 km^2 (57%) of Possible Macrophytes.

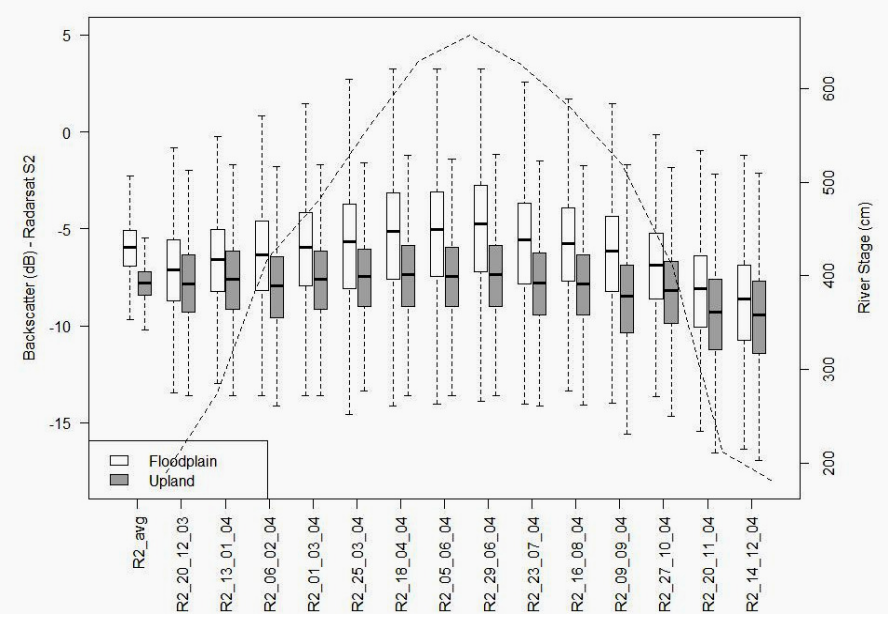

Figure 5.4: Temporal variation in Radarsat S2 (C-HH) backscattering for Level 1 "Upland" and "Floodplain" classes in Monte Alegre lake (Amazon, Brazil). The dashed line indicates river stage (cm) at the nearest gauging station (Óbidos) for each imaged date.

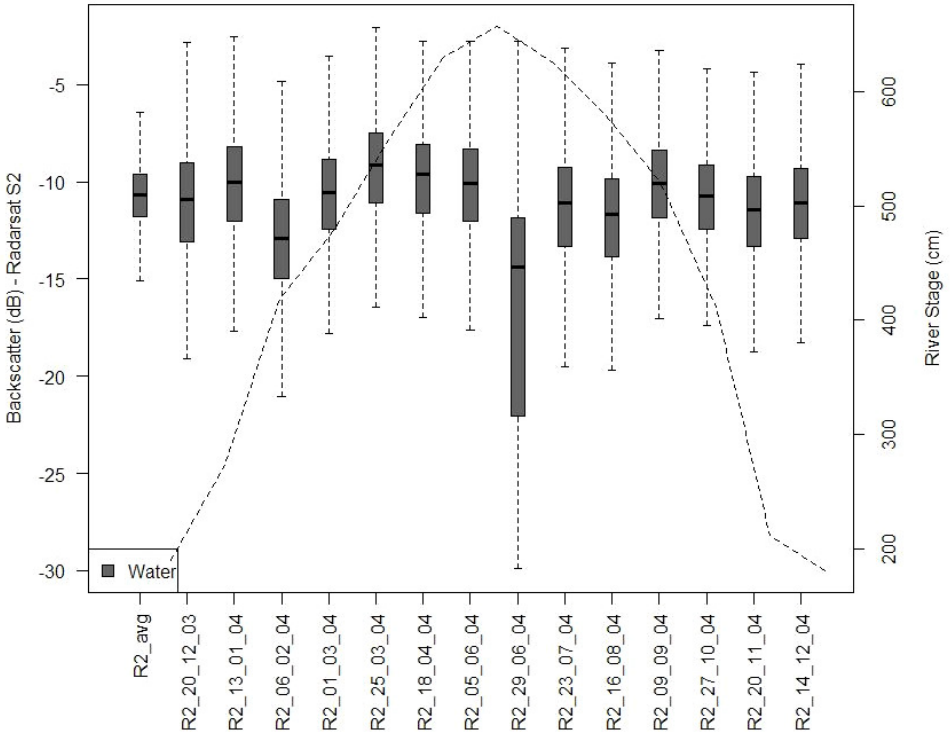

Figure 5.5: Temporal variation in Radarsat S2 (C-HH) backscattering for Level 1 "Water" class in Monte Alegre lake (Amazon, Brazil). The dashed line indicates river stage (cm) at the nearest gauging station (Óbidos). The particularly low values observed on 29/06/04 can be explained by lake surface waters being particularly still at this date.

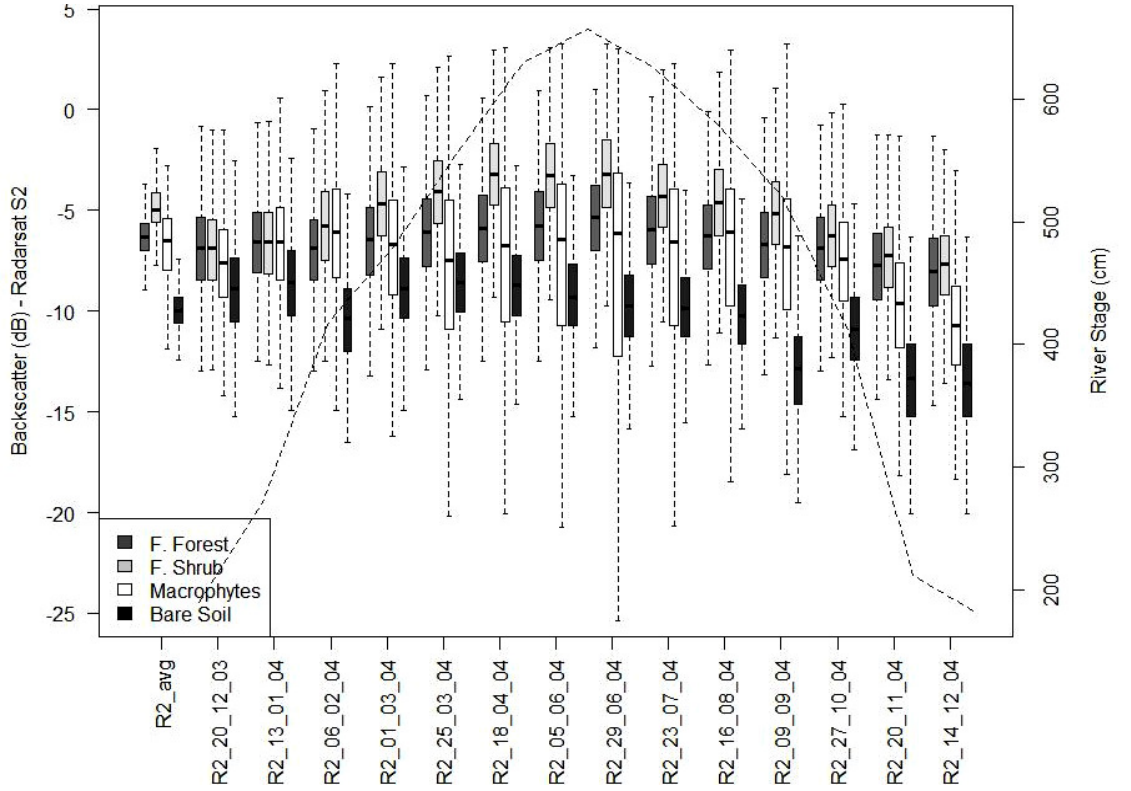

Figure 5.6: Temporal variation in Radarsat S2 (C-HH) backscattering for Level 2 classes in Monte Alegre lake (Amazon, Brazil). The dashed line indicates river stage at the nearest gauging station (Óbidos) for each imaged date.

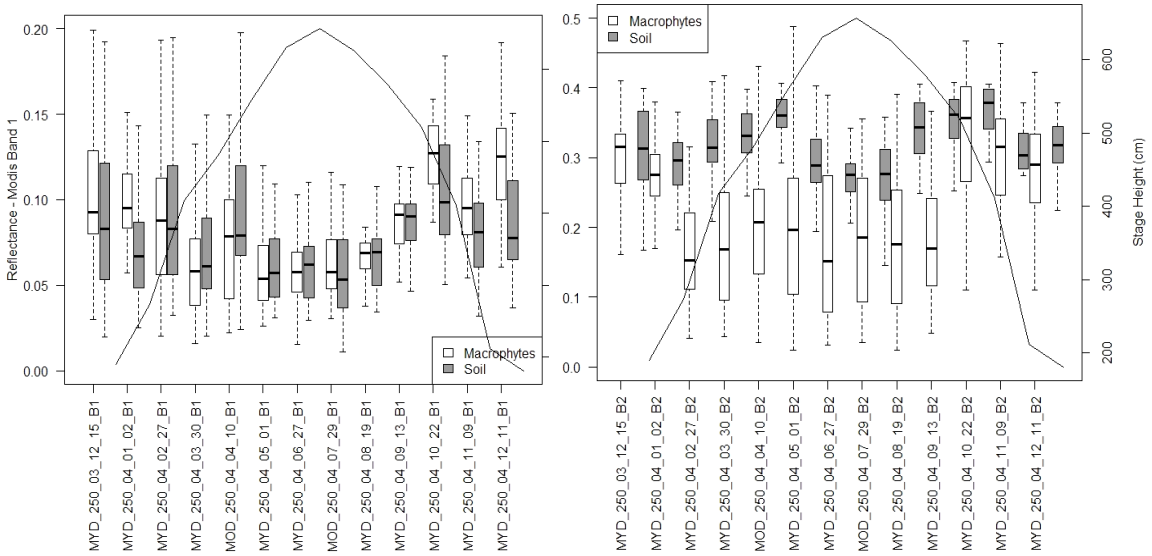

Figure 5.7 - Temporal variation in MODIS Band 1 (left) and and Band 2 (right) spectral signatures of macrophytes and bare soil for Monte Alegre lake (Amazon, Brazil). Secondary y-axis scale (stage height) is equivalent for both graphs.

Actual macrophyte cover (Level 3) ranged from 198 km^2 in January 2004 to 104 km^2 in November 2004 (10% – 20% of floodplain area and 4% – 8% of total scene area), and amounted to about one third of the area mapped as "Possible Macrophytes" at its highest value (Figure 5.10).

5.4.4 Macrophyte Production

The results of macrophyte net primary production simulation are presented in Figure 5.11. The calculated NPP for Monte Alegre Lake during the studied period was approximately 440 x 10^3 MgC yr^{-1}, assuming dead biomass loss rates of 45% and a carbon content of approximately 50% dry mass (Section 4.4). It must be noticed that these results are affected by the partial lake coverage resulting from scene framing, and do not represent NPP figures for the entire lake. Simple NPP estimates for the remaining cover types can be seen on Table 5.4. Overall, the results indicate that macrophytes may be responsible for about half of the primary productivity in the study area.

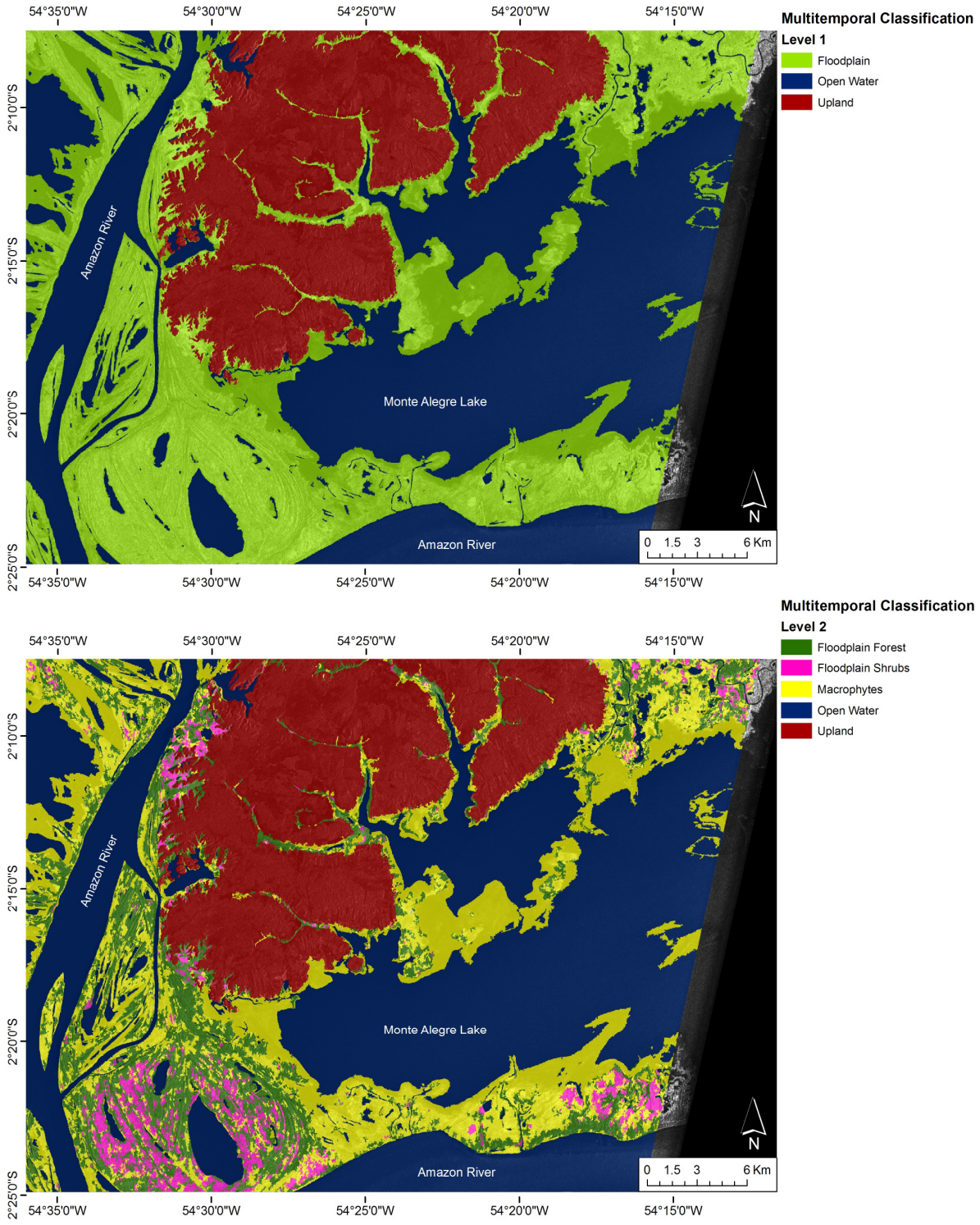

Figure 5.8: Multitemporal classification results for Level 1 classes (above) and Level 2 classes (below) for Monte Alegre lake (Amazon, Brazil).

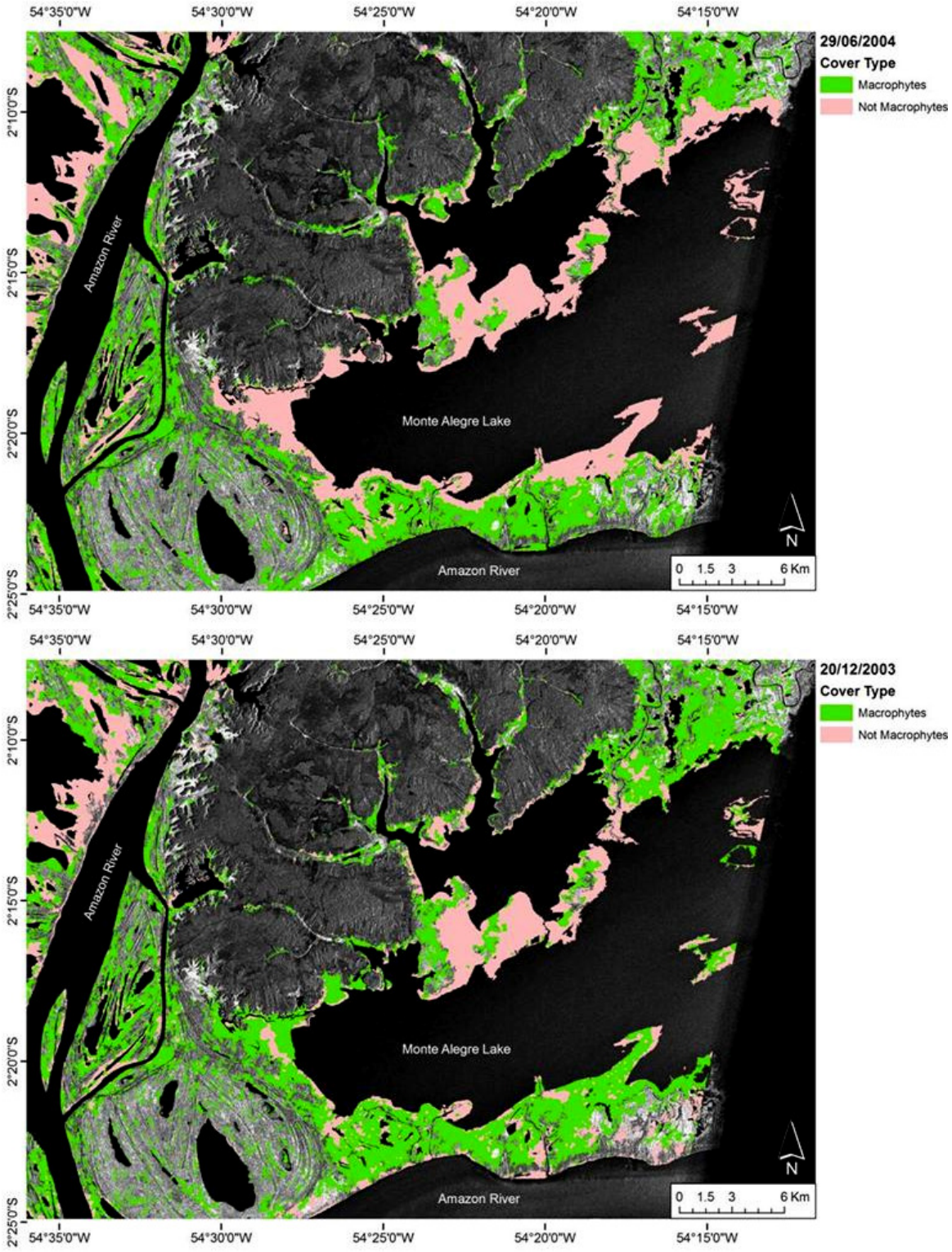

Figure 5.9: Level 3 classification results for June 29, 2004 (above) and December 20, 2003 (below) images pairs for Monte Alegre lake (Amazon, Brazil). See Appendix I for complete series. Background image: Radarsat average annual image.

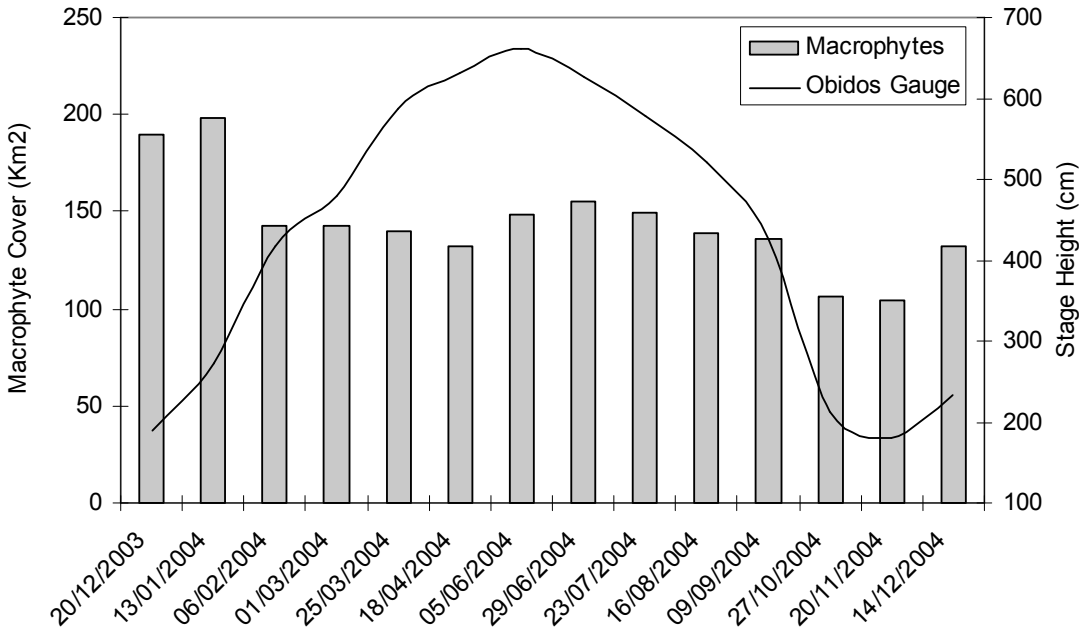

Figure 5.10: Macrophyte cover (km^2) at Monte Alegre lake (Amazon, Brazil) for each studied date.

Table 5.4: Estimated annual net primary production of different vegetation types for Monte Alegre lake (Amazon, Brazil) for the Dec 2003 – Dec 2004 period.

	NPP ($MgC\ km^{-2}\ yr^{-1}$)	Cover Area (km^2)	Annual Net Production ($x\ 10^3\ MgC\ yr^{-1}$)	Annual Net Production (%)
Macrophytes	**3100**[a]	**104 - 198**	**444**[b]	**37.2**
Flooded Forest	1150 [c]	341	392	32.8
Phytoplankton	200 [c]	1040[d]	208	17.5
Flooded Shrub	1150 [c]	80	92	7.7
Periphyton (forest)	100 [c]	421	21	3.5
Periphyton (mac)	110 [c]	144[e]	8	1.3

[a] Average NPP calculated from field data (Section 3.3)
[b] Annual production calculated by simulation, see methods section.
[c] Values according to Melack et al. (in press (b)).
[d] Open water area (Level 1 classification).
[e] Annual production estimated using average macrophyte cover.

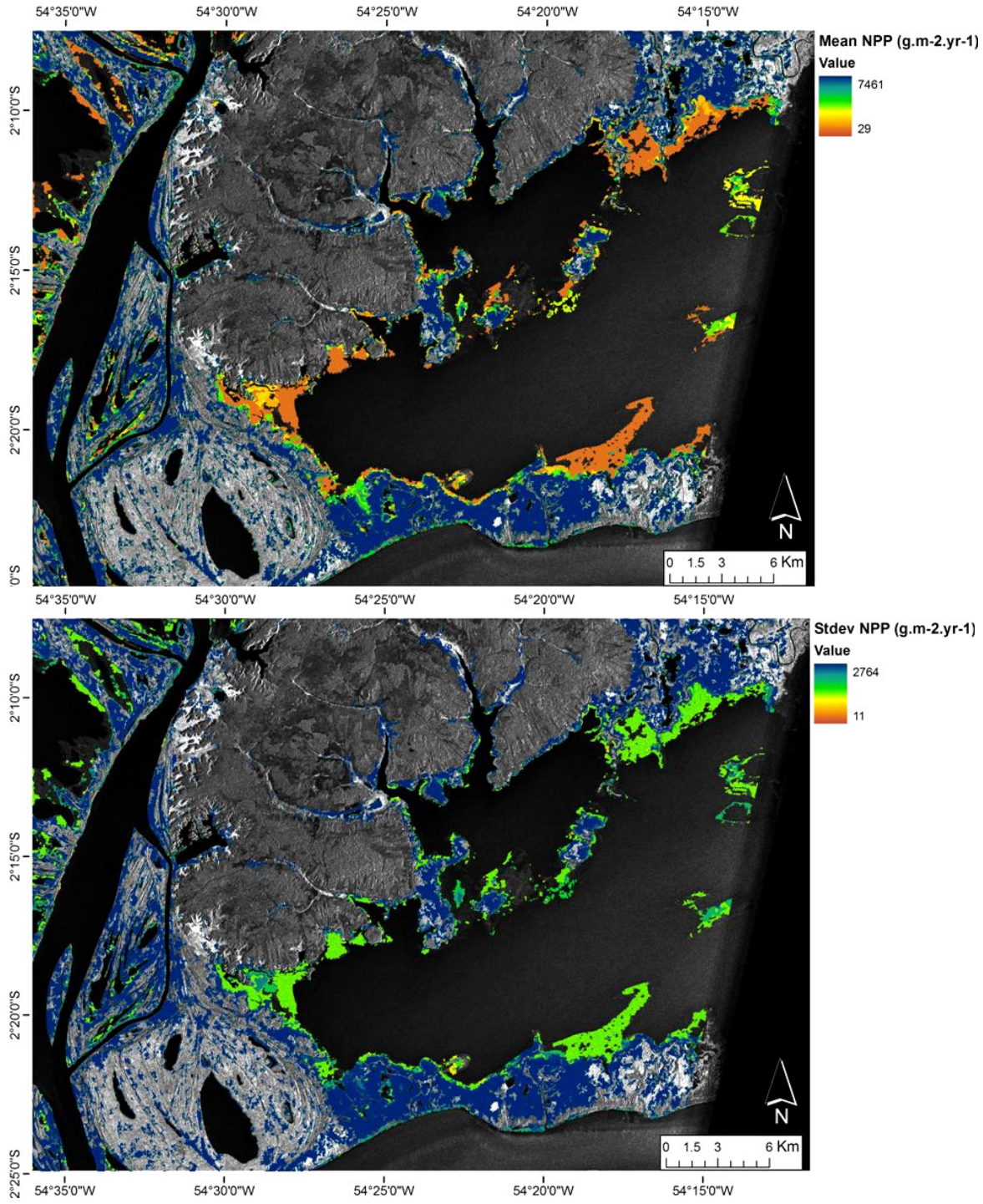

Figure 5.11: Simulated spatial distribution of annual net primary production of macrophytes at Monte Alegre lake (Amazon, Brazil). Above: mean value of 100 simulations; below: standard deviation of 100 simulations.

5.5 Discussion

5.5.1 Classification Method

The present classification method was able to adequately capture the spatial pattern of macrophyte growth and development in the studied area. Temporal information was paramount in minimizing confusion and properly identifying the main vegetation cover types in the floodplain, a task otherwise very difficult to accomplish using single date C band radar imagery. The use of object-oriented classification allowed the extraction of a significantly greater amount of information from the image data, as opposed to a single pixel value. The combination of this capability with the progressive partitioning of the scene through hierarchical classification levels was a predominant factor in obtaining the present results.

The combination of multiple image sources also contributed significantly to the high accuracy observed for Level 1 and Level 2 classifications. At level 1, the inclusion of SRTM data promptly excluded a large portion of upland areas from the classification process, reducing the potential confusion between upland and floodplain classes. For areas below the SRTM height threshold, the marked difference in temporal patterns of radar backscatter between upland floodplain areas was the determining factor (Figure 5.6). The occurrence of flooding favours the radar scattering mechanism known as double-bounce, where radar beams penetrating the vegetation cover are reflected first from the underlying water surface and then from stems and tree trunks, increasing the signal returned to the sensor (Freeman and Durden, 1998; Hess et al, 1995). Open water, on the other hand, caused mostly forward specular reflection of the incoming wave, with resulting very low signals recorded.

At Level 2, the increasing overlap between vegetation signatures decreases accuracy, but structural differences between plant types still resulted in distinct radiometric and temporal characteristics. Flooded shrubs, mostly composed of *Montrichardia arborescens*, exhibited the highest backscatter coefficients during high water season, due to the regular, evenly spaced organization of their vertical stem. Allied to the low leaf area index (LAI), such configuration makes flooded shrubs a very strong double bounce reflector (Costa, 2002; Hess et al., 1995). Flooded forests, on the other hand, may exhibit variable levels of LAI, with variable backscattering signals resulting from the mixture of double-bounce and volumetric scattering. Many floodplain tree species are deciduous and shed leaves during flooding conditions, favouring double-bounce interactions (Wang et al., 1995).

The same combination of volumetric and double bounce can be observed for macrophytes. During early growth season and senescence, plant density and biomass are low, resulting in reduced volumetric and double bounce interactions and predominance of surface scattering from soil or standing water, and overall low backscattering coefficients. As plants stands quickly accumulate biomass, volumetric backscattering starts to be the dominant mode of interaction, resulting in the observed increase of radar return at high water, but not to the levels observed for forest and shrubs due to the lack of double bounce interactions (Costa et al., 2002).

In addition to the advantages of multitemporal object-based classification, the use of MODIS images was essential to obtain correct separation between exposed soil and vegetated areas during the low water stages, despite its coarser spatial resolution. During earlier stages of plant development, surface scattering dominates over other modes of

interaction, making bare soil and newly vegetated areas appear very similar on C-HH radar. On MODIS, however, clear separation can be observed between soil and vegetation, especially in the near infrared region of the spectrum (band 2) (Figure 5.7).

It is reasonable to expect that improved results could be obtained by the simultaneous use of current Radarsat-2 (C-band) and ALOS Palsar (L-band) imagery. The combination of C and L band radar has been shown to greatly improve land cover and vegetation characterization as multiple wavelengths exhibit different responses to structural elements of the floodplain vegetation (Costa, 2004; Costa, 2002; Dobson et. al, 1996; Hess et al., 1995; Wang et al., 1995), Plus, as both sensors offer multiple polarization configurations, a larger set of bands can be used to properly separate between cover types (Silva et al, 2008; Hess et al., 1995).

The observed accuracy reflects the inherent complexity of the floodplain landscape, especially in regard to macrophyte cover, where plant stands can range from a few square meters up to several hectares, have a variety of sizes and shapes, and be isolated or interspersed with other vegetation types. Hess et al (2003) reports similar accuracy values (~65%) for the classification of macrophytes ("herbaceous-flooded") and floodable shrubs ("flooded woodland") for the entire floodplain lake. Martinez and Le Toan (2007) report a value of 68% for macrophytes ("often flooded low vegetation") at Curuai Lake, which exhibits very similar conditions to the present studied area. Furthermore, some degree of deflation in the accuracy measures can be expected due to compounding of GPS positioning and image georeferencing errors when comparing field and image data, and due to the inherent possibility of interpretation error when using the set of visually interpreted validation points.

Although the present method is currently optimized to identify macrophyte cover exclusively, the rationale behind it could easily be extended to contemplate all possible classes in the floodplain, only by the inclusion of additional partitioning of the upper level classes based on temporal information (e.g. differentiation of pasture and agricultural areas, identifying forest clearing and burn, etc.). It could also be readily adapted for any land cover type exhibiting recurring variability and/or transient cover states for the same spatial location over time.

5.5.2 Classification Results

Direct comparison between present results and previous values reported for Lago Grande by Costa et al. (2004) (342 km^2 and 397 km^2 for December and May-June periods respectively) is limited, since a large portion of floodable area at the north-eastern side of the lake is not covered in the present study due to differences in scene framing. However, both studies were conducted at very similar water levels and revealed a ratio of approximately 1.16 between macrophyte cover at high and low water stages.

Hess et al. (2003) suggests herbaceous vegetation represents about 5% – 10% of the floodplain area, based on mapping using JERS L-band radar images at 100m resolution. This value, despite being lower than that observed by the present study, reflects overall macrophyte cover for the whole floodplain. The aforementioned mapping effort includes the large wetland areas of the western and central Amazon floodplain, which are mainly composed of smaller lakes where flooded forest strongly dominates over macrophyte cover (Melack et al., in press (a); Engle et al., 2008). In addition, it is

possible that longer L-band wavelengths miss the low density, shorter vegetation stands (Costa, 2002).

5.5.3 Implications for floodplain ecology and C cycle

Noticeable differences were observed for the macrophyte cover between the months of December 2003 /January 2004, and December 2004, with the former exhibiting a covered area about 1.4 times larger than the latter. Such differences are mainly explained by the difference in flood levels during each year. Stage height data collected for the Amazon River at the nearest location indicates a value of 190 cm for December 2003 and 233 cm for December 2004, and visual inspection of images from both dates clearly reveals the existence of additional areas of exposed substrate during 2003, which were submerged during the following year.

Although most of these exposed areas are comprised of bare substrate, macrophyte establishment can still be observed at many sites due to the very rapid growth rates associated with these plants. A look at the persistence of macrophyte cover over time (Figure 5.12) suggests the existence of two distinct growth strategies for floodplain herbaceous vegetation: plant communities that grow during the low water phase and disappear as soon as water levels start to rise, and plants that are able to grow throughout the entire flood cycle. The sharp decrease in area following the start of the flooding phase suggests that most of these newly established areas are not able to cope with the increased rising water levels and early plant mortality results after a couple of months of flooding, with only some areas being capable of sustaining growth throughout the year.

Zonation of each functional type appears to be determined by substrate topography, with the short term growth plants being clustered towards the interior of the lake on areas of higher depth and more significant water level change, while long term growth plants are distributed in the outer areas of the lake, where flooding would be expected to have shorter durations and lower magnitudes. This distribution is in accordance with previously documented macrophyte growth patterns (Junk and Piedade, 1997). In general, 91 km^2 (35%) of total annual macrophyte cover subsisted during only four months or less, while 117 km^2 (45%) remained growing for 10 months or more. An intersection of field observations regarding dominant species and the two categories indicated predominance of *Paspalum fasciculatum* within the short-lived group and of *Hymenachne amplexicaulis* in the long-lived group.

The observed variation in macrophyte cover has important implications on the total contribution of macrophytes to the carbon balance of Monte Alegre Lake. First, it can be seen that the amount of plants that are able to reach peak biomass and maximum production is restricted to the year-round communities, with lower production resulting from the early mortality observed due to rising water levels. Failure to account for this process can therefore lead to overestimation of production values. Costa et al. (2005), working with 9 images acquired over three different years and representing 5 dates along the seasonal cycle, has obtained an estimate of macrophyte NPP of 1900 x 10^3 MgC of carbon for Monte Alegre Lake.

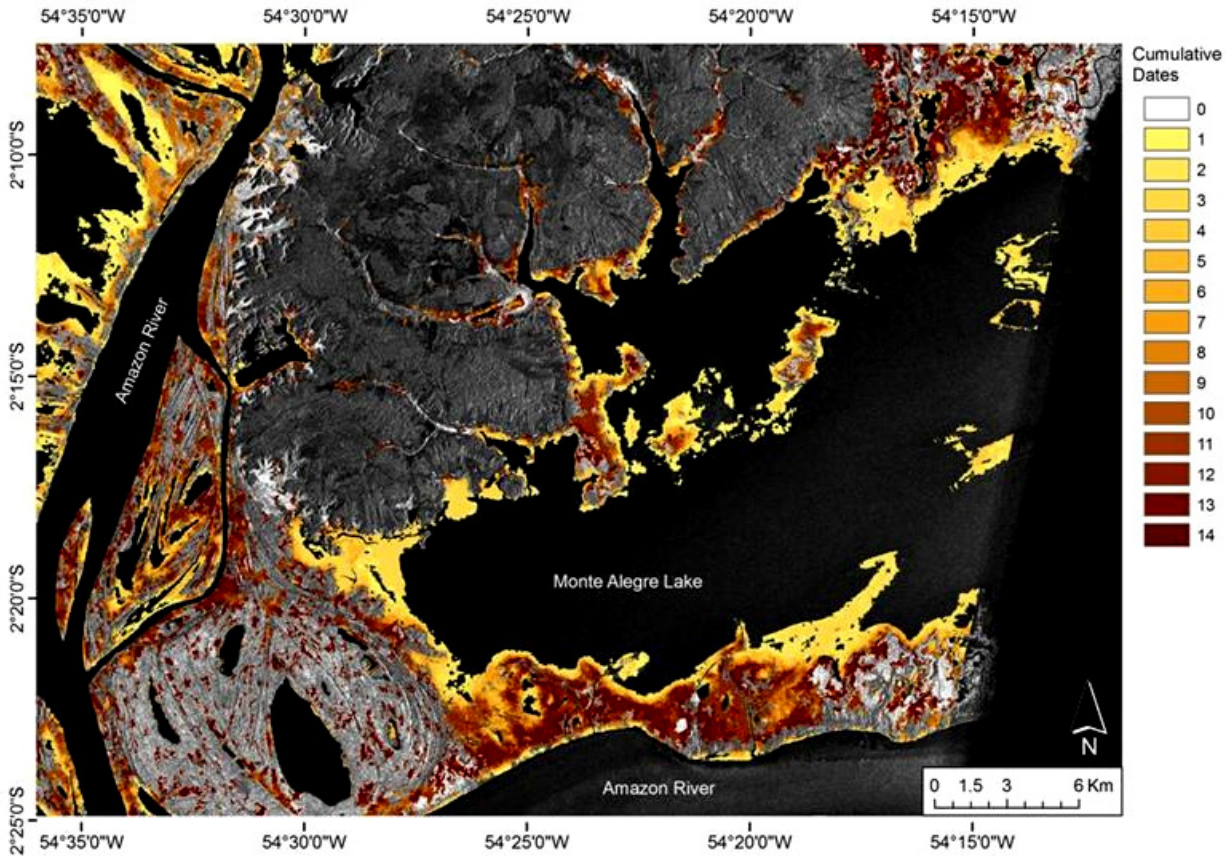

Figure 5.12: Macrophyte spatial distribution according to permanence throughout the flood cycle in Monte Alegre lake (Amazon, Brazil). Legend numbers correspond to the cumulative number of dates where macrophyte cover was observed during the studied period (Dec–03 to Dec–04).

Due to the differences in scene framing, direct comparison of results is prevented, but by taking the ratio of NPP to maximum covered area in both studies, values of approximately 4700 MgC km^{-2} (Costa, 2005) and 3100 MgC km^{-2} (present study) can be observed. It must be also noticed that the former study has assumed linear rates of macrophyte biomass increase /decrease between mapped dates, which might lead to

unrealistically high results given the presently observed early mortality of a significant portion of the macrophyte stands.

Although the majority of macrophyte NPP resulted from the year-round plant communities, 9% (3.5% of total lake NPP) originated from the short-lived communities (four or fewer months of permanence), implying that at least one-fifth of the annual macrophyte NPP is under the direct influence of yearly variations in water level and flood duration. The difference of approximately 64 km^2 in macrophyte area between December 2003 and December 2004 would imply a surplus of at least 12 x 10^3 MgC yr^{-1} (assuming the measured biomass of 250 g m^{-2} for December 2003) in the system between years (~2.6%), potentially more depending on how much growth could be achieved before the death of the short-lived macrophyte stands. The same trend observed over the 1.77 million km^2 of the central Amazon Floodplain region would result in a surplus of 3 TgC yr^{-1}, or roughly 1% of the 298 TgC yr^{-1} of total atmospheric export calculated by Melack et al. (in press b) for the same area.

Even though this sum represents a small percentage of the average annual NPP of macrophytes in the region, such an increase is the result of a difference of about 40 cm in the Amazon River water levels (194 cm in 2003, 233 cm in 2004). During the year 2005, river stages as low as 13 cm have been observed (October), which could potentially result in much larger increases in the area available for colonization by short-lived plant communities. However, as soil desiccation can hinder the growth of new seedlings during extremely dry periods (Piedade et al., 2001), the effect of increasingly lower water levels on macrophyte growth remains to be assessed.

The severe drought observed in the Amazon in 2005 has been associated with unusually warm North Atlantic Sea Surface Temperatures, which are predicted to become more frequent during the 21st century (Cox et al., 2008). Such extreme drought events might not only result in increased contribution from the short lived plant communities, but also cause more significant alterations in plant distribution, affecting the long term trends of vegetation cover and productivity in the floodplain.

Chapter 6 – Conclusion

The present study has established the importance of accounting for spatial and temporal variability of macrophyte growth and productivity when studying large scale macrophyte-related processes in the Amazon floodplain, and provides to date the most detailed analysis of variability and uncertainty in macrophyte NPP estimates for the region. The results indicate that although a series of environmental conditions are likely to contribute to the observed variations, flood dynamics appear to be the major factor determining macrophyte distribution, establishment, growth and productivity.

The effect of spatial variability has been first demonstrated in Chapter 3, which showed that the development of indirect phenometric models for prediction of macrophyte biomass was not as effective as direct selective sub-sampling for the estimation of macrophyte biomass in the Amazon region.

Phenometric modelling results were improved to a certain extent by the use of combined phenometric variables (*i.e.* stem volume and total leaf area) and by establishing species-specific models for each single macrophyte species, but phenotypic variation was still large enough to preclude the generalization of these relationships into single numeric models. The sub-sampling method, on the other hand, was capable of accounting for local variation by relying on direct measurements to estimate individual plant biomass occurring at each specific environmental condition.

By sampling only a small subset, the effort of physically sampling biomass can be reduced, directly translating into wider and more complete sampling coverage, as exemplified by the data set from the present study. While only about 20 complete

measurements of plant biomass were possible (about 50 for emergent biomass only), 182 partial sub-samples could be taken within the same time frame. Thus, we suggest that direct sub-sampling presents the best trade-off between accuracy and coverage for sampling macrophyte populations in extensive wetland environments, and encourage its adoption as an option for a standard method of macrophyte biomass measurement in the Amazon floodplain.

In Chapter 4, the annual growth and productivity of macrophyte communities on the eastern Amazon floodplain was assessed. Plant growth was related to inundation, in terms of stem elongation and biomass. Biomass accumulation was greater during the rising water stage, with some remaining growth still being observed during high and falling water level periods. Actual reduction in biomass due to senescence tended to occur later in the year, and usually at a faster rate than water level decline. Most plants achieved a maximum length of around 300 cm during the growing season, and peak biomass of about 2300 to 6100 g m^{-2}. In general, a lag of zero to three months was observed between water level change and seasonal changes in biomass.

Annual net primary production during the observed period was within the range of 2400 to 3500 g m^{-2}, with above water production between 650 and 1100 g m^{-2}, and below water production between 1700 and 2600 g m^{-2}. Overall, total NPP values varied between 4200 and 7800 g m^{-2} after adjustments for dead biomass loss rates.

The NPP values estimated separately for each dominant species generally agreed with previously published results, with *P. fasciculatum* and *E. polystachya* having lower values than previously reported. *Echinochloa polystachya* and *Paspalum*

fasciculatum were the most productive species at the studied sites, followed by *Paspalum repens, Hymenachne amplexicaulis* and *Oryza perennis*.

Once more, the effect of spatial variability was observed, along with three other sources of variability: macrophyte taxa, sampling design and lack of measurements of dead material loss. This uncertainty implied in ranges of 32 – 79 or 63 – 155 TgC yr^{-1} for scaled up annual macrophyte productivity in the entire central Amazon floodplain, depending on the assumed macrophyte area. The present study agrees with previous results from Quay et al., (1992), which suggest that carbon input from macrophytes might fuel up to half of the C respired in the floodplain.

In Chapter 5, a novel and promising approach for mapping the temporal evolution of aquatic vegetation in the Amazon floodplain was presented. The application of this method allowed for the first time a consistent observation of the seasonal evolution of macrophyte cover in space and time. This observation revealed the existence of distinct spatial and temporal patterns of plant establishment and growth, mostly characterized by a partitioning of macrophyte communities into distinct short-lived and annual communities, the former more susceptible to variations in flood extent and water levels. The occurrence of lower water levels during December 2003 in particular led to an expansion in the area occupied by short-lived macrophyte communities, due to increases in the amount of exposed substrate available for plant colonization.

This direct susceptibility of macrophytes to changes in flooding patterns and environmental conditions raises concerns regarding the response of these communities to long term changes in climatic and environmental conditions. Recent studies suggest an increase in the frequency of droughts for the Amazon region (Cox et al., 2008), which in

turn could lead to an increase in the amount of carbon taken by macrophytes over time. Our results have shown a potential increase of 2.6% in macrophyte NPP between the years 2003 and 2004 as a result of a 40 cm difference in water level between each date, which if observed for the entire floodplain could imply in an 1% increase in total macrophyte production. However, more studies on the effects of extreme droughts and prolonged drought recurrence on the distribution of vegetation in the floodplain are needed to better quantify its repercussions on the carbon cycle.

Furthermore, direct relationships have been established between net primary production and methane production in wetlands (Whiting and Chanton, 1993), and the largest methane emission rates in the Amazon have been associated with macrophyte stands (Bartlett et al., 1990; Devol et al., 1990). Under this scenario, increases in macrophyte cover during drought years could lead to an increase in the conversion of atmospheric CO_2 into CH_4 related to macrophyte assimilation and subsequent anaerobic decomposition.

The spatial and temporal variability of macrophyte growth and productivity remains to be investigated at different locations in the Amazon floodplain, to confirm if the patterns observed by the present study also apply at these locations. In addition, further investigations on the relationship between environmental factors and macrophyte cover and productivity are necessary in order to eventually establish process-based models which can better quantify the role of macrophytes in the biogeochemistry of the Amazon floodplain.

Bibliography

Arraut, E. M. Migração do peixe-boi amazônico: uma abordagem por sensoriamento remoto, radiotelemetria e geoprocessamento. 2008. PhD Thesis. Instituto Nacional de Pesquisas Espaciais, São José dos Campos, Brazil.

Bajjouk, T., Guillaumont, B., Populus, J. 1996. Application of airborne imaging spectrometry system data to intertidal seaweed classification and mapping. Hydrobiologia 326/327: 463–471.

Barnes, W. L., Pagano, T. S., Salomonson, V. V. 1998. Prelaunch Characteristics of the Moderate Resolution Imaging Spectroradiometer (MODIS) on EOS AM-1. IEEE Transactions on Geoscience and Remote Sensing 36(4):1088–1100.

Bartlett, K.B., Crill, P. M., Bonassi, J.A., Richey, J. E., Harriss, R. C. 1990. Methane flux from the Amazon River floodplain – emissions during high water. Journal of Geophysical Research 95 (D10) 16773–16788.

Batzer, D. P., Sharitz, R. R. 2006. Ecology of freshwater and estuarine wetlands. University of California Press, Bekeley, USA 568 pp.

Best, R. G., Wehde, M. E., Linder, R. L. 1981. Spectral reflectance of hydrophytes. Remote Sensing of Environment 11: 27–35.

Boggione, G. A. Restauração de imagens do satélite Landsat-7. 2003. Master's Thesis. Instituto Nacional de Pesquisas Espaciais, São José dos Campos, Brazil.

Bonnet, M. P., Barroux G., Martinez, J. M., Seyler, F., Moreira-Turcq, P., Cochonneau, G., Melack, J. M., Boaventura, G., Maurice-Bourgoin, L., Leon, J. G., Roux, E., Calmant, S., Kosuth, P., Guyot, J. L., Seyler, P. 2008. Floodplain hydrology in an Amazon floodplain lake (Lago Grande de Curuai). Journal of Hydrology 349:18–30.

Boulé, M. E. 1994. An early history of wetland ecology. In Mitsch, W. J., editor, Global Wetlands: Old World and New. Elsevier. 967 pp.

Camarão, A. P., Lourenço, J. B., Dutra, S., Hornick, J. L., da Silva, M. B. 2004. Grazing buffalo on flooded pastures in the Brazilian Amazon region: a review. Tropical Grasslands 38:193–203.

Cao, M., Marshall, S., Gregson, K., 1996. Global carbon exchange and methane emissions from natural wetlands: application of a process-based model. Journal of Geophysical Research 101(D9): 14339–14414.

Congalton, R.G. 1991. A review of assessing the accuracy of classifications of remotely sensed data. Remote Sensing of Environment 37(1), 35–46.

Costa, M. P. F., Niemann, K. O., Novo, E. M. L. M., Ahern, F. 2002. Biophysical properties and mapping of aquatic vegetation during the hydrological cycle of the Amazon floodplain using JERS-1 and RADARSAT. International Journal of Remote Sensing 23: 1401–1426.

Costa, M. P. F. 2004. Use of SAR satellites for mapping zonation of vegetation communities in the Amazon floodplain. International Journal of Remote Sensing 25:1817–1835.

Costa, M. P. F. 2005. Estimate of net primary productivity of aquatic vegetation of the Amazon floodplain using Radarsat and JERS-1. International Journal of Remote Sensing 26:4527–4536.

Cox, P. M., Harris, P. P., Huntingford, C., Betts, R. A., Collins, M., Jones, C. D., Jupp, T. E., Marengo, J. A., Nobre, C. A. 2008. Increasing risk of Amazonian drought due to decreasing aerosol pollution. Nature 453: 212–215.

Dai, T., Wiegert, R. G. 1996. Ramet population dynamics and net aerial primary productivity of *Spartina alterniflora*. Ecology, 77(1): 276–288.

Daoust, R. J., Childers, D.L. 1998. Quantifying aboveground biomass and estimating net aboveground primary production for wetland macrophytes using a non-destructive phenometric technique. Aquatic Botany 62: 115–133.

Definiens Imaging. 2007. Definiens Developer 7.0 Reference Book. Version number 7.0.2.936. München, GB: Definiens Imaging.

Definiens Imaging. 2008. Definiens Developer 7.0 User Guide. Version number 7.0.5.968. München, GB: Definiens Imaging.

Devol, A., Richey, J., Forsberg, B., Martinelli, L. 1990. Seasonal dynamics in methane emissions from the amazon river floodplain to the troposphere. Journal of Geophysical Research 95(D10): 16417–16426.

Dobson, M. C., Pierce, L. E., Ulaby, F. T. 1996. Knowledge-based land-cover classification using ERS-1/JERS-1 SAR composites, IEEE Transactions on Geoscience and Remote Sensing 34(1): 83-99.

Downing, J. A., Anderson, M., 1985. Estimating the standing biomass of aquatic macrophytes. Canadian Journal of Fisheries and Aquatic Sciences 2: 1860–1869.

Efron, B., Tibshirani, R., 1986. Bootstrap methods for standard errors, confidence intervals and other measures of statistical accuracy. Statistical Science 1: 54–77.

Engle, D. L., Melack, J. M., Doyle, R. D., Fisher, T. R. 2008. High rates of net primary production and turnover of floating grasses on the Amazon floodplain: implications for aquatic respiration and regional CO2 flux. Global Change Biology 14:369–381.

Etherington, J. R. (1983). Wetland Ecology. Number 154 in The Institute of Biology's Studies in Biology. Edward Arnold (Publishers) Ltd., London, UK, 66 p.

Field, C. B., Randerson, J. T., Malmstrom, C. M. 1995. Global net primary production: combining ecology and remote sensing. Remote Sensing of Environment 51:74–88.

Fisher, S. G., Carpenter, S. R., 1976. Ecosystem and macrophyte primary production of the Fort River, Massachusetts. Hydrobiologia 49: 175–187.

Fonseca, L. M. G., Mascarenhas, N. D. A. 1987. Determinação da função de transferência do sensor TM do satélite Landsat-5. X Congresso Nacional de Matemática Aplicada e Computacional, Gramado, Brazil, September 21-25, pp. 297-302,

Fonseca, L. M. G., Prasad, G. S. S. D., Mascarenhas, N. D. A. 1993. Combined interpolation-restoration of Landsat images through a FIR filter design technique. International Journal of Remote Sensing 14: 1247–2561.

Forsberg, B. R., Devol, A. H., Richey, J. E., Martinelli, L. A., dos Santos, H. 1988. Factors controlling nutrient concentrations in Amazon floodplain lakes. Limnology and Oceanography 33:41–56.

Fraser, L. H., Keddy, P.A. 2005. The world's largest wetlands: ecology and conservation. Cambridge University Press, Cambridge, UK. 488 pp.

Freeman, A., Durden, S. L. 1998. A three component model for polarimetric SAR data. IEEE Transactions on Geoscience and Remote Sensing, 36: 963–973.

Gorham, E. 1991. Northern peatlands: role in the carbon cycle and probable responses to global warming. Ecological Applications 1:182–195.

Gouraud, C., Giroux, J. F., Mesléard. F., Desnouhes, L. 2008. Non-destructive sampling of Schoenoplectus maritimus in southern France. Wetlands 28: 228–232.

Grace J., Malhi Y., Higuchi N., Meir P. 2001. Productivity and carbon fluxes of tropical rain forests. In: Mooney, H. and Saugier , B. (Eds.). Terrestrial Global Productivity: Past, Present and Future. pp. 401–426. Academic Press, San Diego, USA.

Graciani, S.D., Novo, E. 2003. Determinação da cobertura de macrófitas aquáticas em reservatórios tropicais. XI Simpósio Brasileiro de Sensoriamento Remoto, Belo Horizonte, Brazil, April 05–10, pp. 2509–2516.

Haslam, S. M. 2003. Understanding wetlands: fen, bog and marsh. Taylor & Francis, New York, USA. 296 pp.

Hess, L.L., Melack, J.M., Filoso, S., Wang, Y. 1995. Delineation of inundated area and vegetation along the Amazon floodplain with the SIR-C synthetic aperture radar. IEEE Transaction on Geoscience and Remote Sensing 33(4): 896–904.

Hess, L. L., Novo, E. M. L. M., Slaymaker, D. M., Holt, J., Steffen, C., Valeriano, D. M., Mertes, L. A. K., Krug, T., Melack, J. M., Gastil, M. 2002. Geocoded digital videography for validation of land cover mapping in the Amazon basin. International Journal of Remote Sensing 23: 1527–1555.

Hess, L. L., Melack, J. M., Novo, E. M. L. M., Barbosa, C. C. F., Gastil., M. 2003. Dual-season mapping of wetland inundation and vegetation for the central Amazon basin. Remote Sensing of Environment 87:404–428.

Hopkinson, C. S., Gosselink, J. G., Parrondo, R.T. 1980. Production of coastal Louisiana marsh plants calculated from phenometric techniques. Ecology 61: 1091–1098.

Houghton, R. A. 2003. Why are estimates of the terrestrial carbon balance so different? Global Change Biology 9: 500–509.

Huete, A. R., Didan, K., Shimabukuro, Y. E., Ratana, P., Saleska, S.R., Hutyra, L. R., Yang, W., Nemani, R. R., Myeni, R. 2006. Amazon rainforest green-up with sunlight in the dry season. Geophysical research Letters 33:1–4.

Irion, G., Junk, W. J., de Mello, J. A. S. N. 1997. The physical and chemical environment. In: Junk, W. J. (ed.). The Central Amazon Floodplain. p. 23–46. Springer, Berlin, Germany.

Jakubauskas, M., Kindscher, K., Fraser, A., Debinski, D., Price, K. P. 2000. Close-range remote sensing of aquatic macrophyte vegetation cover. International Journal of Remote Sensing, 21(8): 3533–3538.

Junk, W. J. 1970. Investigations on the ecology and production-biology of the "floating meadows" (*Paspalo-Echinochloetum*) on the Middle Amazon Part I: the floating vegetation and its ecology. Amazoniana 2:449–495.

Junk, W. J., Howard-Williams, C. 1984. Ecology of aquatic macrophytes in Amazonia. In: Sioli, H., Dumont, H. J., Junk, W. J. (eds.). The Amazon: limnology and landscape ecology of a mighty tropical river and its basin. p. 269–253. Vol. 56 of Monographie Biologicae, Kluwer Academic Publisher, Massachusetts, USA.

Junk, W. J. 1997. General aspects of floodplain ecology with special reference to Amazonian floodplains. In: Junk, W. J. (ed.). The Central Amazon Floodplain. p. 3–22. Springer, Berlin, Germany.

Junk, W. J., Bayley, P. B., Sparks, R. E. 1989. The flood pulse concept in river-floodplain system. Canadian special publication of fisheries and aquatic sciences.

Junk, W. J., Furch, K. 1991. Nutrient dynamics in Amazonian floodplains: decomposition of herbaceous plants in aquatic and terrestrial environments. Internationale Vereinigung fuer Theoretische und Angewandte Limnologie Verhandlungen 24:2080–2084.

Junk, W. J., Piedade, M. T. F. 1993a. Biomass and primary-production of herbaceous plant communities in the Amazon floodplain. Hydrobiologia 263(3): 155–162.

Junk, W. J., Piedade, M. T. F. 1993b. Herbaceous plants of the Amazon floodplain near Manaus: Species diversity and adaptations to the flood pulse. Amazoniana 12:467–484.

Junk, W. J., Piedade, M. T. F. 1997. Plant life in the floodplain with special reference to herbaceous plants. p. 147–186. In: Junk, W. J. (ed.). The Central Amazon Floodplain. p. 147–186. Springer, Berlin, Germany.

Justice, C. O., Townshend, J. R. G., Vermote, E. F., Masuoka, E., Wolfe, R. E., Saleous, N., Roy, D. P., Morisette, J. T. 2002. An overview of MODIS Land data processing and product status. Remote Sensing of Environment 83: 3–15.

Kalliola, R., Salo, J., Puhakka, M., Rajasilta, M. 1991. New site formation and colonizing vegetation in primary sucession on the western Amazon floodplains. Journal of Ecology 79: 877–901.

Kasischke, E. S., Bourgeau-Chavez, L. L. 1997. Monitoring South Florida wetlands using ERS-1 SAR imagery. Photogrammetric engineering and remote sensing, 63(3): 281–291.

Kasischke, E. S., Smith, K. B., Borgeau-Chavez, L. L., Romanowicz, E. A., Brunzell, S., Richardson, C. J. 2003. Effects of seasonal hydrologic patterns in south Florida wetlands on radar backscatter measured from ERS-2 SAR imagery. Remote Sensing of Environment 88: 423–441.

Keddy, P. A. 2000. Wetland ecology: principles and conservation. Cambridge University Press , New York, USA. 614 pp.

Laur, H., Bally, P., Meadows, P., Sanchez, J., Schaettler, B., Lopinto, E. 1997. Derivation of the backscatter coefficient sigma0 in ESA ERS SAR PRI products. ESA Document no. ES-TN-RS-PM-HL09.

Leeuw, J., Wielemaker, A., Munck, W., Herman, P. M. J. 1996. Net aerial primary production (NAPP) of the marsh macrophyte *Scirpus maritimus* estimated by a combination of destructive and non-destructive sampling methods. Plant Ecology 123: 101–108.

Le Toan, T., Ribbes, F., Wang, L. F., Floury, N., Ding, K. H., Kong, J. A., Fujita, M., Kurosu, T. 1997. Rice crop mapping and monitoring using ERS-1 data based on experiment and modeling results. IEEE Transactions on Geoscience and Remote Sensing 35(1): 41–56.

Lewis, A., Henderson, F. M. 1998. Manual of Remote Sensing, Vol. 2, Chapt. Radar fundamentals: The geoscience perspective. 3rd ed. pp. 131–187. Wiley, New York, USA.

Linthurst, R. A., Reimold, R. J. 1978. An evaluation of methods for estimating the net aerial primary productivity of estuarine angiosperms. The Journal of Applied Ecology 15: 919–931.

Long, S. P., Garcia-Moya, E., Imbamba, S. K., Kamnalrut, A., Piedade, M. T. F., Scurlock, J. M. O., Shen, Y. K., Hall, D. O. 1989. Primary productivity of natural grass ecosystems of the tropics: a reappraisal. Plant and Soil 115: 155–166.

Malthus, T. J., George, D. G. 1997. Airborne remote sensing of macrophytes in Cefni reservoir, Anglesley, UK. Aquatic Botany 58: 317–332.

Manly, B. F. J. 2001. Randomization, Bootstrap and Monte Carlo Methods in Biology. Chapman & Hall/CRC, Boca Raton, USA. 399 pp.

Martinez, J. M., Le Toan, T. 2007. Mapping of flood dynamics and spatial distribution of vegetation in the Amazon floodplain using multitemporal SAR data. Remote Sensing of Environment 108: 209–223.

McClain, M. E., Elsenbeer, H. 2001. Terrestrial inputs to Amazon streams and internal biogeochemical processing. In: McClain, M. E., Victoria, R. L., Richey, J. E. (eds.). The biogeochemistry of the Amazon Basin. p. 185–208. Oxford University Press, New York, USA.

Melack, J. M., Hess L. L. In press (a). Remote Sensing of the distribution and extent of wetlands in the Amazon basin. In: Junk, W. J., Piedade, M. T. F. (eds.). Amazonian floodplain forests: Ecophysiology, biodiversity and sustainable management. Ecological Studies – Springer.

Melack, J.M., Novo, E.M.L.M., Forsberg, B. R., Piedade, M.T.F., Maurice, L. In press (b). Floodplain ecosystem processes. American Geophysical Union, Geophysical Monograph Series.

Melack, J. M., Forsberg, B. R. 2001. Biogeochemistry of Amazon floodplain lakes and associated wetlands. In: McClain, M. E., Victoria, R. L., Richey, J. E. (eds.). The biogeochemistry of the Amazon Basin. p. 235–276. Oxford University Press, New York, USA.

Melack, J. M., Hess, L. L., Gastil, M., Forsberg, B. R., Hamilton, S. K., Lima, I. B. T., Novo, E. M. L. M. 2004. Regionalization of methane emissions in the Amazon Basin with microwave remote sensing. Global Change Biology 10:530–544.

Miao, S., Sindhøj, E., Edelstein, C. 2008. Allometric relationships of field populations of two clonal species with contrasting life histories, *Cladium jamaicense* and *Typha domingensis*. Aquatic Botany 88: 1–9.

Milner, C., Hughes, R. E. 1968. Methods for the measurement of the primary production of grassland. IBP Handbook, vol. 6. Blackwell Scientific, Oxford, UK.

Mitsch, W. J., Gosselink, J. G. 2000. Wetlands. 3d. edition. John Wiley & Sons, Hoboken, USA. 920 pp.

Moreau, S., Le Toan, T. 2003. Biomass quantification of Andean wetland forages using ERS satellite SAR data for optimizing livestock management. Remote Sensing of Environment 84: 477–492.

Moreira-Turcq, P., Seyler, P., Guyot, J. L., Etcheber, H. 2003. Exportation of organic carbon from the Amazon River and its main tributaries. Hydrological Processes 17: 1329–1344.

Morison, J. I. L., Piedade, M. T. F., Muller, E., Long, S.P., Junk, W. J., Jones. M. B. 2000. Very high productivity of the C-4 aquatic grass *Echinochloa polystachya* in the Amazon floodplain confirmed by net ecosystem CO_2 flux measurements. Oecologia 125: 400–411.

Morris, J. T., Haskin, B. 1990. A 5-yr record of aerial primary production and stand characteristics of *Spartina alterniflora*. Ecology 71: 2209–2217.

Nemani, R., Running, S. 1997. Land cover characterization using multitemporal red, near-IR, and thermal-IR data from NOAA/AVHRR. Ecological Applications 7(1): 79–90.

Noernberg, M. A., Novo, E., Krug, T. 1999. The use of biophysical indices and coefficient of variation derived from airborne synthetic aperture radar for monitoring the spread of aquatic vegetation in tropical reservoirs. International Journal of Remote Sensing 20: 67–82.

Novo, E. M. L. M., Costa, M. P. F., Mantovani, J. E., Lima, I. B. T. (2002). Relationship between macrophyte stand variables and radar backscatter at L and C band, Tucurui reservoir, Brazil. International Journal of Remote Sensing 23: 1241–1260.

Oechel, W. C., Vourlitis, G. L., Verfaillie, J., Crawford, T., Brooks, S., Dumas, E., Hope, A., Stow, D., Boynton, B., Nosov, V., Zulueta, R. 2000. A scaling approach for quantifying the net CO_2 flux of the Kuparuk River basin, Alaska. Global Change Biology 6: 160–173.

Ohly, J. J., Hund, M. 2000. Floodplain animal husbandry in central Amazonia. In: Junk, W. J., Ohly, J. J., Piedade, M. T. F., Soares, M. G. M. (eds.). The Central Amazon Floodplain: Actual Use and Options for a Sustainable Management. p. 313–341. Backhuys Publishers, Leiden, Netherlands.

Ometto, J. P. H. B., Nobre, A. D., Rocha, H. R., Artaxo, P., Martinelli, L. A. 2005. Amazonia and the modern carbon cycle: lessons learned. Oecologia 143: 483–500.

Peñuelas, J., Filella, I., Gamon, J. A., Field, C. 1997. Assessing photosynthetic radiation-use efficiency of emergent aquatic vegetation from spectral reflectance. Aquatic Botany 58: 307–315.

Peñuelas, J., Gamon, J. A., Griffin, K. L., Field, C. B. 1993. Assessing community type, plant biomass, pigment composition and photosynthetic efficiency of aquatic vegetation from spectral reflectance. Remote Sensing of Environment, 46: 110–118.

Piedade, M. T. F., Junk, W. J., Long, S. P. 1991. The productivity of the C4 grass *Echinochloa polystachya* on the Amazon Floodplain. Ecology 72: 1456–1463.

Piedade, M. T. F., Junk, W. J., de Mello, J. A. N. 1992. A floodplain grassland of the central Amazon. In: Long, S. P., Jones, B. J., Roberts, M. J. (Eds.) Primary productivity of grass ecosystems of the tropics and sub-tropics. Chapman-Hall/UNEP.

Piedade, M. T. F., Long, S. P., Junk, W. J. 1994. Leaf and canopy photosynthetic CO_2 uptake of a stand of *Echinochloa polystachya* on the central Amazon floodplain. Oecologia 97: 193–201.

Piedade, M. T. F., Junk, W. J., Long, S. P. 1997. Nutrient dynamics of the highly productive C4 macrophyte *Echinochloa polystachya* on the Amazon floodplain. Functional Ecology 11: 60–65.

Piedade, M. T. F., Worbes, M., Junk, W. J. 2001. Geo-ecological controls on elemental fluxes in communities of higher plants in Amazonian floodplains. In: McClain, M. E., Victoria, R. L., Richey, J. E. (eds.). The biogeochemistry of the Amazon Basin. p. 209–234. Oxford University Press, New York, USA.

Pope, K. O., Rejmankova, E., Paris, J. F., Woodruff, R. 1997. Detecting seasonal flooding cycles in marshes of the Yucatán peninsula with SIR-C polarimetric radar imagery. Remote Sensing of Environment 59: 157–166.

Potter, C., Klooster, S., Steinbach, M., Tan, P. N., Kumar, V., Shekhar, S., Carvalho, C. 2004. Understanding global teleconnections of climate to regional model estimates of Amazon ecosystem carbon fluxes. Global Change Biology 10: 693–703.

Proisy, C., Mougin, E., Fromard, F., Karam, M. A. 2000. Interpretation of polarimetric radar signatures of mangrove forests. Remote Sensing of Environment 71: 56–66.

Quay, P. D., Wilbur, D. O. , Richey, J. E., Hedges, J. I., Devol, A. H. 1992. Carbon cycling in the Amazon River - implications from the ^{13}C compositions of particles and solutes. Limnology and Oceanography 37: 857–871.

Quegan, S., Le Toan, T., Yu, J. J., Ribbes, F., Floury, N. 2000. Multitemporal ERS SAR analysis applied to forest mapping. IEEE Transactions on Geoscience and Remote Sensing, 38(2): 741–753.

Radarsat International. 2002. RADARSAT Data Products Specification. RSI-GS-026 V3. Richmond, Canada.

Richey, J. E., Melack, J. M., Aufdenkampe, A. K., Ballester, V. M., Hess, L. L. 2002. Outgassing from Amazonian rivers and wetlands as a large tropical source of atmospheric CO_2. Nature 416: 617–620.

Rosenqvist, Å., Forsberg, B. R., Pimentel, T., Rauste, Y. A., Richey, J. E. 2002. The use of spaceborne radar data to model inundation patterns and trace gas emissions in the central Amazon floodplain. International Journal of Remote Sensing 23: 1303–1328.

Sala, O. E., Biondini, M. E., Lauenroth, W. K. 1988. Bias in estimates of primary production: An analytical solution. Ecological Modelling, 44(1): 43–55.

Saleska, S. R., Miller, S. D. , Matross, D. M., Goulden, M. L., Wofsy, S. C., da Rocha, H. R., de Camargo, P. B., Crill, P., Daube, B. C., de Freitas, H. C., Hutyra, L., Keller, M., Kirchhoff, V., Menton, M., Munger, J. W., Pyle, E. H., Rice, A. H., Silva, H. 2003. Carbon in Amazon forests: unexpected seasonal fluxes and disturbance-induced losses. Science 302: 1554–1557.

Schlesinger, W. H. 1997. Biogeochemistry: An analysis of global change. 2nd Edition. Academic Press, San Diego, USA. 588 pp.

Shepherd, N. 2000. Extraction of Beta Nought and Sigma Nought from RADARSAT CDPF Products. ALTRIX Systems Report No.: AS97-5001, Ottawa, Canada.

Silva, T. S. F., Freitas, R. M., Novo, E. M. L. M. 2007a. Monitoramento de áreas alagáveis.. In Rudorff, B. F. T., Shimabukuro, Y. E., Ceballos, J. C. (eds.). O Sensor Modis e suas Aplicações Ambientais no Brasil. p. 255–263. Parêntese Editora, São José dos Campos, Brazil.

Silva, T.S.F., Lima, A., Fonseca, L. M. G. F., Novo, E. M. L. M., Ribeiro, M. C. 2007b. Assessment of image restoration techniques to enhance the applicability of MODIS images on Amazon floodplain landscape studies. XIII Simpósio Brasileiro de Sensoriamento Remoto. Florianópolis, Brazil, pp. 6969-6976.

Silva, T. S. F., Costa, M. P. F. , Melack, J. M., Novo, E. M. L. M. 2008. Remote sensing of aquatic vegetation: theory and applications. Environmental Monitoring and Assessment 140: 131–145.

Simard, M., Saatchi, S. S., De Grandi, G. 2000. The use of decision tree and multiscale texture for classification of JERS-1 SAR data over tropical forest. IEEE Transactions on Geoscience and Remote Sensing 38(5): 2310–2321.

Simard, M., Zhang, K., Rivera-Monroy, V. H., Ross, M. S., Ruiz, P. L., Castaneda-Moya, E., et al. (2006). Mapping height and biomass of mangrove forests in Everglades National Park with SRTM elevation data. Photogrammetric Engineering and Remote Sensing 72(3): 299–311.

Sippel, S. J., Hamilton, S. K., Melack, J. M., Novo, E. M. L. M. 1998. Passive microwave observations of inundation area and the area/stage relation in the Amazon River floodplain. International Journal of Remote Sensing 19: 3055–3074.

Solomon, S., Qin, D., Manning, M., Marquis, M., Averyt, K., Tignor, M. M. B., Miller, H. L. 2007. Climate change 2007: the physical science basis: contribution of working group I to the fourth assessment report of the intergovernmental panel on climate change. Cambridge University Press, Cambridge, UK, 996 pp.

Srivastava, S. K., Hawkins, R. K., Lokowski, T. I., Banik, B. T., Adamovic, M., Jefferies, W. C. 1999. RADARSAT image quality and calibration – Update. Advances in Space Research 23: 1487–1496.

Tilley, D. R., Ahmed, M., Son, J. H., Badrinayanan, H. 2003. Hyperspectral reflectance of emergent macrophytes as an indicator of water column ammonia in an oligohaline, subtropical marsh. Ecological Engineering 21: 153–163.

Tockner, K., Malard, F., Ward, J. V. 2000. An extension of the flood pulse concept. Hydrological Processes 14: 2861–2883.

Vartapetian, B. B., Jackson, M. B. 1997. Plant adaptations to anaerobic stress. Annals of Botany 79 (Supplement A): 3–20.

Vermote, E. F., Tanre, D., Deuze, J. L., Herman, M., & Morcette, J. J. 1997. Second simulation of the satellite signal in the solar spectrum, 6S: an overview. IEEE Transactions on Geoscience and Remote Sensing, 35(3): 675–686.

Vermote, E. F., Vermeulen, A. 1999. Atmospheric correction algorithm: spectral reflectances (MOD09). MODIS Algorithm Theoritical Basis Document, version 4.

Vermote, E. F., Kotchenova, S. 2008. Atmospheric correction for the monitoring of land surfaces. Journal of Geophysical Research 113(D23): D23S90.

Vis, C., Hudon, C., Carignan, R. 2003. An evaluation of approaches used to determine the distribution and biomass of emergent and submerged aquatic macrophytes over large spatial scales. Aquatic Botany 77: 187–201.

Wang, Y., Hess, L. L., Filoso, S., Melack, J. M. 1995. Understanding the radar backscattering from flooded and nonflooded Amazonian forests: Results from canopy backscatter modeling. Remote Sensing of Environment 54: 324–332.

Whiting, G. J., Chanton, J. P. 1993). Primary production control of methane emission from wetlands. Nature 364: 794–795.

Williams, D. J., Rybicki, N. B., Lombana, A. V., O'Brien, T. M., Gomez, R. B. 2003. Preliminary investigation of submerged aquatic vegetation mapping using hyperspectral remote sensing. Environmental Monitoring and Assessment 81: 383–392.

Wrona, F. J., Prowse, T. D., Reist, J. D. 2005. Freshwater ecosystems and fisheries. In: Symon, C., Arris, L., Heal, B. (eds.). Arctic Climate Impact Assessment. p. 353–452. Cambridge University Press, New York, USA.

Wuebbles, D., Hayhoe, K. 2002. Atmospheric methane and global change. Earth–Science Reviews 57: 177–210.

Appendix A – Monthly maps of macrophyte cover at Monte Alegre Lake

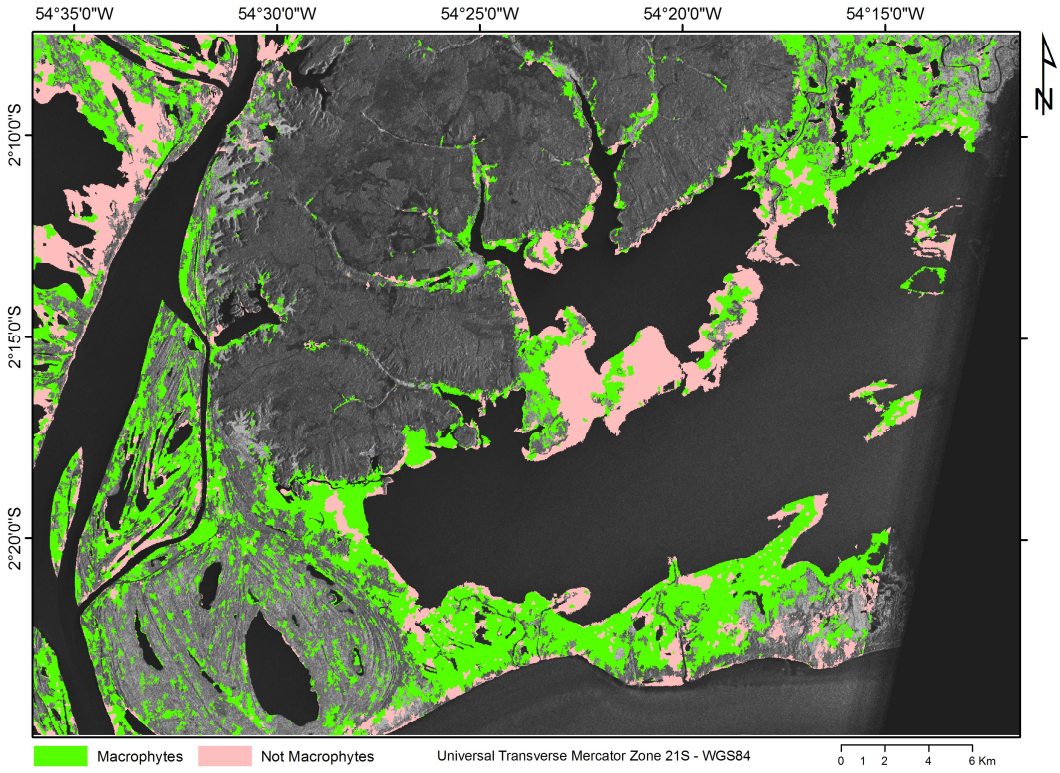

Figure A.1 - Macrophyte cover for Monte Alegre Lake for the date of December 20th, 2003. "Not Macrophytes" areas correspond to areas classified as "Possible Macrophytes" at Level 2 classification, but which do not correspond to macrophyte cover at the mapped date.

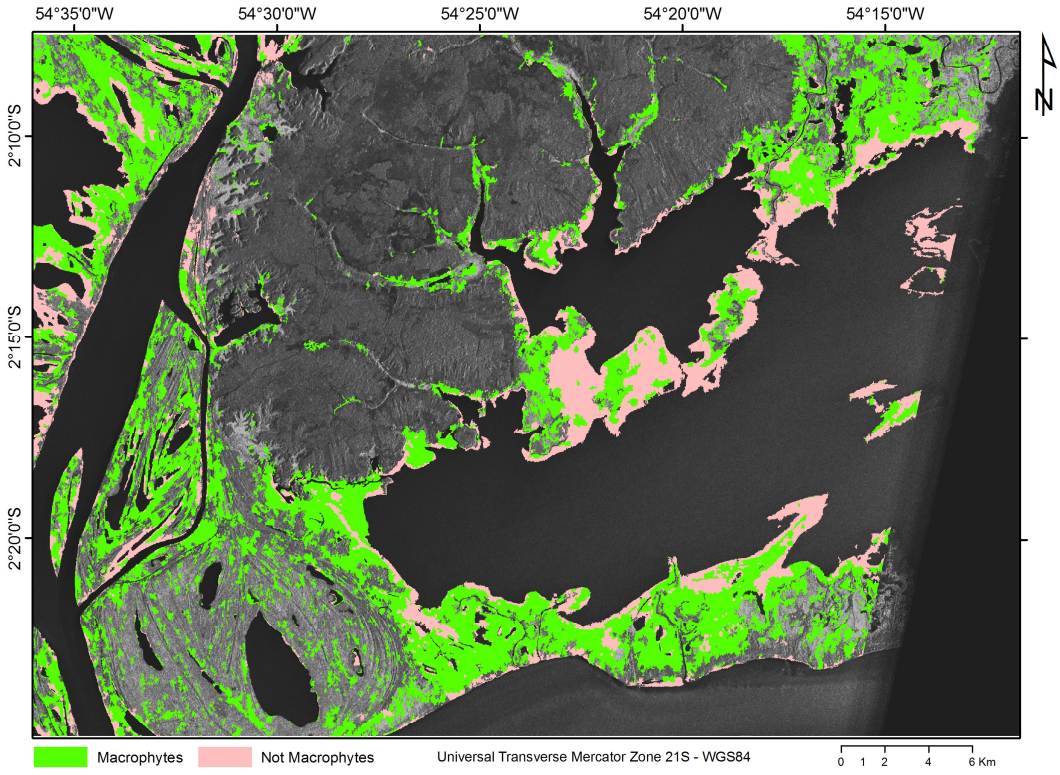

Figure A.2 - Macrophyte cover for Monte Alegre Lake for the date of January 13th, 2004. "Not Macrophytes" areas correspond to areas classified as "Possible Macrophytes" at Level 2 classification, but which do not correspond to macrophyte cover at the mapped date.

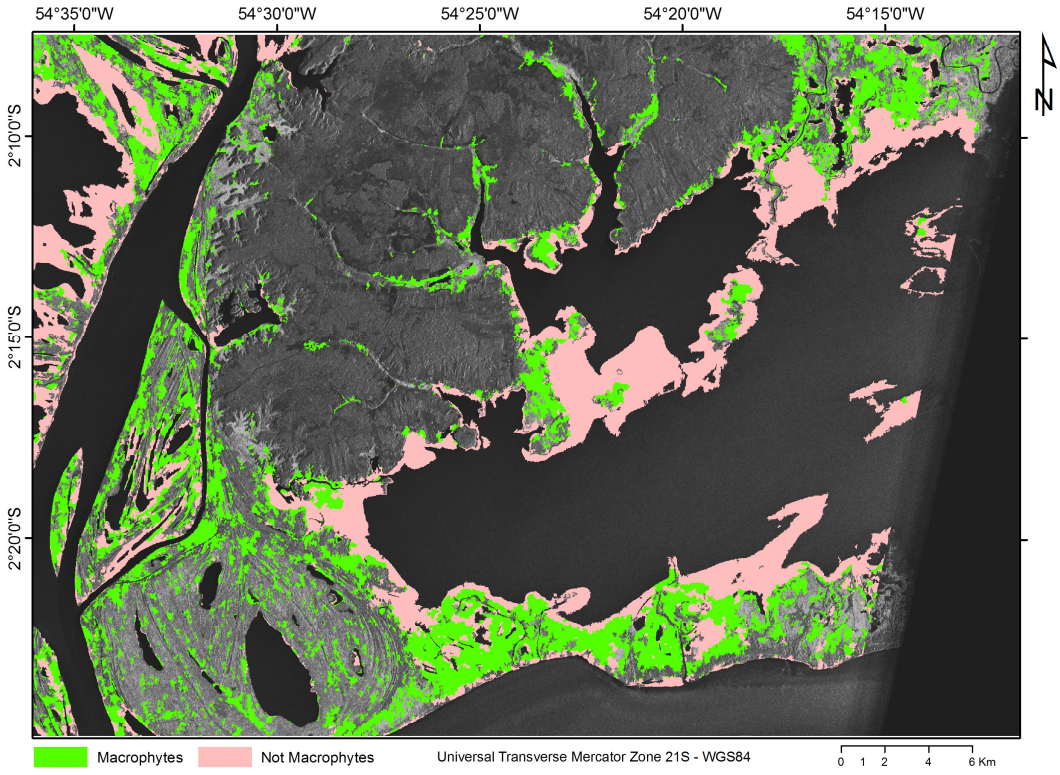

Figure A.3 - Macrophyte cover for Monte Alegre Lake for the date of February 6th, 2004. "Not Macrophytes" areas correspond to areas classified as "Possible Macrophytes" at Level 2 classification, but which do not correspond to macrophyte cover at the mapped date.

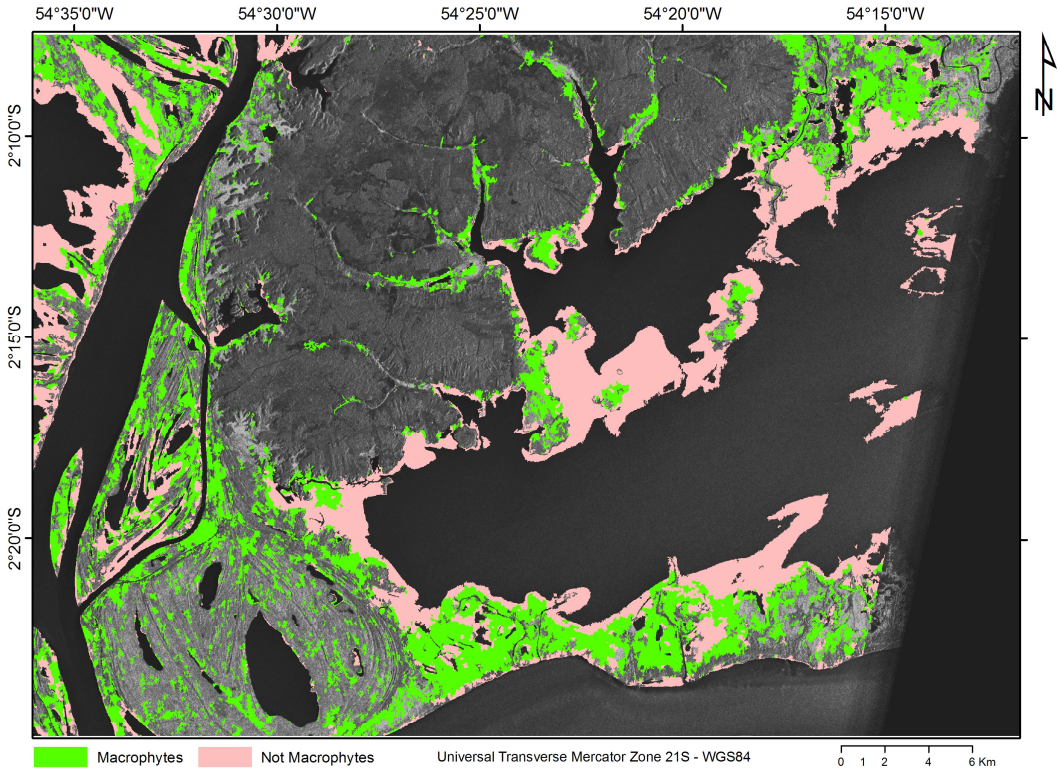

Figure A.4 - Macrophyte cover for Monte Alegre Lake for the date of March 1st, 2004. "Not Macrophytes" areas correspond to areas classified as "Possible Macrophytes" at Level 2 classification, but which do not correspond to macrophyte cover at the mapped date.

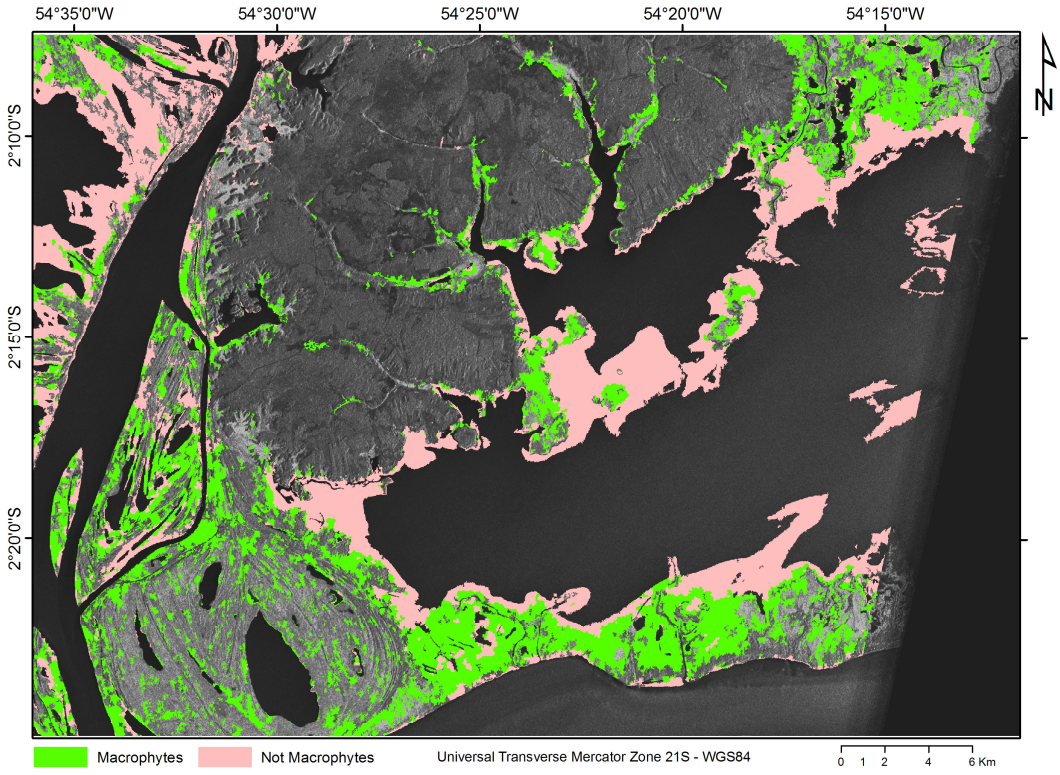

Figure A.5- Macrophyte cover for Monte Alegre Lake for the date of March 25th, 2004. "Not Macrophytes" areas correspond to areas classified as "Possible Macrophytes" at Level 2 classification, but which do not correspond to macrophyte cover at the mapped date.

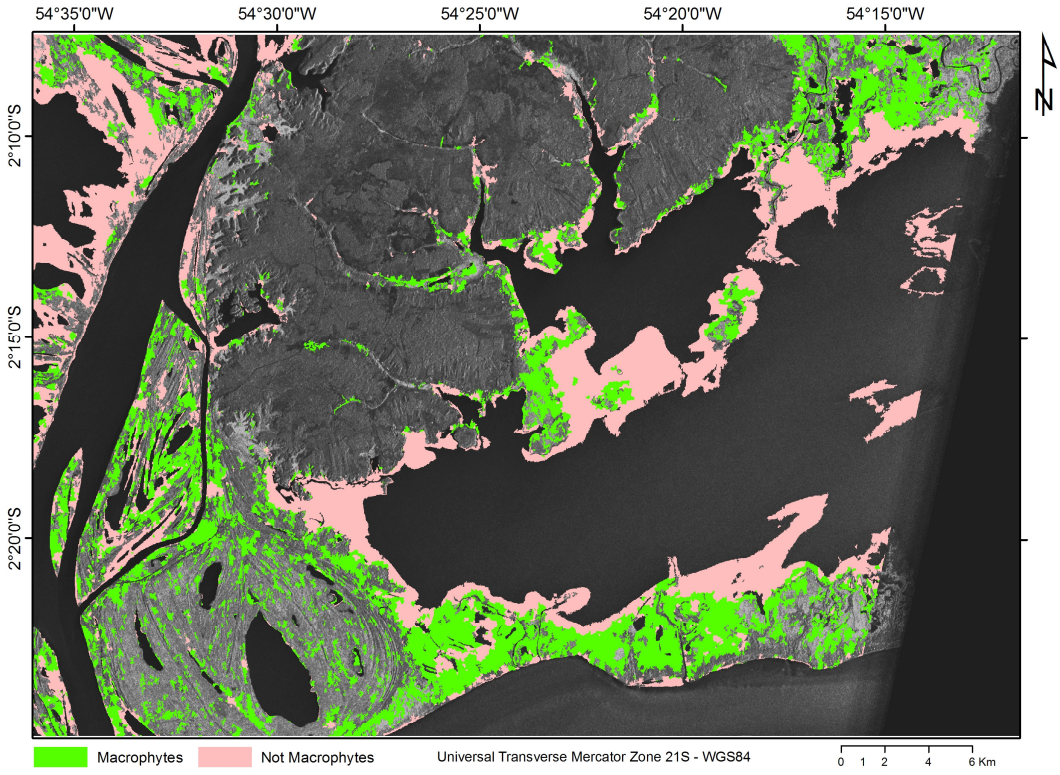

Figure A.6 - Macrophyte cover for Monte Alegre Lake for the date of April 18th, 2004. "Not Macrophytes" areas correspond to areas classified as "Possible Macrophytes" at Level 2 classification, but which do not correspond to macrophyte cover at the mapped date.

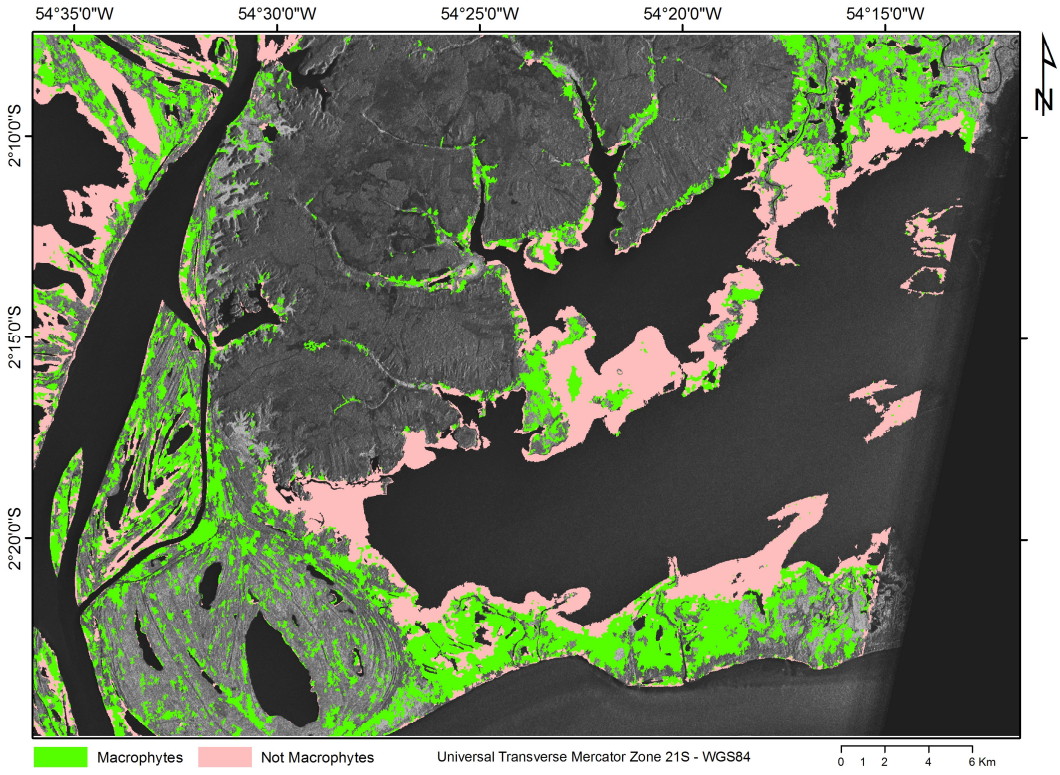

Figure A.7 - Macrophyte cover for Monte Alegre Lake for the date of June 5th, 2004. "Not Macrophytes" areas correspond to areas classified as "Possible Macrophytes" at Level 2 classification, but which do not correspond to macrophyte cover at the mapped date.

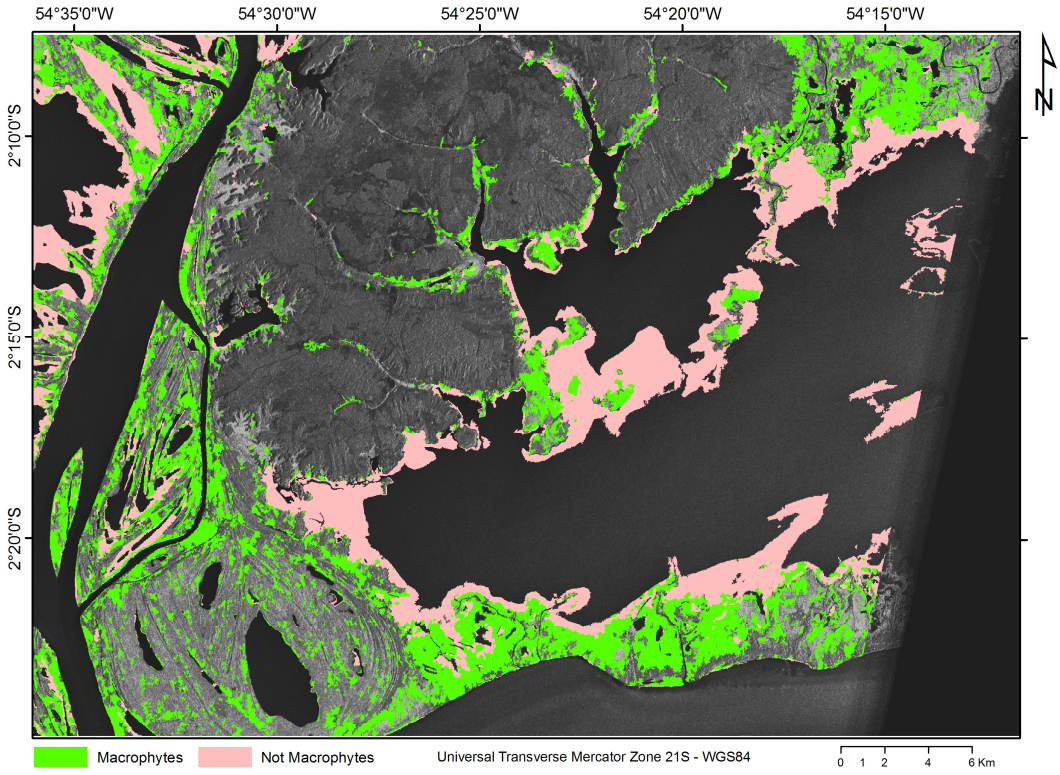

Figure A.8 - Macrophyte cover for Monte Alegre Lake for the date of June 29th, 2004. "Not Macrophytes" areas correspond to areas classified as "Possible Macrophytes" at Level 2 classification, but which do not correspond to macrophyte cover at the mapped date.

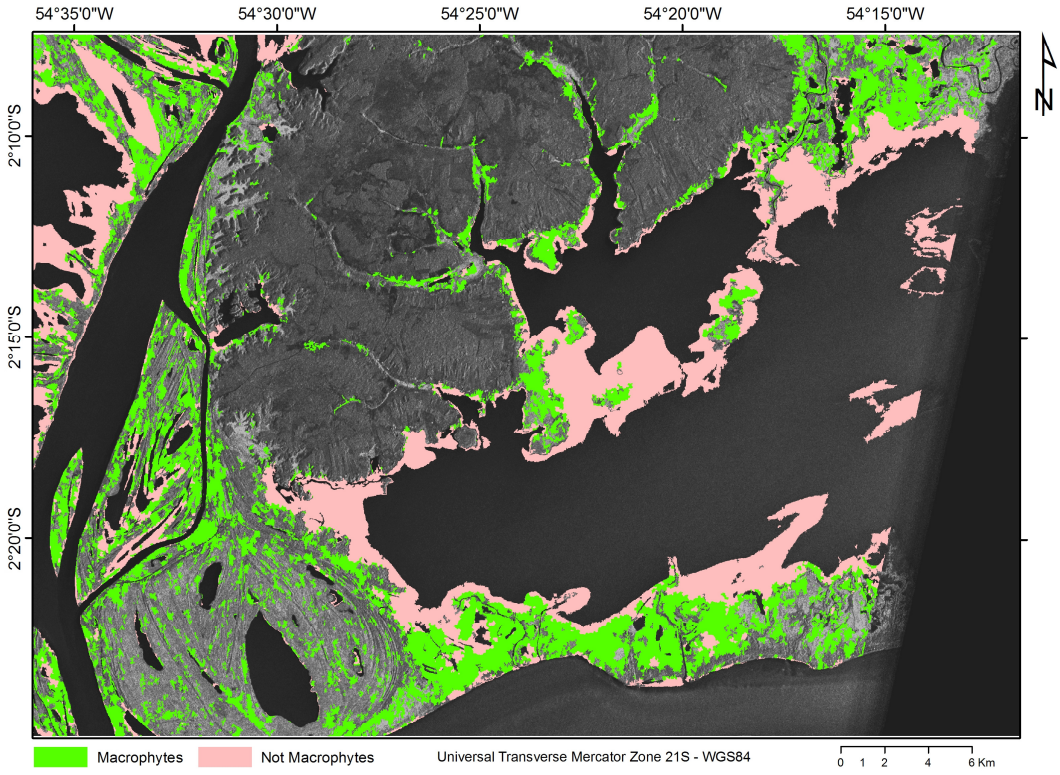

Figure A.9 - Macrophyte cover for Monte Alegre Lake for the date of July 23rd. , 2003. "Not Macrophytes" areas correspond to areas classified as "Possible Macrophytes" at Level 2 classification, but which do not correspond to macrophyte cover at the mapped date.

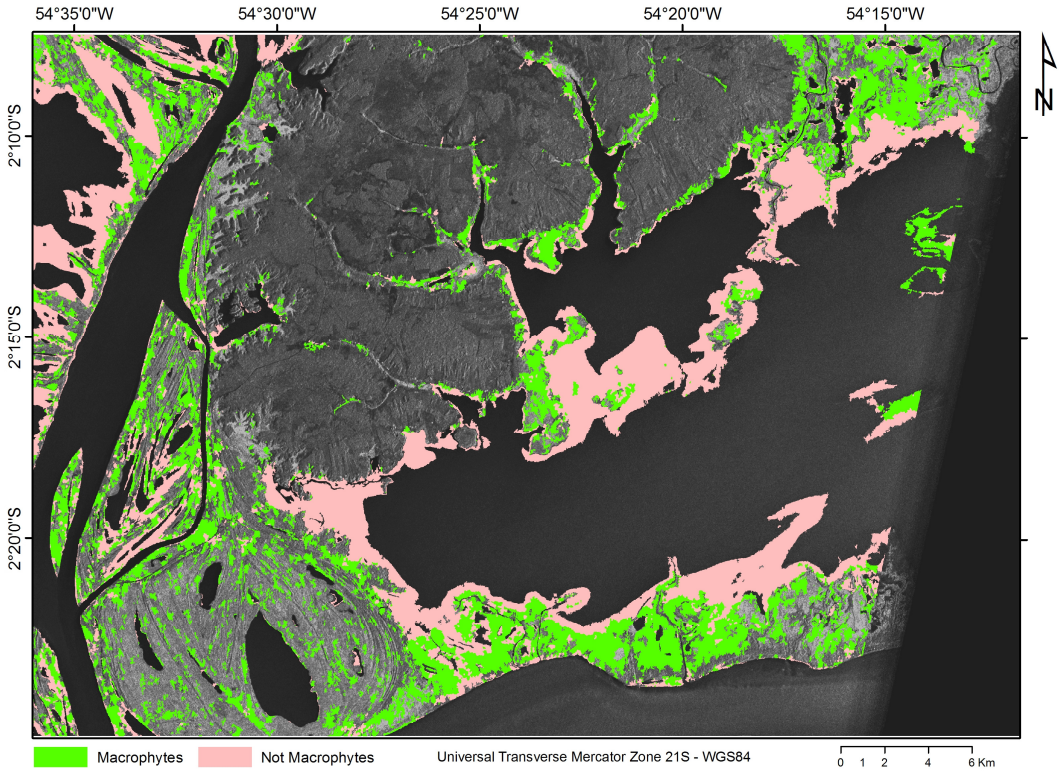

Figure A.10 - Macrophyte cover for Monte Alegre Lake for the date of August 16th, 2004. "Not Macrophytes" areas correspond to areas classified as "Possible Macrophytes" at Level 2 classification, but which do not correspond to macrophyte cover at the mapped date.

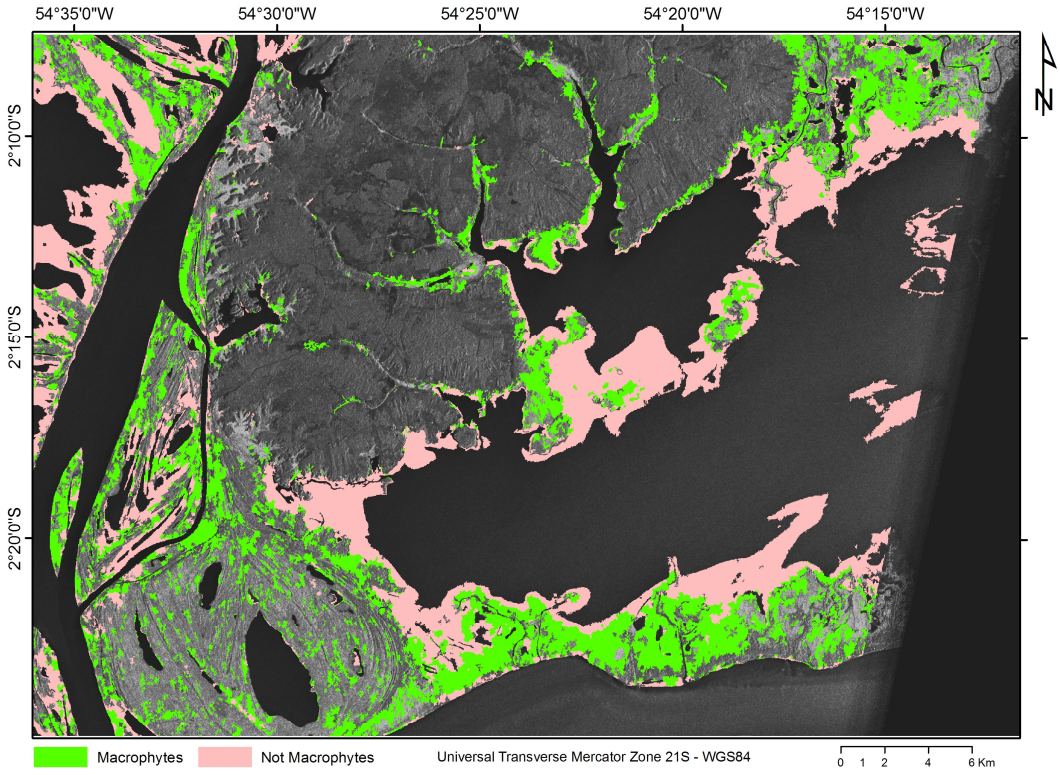

Figure A.11 - Macrophyte cover for Monte Alegre Lake for the date of September 9th, 2004. "Not Macrophytes" areas correspond to areas classified as "Possible Macrophytes" at Level 2 classification, but which do not correspond to macrophyte cover at the mapped date.

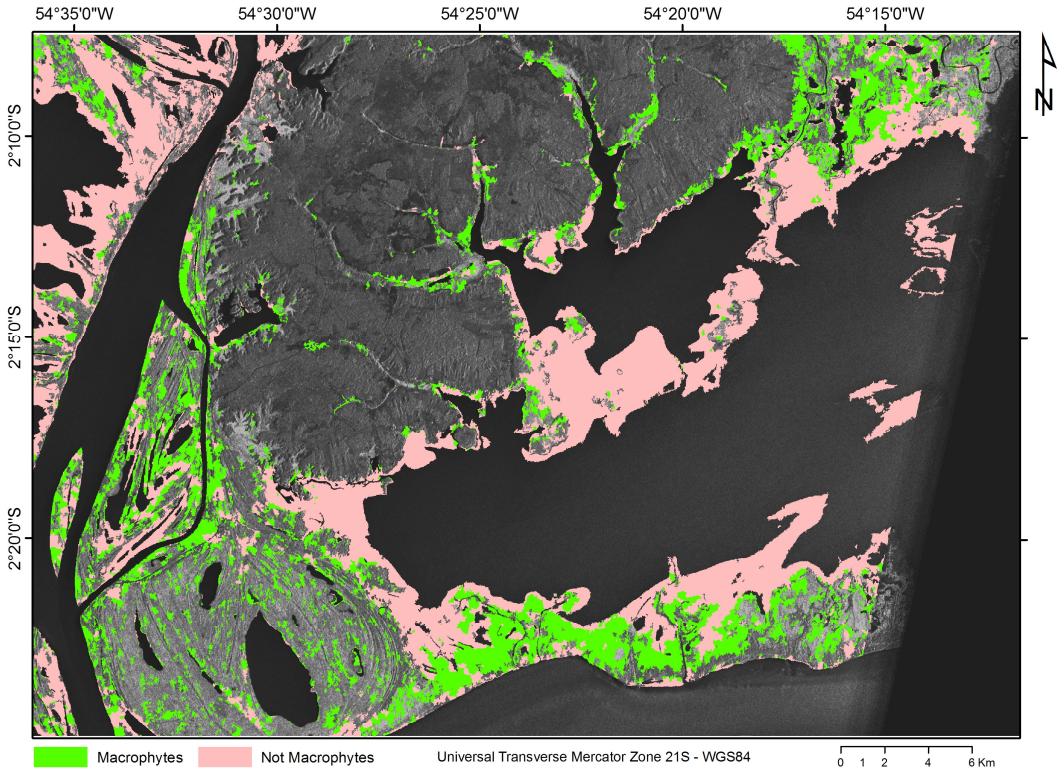

Figure A.12 - Macrophyte cover for Monte Alegre Lake for the date of October 27th, 2004. "Not Macrophytes" areas correspond to areas classified as "Possible Macrophytes" at Level 2 classification, but which do not correspond to macrophyte cover at the mapped date.

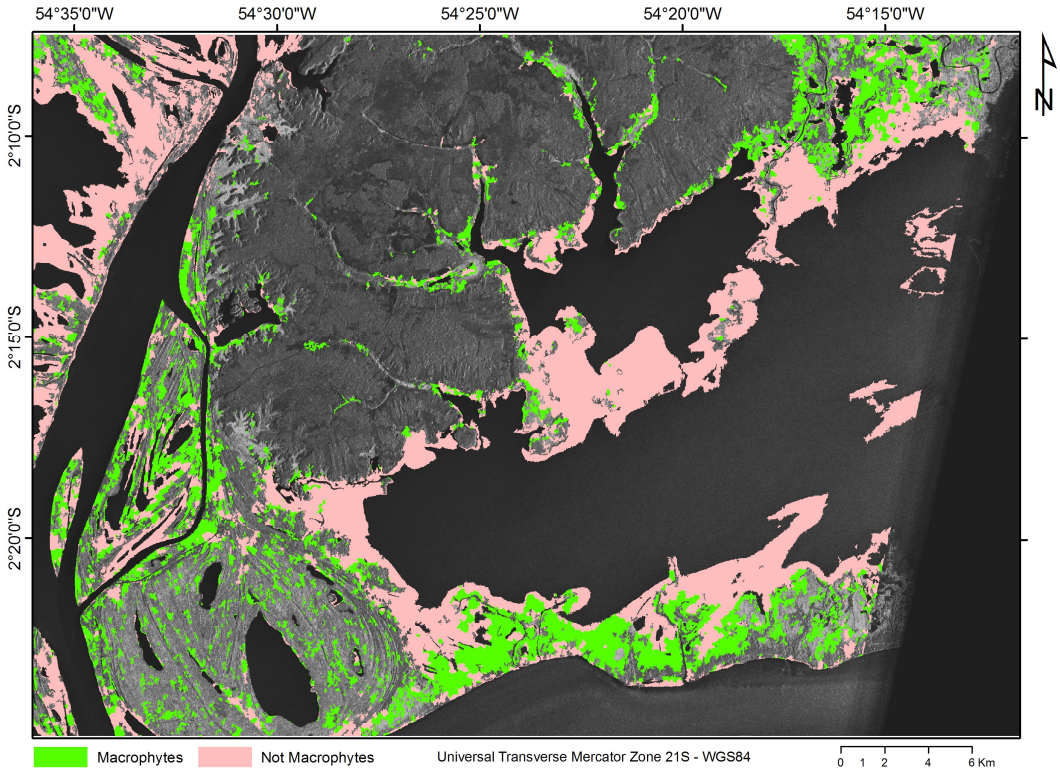

Figure A.13 - Macrophyte cover for Monte Alegre Lake for the date of November 20th, 2004. "Not Macrophytes" areas correspond to areas classified as "Possible Macrophytes" at Level 2 classification, but which do not correspond to macrophyte cover at the mapped date.

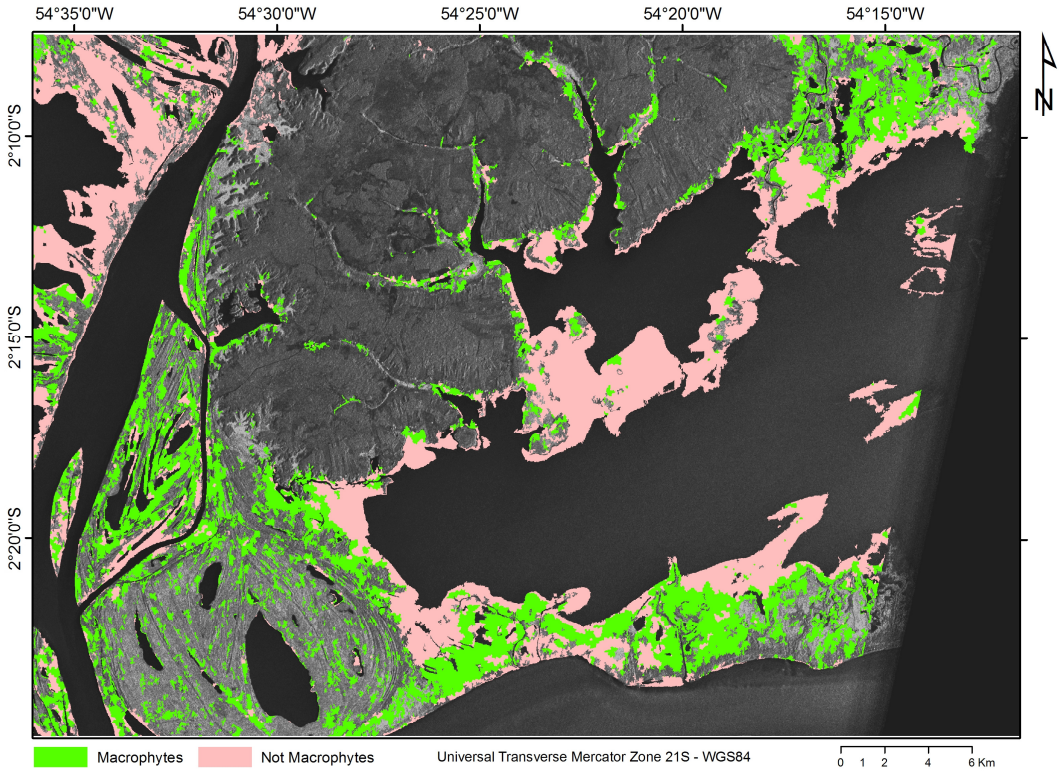

Figure A.14 - Macrophyte cover for Monte Alegre Lake for the date of December 14th, 2004. "Not Macrophytes" areas correspond to areas classified as "Possible Macrophytes" at Level 2 classification, but which do not correspond to macrophyte cover at the mapped date.